Analysis and review of the literature for the computation of the (global) probability of collision between space objects: Multiple long-term/short-term encounters

D. Arzelier, F. Bréhard, M. Joldeş, J.B. Lasserre, A. Rondepierre

Equipe MAC (Méthodes et Algorithmes en Commande), LAAS-CNRS
7, avenue du Colonel Roche 31031 Toulouse
florent.brehard@laas.fr
Equipe ROC (Recherche Opérationnelle Optimisation Contraintes)
LAAS-CNRS
7, avenue du Colonel Roche 31031 Toulouse
denis.arzelier@laas.fr, mioara.joldes@laas.fr, aude.rondepierre@insa-toulouse.fr

Ref:
R & T: R-S19-BS-0005-051
Technical report TR 1
Version 1.0

April 26, 2022

Contents

Notations

Mathematics

Proofs are ended by the $\square$ symbol.
Sets

- $\mathbb{N}$: set of natural numbers.
- $\mathbb{Z}$: set of integers.
- $\mathbb{R}$: set of real numbers.
- $\mathbb{C}$: set of complex numbers.
- $\mathbb{N}^* = \{n \in \mathbb{N} \text{ s.t. } n \geqslant 1\}$.
- $\mathbb{R}^n$: linear space of real vectors of dimension n, $n \in \mathbb{N}^*$.
- $\mathbb{S}^2 = \left\{x \in \mathbb{R}^3 \text{ s.t. } \|x\|_2 = 1\right\}$ is the unit sphere.
- ${}^{c}_{A}B := A \backslash B = \{x \in A \text{ s.t. } x \notin B\}$: complement of B in A. The prescript A may be omitted if the context makes it clear and obvious.
- ∂A: boundary of the topological space A.
- $\mathrm{cl}\,(A) = A \cup \partial A$: closure of the topological space A.
- $\overline{B}\,(x, R) = \{y \in \mathbb{R}^n \text{ s.t. } \|x - y\|_2 \leqslant R\}$ ($n \in \mathbb{N}$, $x \in \mathbb{R}^n$, $R > 0$).
- $\mathrm{supp}(f) = \mathrm{cl}\,(\{x \in A \text{ s.t. } f\,(x) \neq 0\})$: support of $f : A \to \mathbb{R}$.
- $\mathrm{supp}(\mu)$: support of the measure μ.
- $\mathbb{R}\,[x]$: ring of real polynomials in the variables $(x_i)_{i=1,\cdots,n}$ ($n \in \mathbb{N}$).
- $\mathbb{R}\,[x]_r = \{p \in \mathbb{R}^n\,[x] \text{ s.t. } \deg(p) \leqslant r\}$: ring of real polynomials in the variables $(x_i)_{i \in [\![1,n]\!]}$ ($n \in \mathbb{N}$) and of maximal degree $r \in \mathbb{N}$.
- $\mathbb{N}^n$: multi-indices of dimension $n \in \mathbb{N}$.
- $\mathbb{N}^n_r = \{\alpha \in \mathbb{N}^n \text{ s.t. } \sum_{i=1}^n \alpha_i \leqslant r\}$ multi-indices of dimension $n \in \mathbb{N}$ and of maximal degree $r \in \mathbb{N}$.

Functions and Measures

- $\mathrm{Id}_{\mathbb{R}^n}$: identity function i.e. $\mathrm{Id}_{\mathbb{R}^n} : \mathbb{R}^n \to \mathbb{R}^n$, $x \mapsto x$.
- 1_B: indicator function of a set B.
- $|.|$: absolute value.
- $|\alpha| = \displaystyle\sum_{i=1}^{n} \alpha_i$ ($\alpha \in \mathbb{N}^n$, $n \in \mathbb{N}$).

- $\|x\|_2 = \left[x \in \mathbb{R}^n \mapsto \sqrt{\sum_{i=1}^n x_i^2}\right]$: Euclidean norm.
- $\mu_1 \otimes \mu_2$: product measure of the measures μ_1 and μ_2.
- $x^\alpha = \prod_{i=1}^n x_i^{\alpha_i}$ ($n \in \mathbb{N}$, $x = (x_i)_{i=1,\cdots,n}$, $\alpha \in \mathbb{N}^n$).

Derivatives and vector analysis

Let $\mathcal{T} \subseteq \mathbb{R}$, $n \in \mathbb{N}$, $m \in \mathbb{N}$, $f : \mathcal{T} \times \mathbb{R}^n \to \mathbb{R}$ be a scalar field, and $g : \mathcal{T} \times \mathbb{R}^n \to \mathbb{R}^n$ be a vector field.

- $\partial_{x_i} f = f_{x_i} = \frac{\partial f}{\partial x_i}$: partial derivative of f with respect to the variable x_i ($i = 1, \cdots, n$).
- $\partial_x^\alpha = \partial_{x_1}^{\alpha_1} \cdots \partial_{x_n}^{\alpha_n}$.
- $\dot{g} = \partial_t g = (\partial_t g_1, \partial_t g_2, \ldots, \partial_t g_m)$: element-wise partial time derivative of g.
- $\nabla f = (\partial_t f, \partial_{x_1} f, \partial_{x_2} f, \ldots)^T$: gradient operator.
- $\mathrm{div}(g) = \partial_{x_1} g_1 + \partial_{x_2} g_2 + \cdots + \partial_{x_n} g_n$: divergence operator.
- $J(g) = (\partial_{x_1} g, \partial_{x_2} g, \ldots \partial_{x_n} g)$: Jacobian operator.
- $d_t f = \frac{df}{dt} = \partial_t f + (\nabla f) \cdot g$: total derivative of f under the vector field g.

Linear Algebra

- $(\boldsymbol{e_1}, \ldots, \boldsymbol{e_n})$: canonical basis of linear space $\mathbb{R}^n$.
- $\mathcal{M}_{m,n}(\mathbb{K})$: matrices with $m \in \mathbb{N}$ rows and $n \in \mathbb{N}$ columns, and which components are in the field $\mathbb{K}$ ($\mathbb{R}$ or $\mathbb{C}$).
- I_n: identity square matrix of dimension n.
- A^{-T}: transpose of the inverse of the square matrix A.
- Let $(A, B) \in (\mathcal{M}_{n,n}(\mathbb{K}))^2$ ($n \in \mathbb{N}$). The notation "$A \succeq 0$" means A is positive semidefinite. "$A \succeq B$" means "$A - B \succeq 0$".
- $u \cdot v$: scalar product between the vectors u and v.
- $\langle A, B \rangle_F = \mathrm{trace}\left(A^T B\right) = \sum_{i,j} A_{ij} B_{ij}$: Frobenius inner product of two matrices $(A, B) \in (\mathcal{M}_{n,m}(\mathbb{K}))^2$ ($n, m \in \mathbb{N}$).
- $0_{n,m}$ is a matrix of zeros of dimensions $n \times m$.
- v = diag2vec(A): transform the diagonal elements of the square matrix A in the vector v.
- v = vec2diag(v): puts the entries of the vector v on the diagonal of the square matrix A.

Probabilities and Statistics

- $\mathbb{P}(E)$: probability of the event E.
- $x \sim \mathcal{N}(\mu, \Sigma)$: x is a n-dimensional ($n \in \mathbb{N}$) random vector following a multivariate Gaussian distribution with mean vector $\mu \in \mathbb{R}^n$ and with covariance matrix $\Sigma \in \mathcal{M}_{n,n}(\mathbb{R})$ ($\Sigma \succeq 0$).

- E[X]: mean value vector of the random vector X ;

Orbital Mechanics

Notations for orbital state-space model

Those notations describe what the adopted letters usually denote in this report, unless otherwise stated.

- $r_\star = (r_{\star 1},\ r_{\star 2},\ r_{\star 3})^T$: position vector of object $\star$ in some reference frame, (primary: $\star = p$, secondary: $\star = s$, relative: $\star = r$).
- $v_\star = (v_{\star 1},\ v_{\star 2},\ v_{\star 3})^T$: velocity vector of object $\star$.
- $x_\star = (r_\star^T,\ v_\star^T)^T$: state vector of object $\star$.
- $X_{\star\flat} = (x_\star^T,\ x_\flat^T)^T$: state vector of combined object composed of $\star$ and $\flat$.
- $f\left(.,.\right)$: system dynamics.
- $X\left(.|X^0\right)$: trajectory, solution of the equations of motion starting from the initial condition X^0.

Constant and orbital parameters

- $\mu = GM_\oplus = 3.9860047\ 10^{14}\ \mathrm{m^3 s^{-2}}$: standard geocentric gravitational constant from US potential model GEM-T1 ;

- a: semimajor axis ;
- Ω : right ascenascension droite du noeud ascendant ;
- ω : argument of perigee ;
- i : inclination ;
- e : eccentricity ;
- ν : true anomaly ;
- M : mean anomaly ;
- E : eccentric anomaly ;
- $n = \sqrt{\frac{\mu}{a^3}}$: mean motion ;
- T^o : orbital period ;

Abbreviations

- CSM: Conjunction Summary Report.
- CAR: Conjunction Assessment Report.
- TLE: Two-Line Elements.
- TCA: Time of Closest Approach.

1 Introduction

The most general methods to accurately compute the global collision probability, without any additional assumption, are based on Monte-Carlo simulations, see e.g. [7, 33] in the context of a simple encounter or [37] in the context of a multiple encounter. These methods use a random sampling of N vectors in the space of initial conditions. For each of them, the corresponding trajectories are propagated according to the dynamical model adopted on the discretized time interval $[0, T]$. We count 1 if there is a collision, 0 otherwise. At the end, the collision probability is given by the formula: $\mathcal{P}_c([0,T]) = \frac{1}{N}\sum_{i=1}^{N} \delta_i$. The number of trials to be made depends on the requested precision as well as the value of the probability: a low value requires a lot of samples to be correctly estimated, and simulations can be dramatically time-consuming. This is one of the major disadvantages of Monte Carlo methods which makes them unsuitable for detecting low probability events in high dimension such as multiple events [37]. Therefore alternative approaches had to be explored to assess the risk of collision between two or more objects.

In the particular context of encounters between two objects, encounters are usually classified into two families: the short-term encounters [1, 21, 28, 35] and the long-term encounters [21, 33] for which many simplifying assumptions, enabling the computation of the collision probability can be made. In the context of short-term encounters, conjunctions are assumed to be short and rare. The relative velocity between the two objects is assumed to be very high (higher than the km/s) and the relative motion is assumed rectilinear on the time interval of the encounter. Finally, it is also assumed that the cross-correlations between the estimated states of the two objects are very small and therefore negligible. Such encounters typically occur in low orbits where the orbital velocities are high. Long-term encounters are characterized by relative velocities of the order of m/s, and correspond to situations where both objects spend significant time in proximity to each other. The motion equations of both objects are linearized around the reference orbit. This type of encounter is more common in the context of formation flying or proximity operations.

In the specific context of short-term encounters, several techniques for calculating the probability of collision have been developed. In historical order, the main methods are identified as those of Foster (1992) [35], Patera (2001) [61] and Alfano (2002) [2], based on numerical integration schemes and the method of Chan (1997) [20, 21] based on an analytic formula of the probability of collision in the form of a convergent series with positive terms. All these methods have already been the subject of several comparative studies [6, 21]. A new method for calculating the collision probability in short-term encounter and the instantaneous probability of collision under Gaussian uncertainty, has been developed during the PhD thesis of R. Serra [71] and published in [73, 74, 72]. The first gives a conservative estimate of the risk for a large part of actual encounters, those falling within the short-term encounter framework, while the second provides, in a more general context, an instantaneous information which then makes it possible to obtain lower bounds for the risk of collision over time intervals. This new method has the advantage of being based on an exact analytical formula, in the form of a convergent series with positive terms, and is the exact version of the approximate one by Chan [20, 21]. Numerical examples are given and demonstrate the efficiency of the proposed formulas compared to existing methods. In addition, analytical bounds are obtained for the probability of collision: they represent a significant tool for mission analysis since their efficient evaluation, allows in many real cases to rule on the importance of the risk.

In the general context of satellite flying formation or proximity operations, the hypothesis of short-term encounters can no longer be considered valid for the calculation of the overall risk of collision [37, 19]. The assumption of short-time spent in the encounter area is no longer verified when considering a cluster of satellites and, even in the case of only two space objects, the encounter could sometimes occur several times per orbit, for several consecutive orbits [37]. For such multiple

encounters, the cross-correlations between the estimated states are not negligible anymore, and assessing the risk separately for each individual encounter as if they were independent events, is not sufficient to characterize the real risk of such a conjunction.
The extension of the probability calculation in the case of long-term encounters, also called nonlinear framework, represents a first generalization attempt for specific cases of configurations [62, 58, 21, 33]. Unfortunately, these approaches are relatively limited because of their characterization for particular relative trajectories and are only imperfectly generalized to other cases [63]. In this last reference or more recently in [31], different metrics are proposed: distribution sampling, the Mahalanobis minimum distance and its upper bound on the collision probability, the Maximum Instantaneous probability and its lower bound on the collision probability, a hybrid probability combining the last two metrics for which the calculations can be shared or the symmetric Kullback-Leibler (KL) divergence. Roughly, the Mahalanobis distance or the symmetric KL divergence can be seen as a measure of similarity between two pdfs. The idea is to reduce the computational complexity of the distribution sampling approach by improving the determination of an interval over which two objects are in close proximity while accounting for the uncertainties of these objects. A similar approach based on computational tools of increasing complexity and precision (approximate ellipsoids for the probability density, probability density level curves, etc.) is also proposed in [18]. In [28], V. Coppola proposes a mathematical formalization and generalization of the short-term encounter formula: the two objects are modeled with uncertainty in both position and velocity, and their trajectories are not assumed to be rectilinear anymore. However, this formulation needs the assumption that the distribution of the uncertainty is Gaussian during the encounter interval to be fulfilled. The reference [32] proposes to generalize the Coppola's formulation by extending it to mixtures of Gaussian densities used for a more realistic representation of the uncertainty. More recently, the Coppola's formula has been also revisited and generalized to non-spherical objects [46]: instead of directly computing the collision probability, G. Krier first computes the collision probability per time unit, called the hazard function. The total probability of collision is the time integral of this hazard function, and this integration is performed numerically. This method has been successfully validated by comparing the obtained results with Monte Carlo simulations.
The objective of this report is to give first an exact and rigorous mathematical modeling of the problem of the computation of the probability of collision as derived by V. Coppola in the reference [28] using the measure theory. This theoretical framework enables to define the computation of the collision risk in a very general way encompassing the one used in [28]. This formalism clarifies the different assumptions and their mathematical implications at every step of the derivation. From the obtained so-called 3D integral of Coppola, additional simplifying assumptions are revisited step-by-step to obtain the classical 2D integral used for short-term encounters. Some criteria of validity of this last model, found in the literature, are then reviewed and analyzed. The numerical implementations from Coppola, CARA and CNES of the 3D integral are detailed as far as possible based on the available references. This section ends with the critical analysis of counter-examples to the 3D integral proposed by K. Chan. This analysis shows that these examples cannot be considered as threatening the validity of the derivations since they do not comply with one basic assumption used to derive the 3D integral.
If the Coppola's formulation appears to be theoretically strongly rooted and useful in cases satisfying the model used, it remains necessary to challenge this still restrictive modeling frame which is no more realistic for repeated conjunctions for instance. The fundamental assumption that there must be only one entering crossing in the forbidden region is indeed not respected in every case and an alternative method is proposed in this report. The method is based on two steps: (1) the higher-order implicit representation of the swept-volume (volume generated by the hard body during the encounter duration) by a polynomial superlevel sets. This is a method developed in the

framework of polynomial optimization, which has the advantage of providing approximate closed-form descriptions of the collision-prone states, which can then be effectively used for long-term and repeated conjunctions analysis. From a computational viewpoint, a hierarchy of linear matrix inequality problems is solved, which provides approximations that are convergent in volume to the original set. (2) Once such a polynomial representation is computed, a high-order quadrature scheme for volumes implicitly defined by a polynomial superlevel sets is employed. Numerical examples borrowed from the literature are then used to illustrate the pros and cons of the method.

2 Coppola's method for risk assessment for long-term spacecraft encounters

2.1 Encounter modeling and problem statement

Consider an operational spacecraft (called the primary) in orbit around the Earth and a space debris (called the secondary). The state of each orbiting object is described by their position and velocity in a reference frame $\hat{\mathcal{R}}$, and gathered in a global state vector X_{ps}:

$$X_{ps} = (r_p, v_p, r_s, v_s)^T \in \mathbb{R}^n,$$

where $n = 12$.
Let $[t_0, t_0 + T]$ be the time interval of the encounter. Consider now the dynamics of the 2 objects:

$$\left\{ \begin{array}{rcl} \dot{X}_{ps}(t) & = & f(t, X_{ps}(t)), \quad t \in [t_0, t_0 + T], \\ X_{ps}(t_0) & = & X^0_{ps}. \end{array} \right. \tag{1}$$

where f is a real vector field, which is supposed to be at least Lipschitz continuous, T is a given positive real number defining the time interval of the encounter and t_0 is the initial time (time at epoch for instance). The initial conditions $X^0_{ps} \in \mathbb{R}^n$ (e.g. position and velocity) are usually subject to uncertainties, and so, they are supposed to be distributed according to a given probability measure μ_I with its density function $\rho_I = \dfrac{d\mu_I}{d\lambda}$ (cf. the notation defined in Appendix B). These equations include the Newtonian gravitational central field and possible orbital perturbations (non spherical Earth, atmospheric drag, e.g.). Whatever model is adopted, it is assumed that, for given initial conditions, the solutions of the system (1) exist and are unique. For each fixed initial condition $X^0_{ps} \in \mathbb{R}^n$, a trajectory, or sample path, is then defined as follows:

Definition 1 (Trajectory/Sample path)**.**
Given an initial condition $X^0_{ps} \in \mathbb{R}^n$, a trajectory, or sample path, starting from X^0_{ps} is the unique solution of:

$$X_{ps}(t|X^0_{ps}) = X^0_{ps} + \int_{t_0}^{t} f(\tau, X_{ps}(\tau|X^0_{ps}))\mathrm{d}\tau. \tag{2}$$

Classically the objects are assumed to be spherical [1, 62, 4, 21, 28]: this assumption enables one to ignore the orientation of the objects, and to model conservatively the secondary object whose geometry is often poorly known (see Figure 1).

Assumption 1 (Spherical geometry)**.**
The objects involved in the conjunction have a spherical shape.

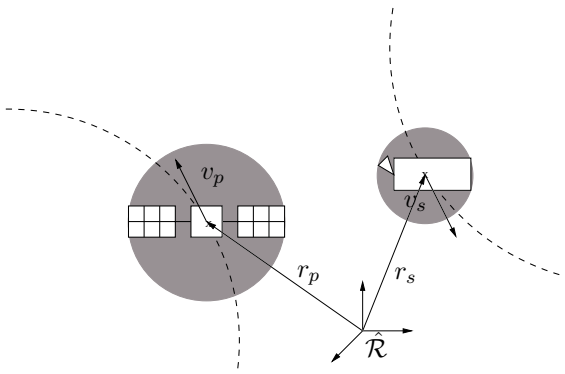

Figure 1: Encounter between two spherical objects.

Let us now define the notion of a collision. Suppose that for any initial condition $X_{ps}^0 \in \mathbb{R}^n$ the corresponding trajectory exists on the time interval $[t_0, t_0 + T]$, then roughly speaking, a collision occurs when a trajectory enters a certain *forbidden region* $\mathcal{X}_R$. For instance, in practice, this describes the fact that the relative distance between two objects is less than a certain given radius threshold $R > 0$.
If the state X_{ps} is given by the positions and velocities of 2 objects, then the *forbidden region* is expressed as

$$\mathcal{X}_R = \{X_{ps} = (r_p, v_p, r_s, v_s) \in \mathbb{R}^{12} \mid \|r_s - r_p\|^2 - R^2 < 0\}. \tag{3}$$

Note that, in case of two objects, the forbidden region (which depends on R) $\mathcal{X}_R$ is also called the combined spherical object and let its complement, so-called *safe/admissible region*, be ${}^c\mathcal{X}_R := \mathbb{R}^n \backslash \mathcal{X}_R$.

Definition 2 (Collision)**.**
Given an initial condition $X_{ps}^0 \in \mathbb{R}^n$, a maximum time of interest $T + t_0 > 0$, and a forbidden region $\mathcal{X}_R$, a collision occurs if there exists $t \in [t_0, t_0 + T]$ such that $X_{ps}(t|X_{ps}^0) \in \mathcal{X}_R$.

Definition 3 (Collision domain)**.**
The domain of collision $\mathcal{X}_T^0$ over the time interval $[t_0, t_0 + T]$ is the set of initial conditions leading to a collision between any pair of objects during $[t_0, t_0 + T]$, namely:

$$\mathcal{X}_T^0 = \{X_{ps}^0 \in \mathbb{R}^n \mid \exists t \in [t_0, t_0 + T],\ X_{ps}(t|X_{ps}^0) \in \mathcal{X}_R\}. \tag{4}$$

Remark 1. *In Equation (3) and Definition 3, the sets $\mathcal{X}_R$ and $\mathcal{X}_T^0$ have been defined based on the combined object state vector X_{ps}. Equivalent definitions could be given by using any combined state vector such as X_{rp} for instance, as it is the case in the rest of this report.*

Historically, the first criterion for collision risk assessment between two space objects was geometric: it relies on checking whether or not the nominal trajectory enters a *no-go* zone [9, 29] (including the forbidden region) whose size is either arbitrarily set or calculated with respect to uncertainties' standard deviations. A more natural formulation of the problem of collision risk assessment consists in *computing the probability that a collision occurs*:

Problem 1. *Let the dynamics in* (1)*, a maximum time of interest $t_0 + T > 0$ and a safe region ${}^c\mathcal{X}_R$. Provided that the initial conditions $X_{ps}^0 \in \mathbb{R}^n$ are distributed according to a given probability measure μ_I with its density function ρ_I, the probability that a collision occurs is computed simply by:*

$$\mathcal{P}_c([t_0, t_0 + T]) = \mathcal{P}_c(T, t_0) = \mathbb{P}(X_{ps}^0 \in \mathcal{X}_T^0) = \mu_I(\mathcal{X}_T^0) = \int_{\mathcal{X}_T^0} \mathrm{d}\mu_I. \tag{5}$$

The analytical calculation of the collision probability as defined in (5) is a very difficult problem: the first issue is to determine the domain of integration, which strongly depends on the chosen model for the dynamics when propagating the distribution of probability of the initial state. In addition, the integration of the density of probability on this set may be very complex, even for a Gaussian distribution [21].

2.2 Measures for the modelling of the collision probability

As in [28], we define the set $\mathcal{X}_T^{00}$ of initial states for which a collision occurs at $t = t_0$ and the set $\mathcal{X}_T^{0t_c} := \mathcal{X}_T^0 \backslash \mathcal{X}_T^{00}$ of the remaining initial states for which a collision occurs later. The collision

probability $\mathcal{P}_c := \mu_I(\mathcal{X}_T^0)$ is thus, $\mathcal{P}_c = \mu_I(\mathcal{X}_T^{00}) + \mu_I(\mathcal{X}_T^{0t_c})$. Often, in practice, the probability that a collision occurs at $t = 0$ is very small. However, the general computation of an *instantaneous* collision probability for a fixed $t = t_0$ (when the distribution of states at t_0 is Gaussian) is of interest and may be analyzed independently.
We now focus on computing $\mu_I(\mathcal{X}_T^{0t_c})$. More precisely, we are given the distribution (measure) of all initial states μ_I, the dynamics, as well as the forbidden region $\mathcal{X}_R$. The computation of $\mu_I(\mathcal{X}_T^{0t_c})$ amounts in *finding* (in some sense) an unknown initial measure μ_0 which can be seen as the restriction of μ_I to initial points leading to a collision on the time interval $(t_0, t_0 + T]$, denoted by $1_{\mathcal{X}_T^{0t_c}}\mu_I$. Assume that trajectories $X_{ps}(\cdot|X_{ps}^0)$ starting at $X_{ps}^0 \in {}^c\mathcal{X}_R$ are continuous functions and let $({}^c\mathcal{X}_R)^\circ$ be the interior of ${}^c\mathcal{X}_R$. Then, over the fixed period $[t_0, t_0 + T]$, these trajectories either are in $({}^c\mathcal{X}_R)^\circ$ or will touch its topological boundary $\partial\,{}^c\mathcal{X}_R := {}^c\mathcal{X}_R \backslash ({}^c\mathcal{X}_R)^\circ$ at a so-called first hitting time $\tau(X_{ps}^0) \in (t_0, t_0 + T]$,

$$\tau(X_{ps}^0) := \min\{t_0 + T, \inf(t \geqslant t_0 \text{ s.t. } X_{ps}(t|X_{ps}^0) \in \partial\,{}^c\mathcal{X}_R)\}.$$

Finally, one defines the final measure $\mu_F \in M([t_0, t_0 + T] \times \mathbb{R}^n)_+$ which captures the distribution of the first hitting times $\tau(X_{ps}^0)$ and the corresponding state $X_{ps}(t|X_{ps}^0)$ after it has been propagated by the dynamics starting at $t = t_0$ from the initial measure μ_0:

$$\mu_F\left(A \times B\right) := \int_{[t_0, t_0+T]\times\mathbb{R}^n} 1_{A\times B}(\tau(X_{ps}^0), X_{ps}(\tau(X_{ps}^0)|X_{ps}^0))\mathrm{d}\mu_0\left(X_{ps}^0\right), \tag{6}$$

for all Borel measurable sets $A \times B \subseteq (t_0, t_0 + T] \times \mathbb{R}^n$. The final measure μ_F is the pushforward measure $h_{\tau\star}\mu_0$ of μ_0, via the mapping:

$$\begin{array}{rccc} h_\tau : & \mathbb{R}^n & \to & [t_0, t_0 + T] \times \mathbb{R}^n, \\ & X_{ps}^0 & \mapsto & (\tau(X_{ps}^0), X_{ps}(\tau(X_{ps}^0)|X_{ps}^0)), \end{array} \tag{7}$$

that is:

$$\mu_F(A \times B) = \mu_0(h_\tau^{-1}(A \times B)), \tag{8}$$

for any Borel measurable sets $A \times B \subseteq (t_0, t_0 + T] \times \mathbb{R}^n$ (cf. Figure 2).

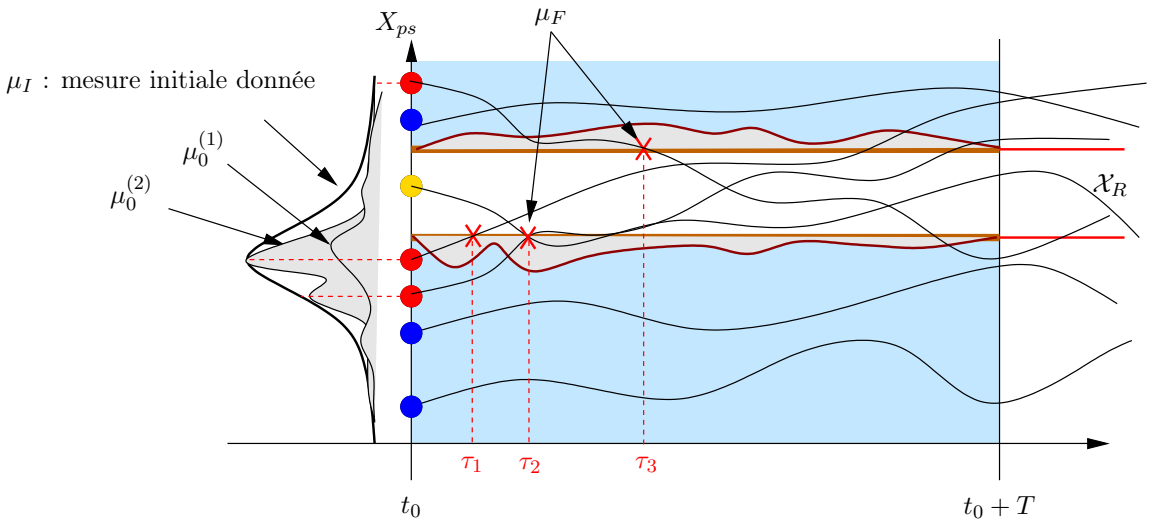

Figure 2: Yellow points: $X_{ps}^0 \in \mathcal{X}_T^{00}$, red points: $X_{ps}^0 \in \mathcal{X}_T^{0\tau_i}$, blue points: $X_{ps}^0 \in {}^c\mathcal{X}_T^0$.

2.3 Coppola's formula revisited via measure theory

The objective of this section is twofold: First to derive the formula for the computation of the probability of collision given in [28] and obtained in a general context. The method for computing the long-term probability of collision with velocity uncertainty and proposed by Coppola is also known as the *direct method* [32]. Our intention is to give a thorough and rigorous treatment to the solution proposed in [28] (the so-called 3D PoC method). The second objective is to review the literature dedicated to the 3D PoC, its limitations and possible alternatives.
We assume that the dynamical model under consideration (regardless of how the state vector X_{**} of the combined object is defined) $\dot{X}(t) = f(t, X(t))$ gives rise to an invertible flow $\varphi_{t_0}^t$, behaving as a C^1-diffeomorphism for $t \in [t_0, t_0 + T]$:

$$\begin{array}{rccc} \varphi_{t_0}^t & : & \mathbb{R}^{12} & \to & \mathbb{R}^{12} \\ & & X^0 & \mapsto & X(t|X^0), \end{array}$$

where $\varphi_{t_0}^t(\cdot)$ is the map $\varphi(t, t_0, \cdot)$ for a given $(t, t_0) \in \mathbb{R} \times \mathbb{R}$. Assuming that the function $\varphi(\cdot, \cdot, \cdot) : \mathbb{R} \times \mathbb{R} \times \mathbb{R}^{12} \to \mathbb{R}^{12}$ remains unchanged under time translation, we could set $t_0 = 0$ without loss of generality [38]. The two parameter family of mappings satisfies:

$$\frac{\partial}{\partial t}\varphi_{t_0}^t(X^0) = f(t, \varphi_{t_0}^t(X^0)).$$

Its inverse is given by:

$$\left(\varphi_{t_0}^t\right)^{-1} = \varphi_t^{t_0} : X(t|X^0) \mapsto X^0.$$

When manipulating density functions and the change of variable formula in the calculations below, we will also need the *local linearization of the flow* with respect to the initial conditions, denoted by $\mathrm{D}\varphi_{t_0}^t(X^0) \in \mathbb{R}^{12\times 12}$. Indeed, if $\tilde{X}^0$ is close to X^0, then:

$$\varphi_{t_0}^t(\tilde{X}^0) \approx \varphi_{t_0}^t(X^0) + \mathrm{D}\varphi_{t_0}^t(X^0)(\tilde{X}^0 - X^0).$$

Note that the local linearization of the inverse flow $\varphi_t^{t_0}$ satisfies the relation:

$$\mathrm{D}\varphi_t^{t_0}(\varphi_{t_0}^t(X^0)) = \left(\mathrm{D}\varphi_{t_0}^t(X^0)\right)^{-1},$$

since by differentiating with respect to X^0 the equation $\varphi_t^{t_0} \circ \varphi_{t_0}^t = \mathrm{Id}_{\mathbb{R}^{12}}$, we get $\mathrm{D}\varphi_t^{t_0}(\varphi_{t_0}^t(X^0)) \circ \mathrm{D}\varphi_{t_0}^t(X^0) = \mathrm{Id}_{\mathbb{R}^{12}}$.

Example 1.
Under the assumption that the flow is linear, $\dot{X}(t) = A(t)X(t)$, *the solution of the dynamics equation via the state transition matrix* $\Phi(t, t_0)$, *is such that*

$$X(t|X^0) = \varphi_0^t(X^0) = \Phi(t, t_0)X^0,$$

that is, the initial conditions are propagated from time 0 *to time* t *via the matrix* $\Phi(t, t_0)$. *One has also* $X^0 = \Phi(t, t_0)^{-1}X(t) = \Phi(t_0, t)X(t)$.

Also, suppose that there is a suitable surface parametrization of the whole or part of $\partial^c\mathcal{X}_R$ given by $P : S \to \mathbb{R}^n$, with $S \subseteq \mathbb{R}^{n-1}$ and with $P(s) = (p_1(s), \ldots, p_n(s)) \in \partial^c\mathcal{X}_R$.

Example 2.

(a) (Circle) The coordinates $(x, y) \in \mathbb{R}^2$ of a point on the circle of radius R are parameterized on the circle via the change of coordinates:

$$(x, y)^T := P(\theta) = (R\cos(\theta), R\sin(\theta))^T,$$

with $\theta \in S = [0, 2\pi]$.

(b) (Sphere) The coordinates $(x, y, z) \in \mathbb{R}^3$ of a point on the sphere of radius R are parameterized on the sphere via the change of coordinates:

$$(x, y, z)^T := P(\theta, \phi) = (R\cos(\theta)\sin(\phi), R\sin(\theta)\sin(\phi), R\cos(\phi))^T,$$

with $\theta \in [0, 2\pi), \phi \in [0, \pi]$ and $S = [0, 2\pi) \times [0, \pi]$.

(c) (Practical case in Coppola's article)
For $X_{rp} = (r_{r1}, r_{r2}, r_{r3}, v_{r1}, v_{r2}, v_{r3}, r_{p1}, r_{p2}, r_{p3}, v_{p1}, v_{p2}, v_{p3})^T \in \mathbb{R}^{12}$ the surface ${r_{r1}}^2 + {r_{r2}}^2 + {r_{r3}}^2 = R^2$, is parameterized on $\mathbb{R}^{11}$ via the change of coordinates:

$$X_{rp} = (r_{r1}, r_{r2}, r_{r3}, v_{r1}, v_{r2}, v_{r3}, r_{p1}, r_{p2}, r_{p3}, v_{p1}, v_{p2}, v_{p3})^T := P(\theta, \phi, v_{r1}, \ldots, v_{p3}), \quad (9)$$
$$= (R\cos(\theta)\sin(\phi), R\sin(\theta)\sin(\phi), R\cos(\phi), v_{r1}, v_{r2}, v_{r3}, r_{p1}, r_{p2}, r_{p3}, v_{p1}, v_{p2}, v_{p3})^T, \quad (10)$$

with $\theta \in [0, 2\pi), \ \phi \in [0, \pi]$ and $S = [0, 2\pi) \times [0, \pi] \times \mathbb{R}^9$. Note that this parametrization is based on spherical coordinates used in Mathematics and which convention is different (θ and ϕ are swapped) from the one preferentially used in Physics and in Geography as in [28] (radius R, longitude φ and latitude $\lambda = \frac{\pi}{2} - \theta$ (denoted θ in [28])).

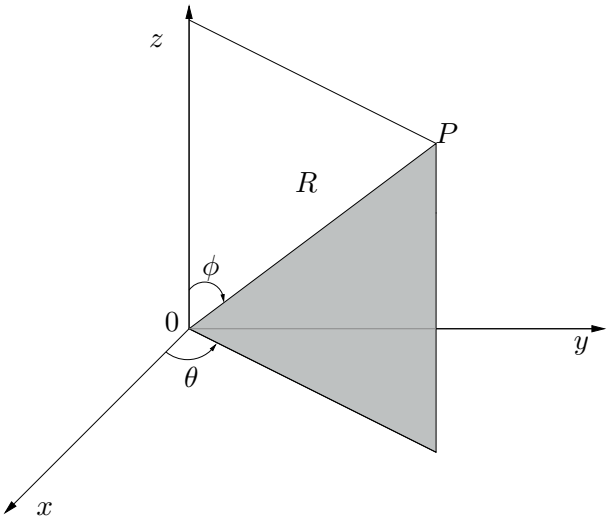

Figure 3: Spherical coordinates for the parametrization of a sphere.

The *a priori* unknown and possibly complicated shape of $\mathcal{X}_T^{0t_c}$ makes it difficult to get the probability of collision by directly computing an integral over this set. The principle of Coppola's formula is

to compute an equivalent integral over the set of collision states instead, via a change of variables given by the function $\psi : [t_0, t_0 + T] \times S \to \mathcal{X}_T^{0t_c}$, $\psi(t, s) = \varphi_t^{t_0}(P(s))$ (note that this definition is a partial composition only, since $\varphi_t^{t_0}$ depends on the first argument t of ψ). For this substitution to be licit, as stated by the following lemma, we need ψ to be 1-1 (more precisely, a C^1-diffeomorphism). The following assumption is sufficient for the bijectivity of ψ.

Assumption 2 (Only one entering crossing)**.**
For each trajectory leading to a collision, there is only one entering crossing in (or only one tangent to) the forbidden region $\mathcal{X}_R$ for all $t \in (t_0, t_0 + T]$. Therefore, the collision domain $\mathcal{X}_T^{0t_c}$ and the surface S are respectively defined by:

$$\mathcal{X}_T^{0t_c} = \left\{ X^0 \in \mathbb{R}^n \mid \exists! t \in (t_0, t_0 + T],\ X(t|X^0) \in \mathcal{X}_R \text{ and } v_r(t)^T r_r(t) \leqslant 0 \right\}, \tag{11}$$

and

$$S = \left\{ (\theta, \phi, v_r, r_p, v_p) \in [0, 2\pi) \times [0, \pi] \times \mathbb{R}^9 :\ v_{r1} \cos(\theta) \sin(\phi) + v_{r2} \sin(\theta) \sin(\phi) + v_{r3} \cos(\phi) \leqslant 0 \right\}. \tag{12}$$

In order to compute the part of the collision probability $\mathcal{P}_c$ given by $\mu_I(\mathcal{X}_T^{0t_c}) := \mu_0(\mathbb{R}^n)$, the next derivations rely on the following lemma:

Lemma 1.

(i) $\mu_F = ((\mathrm{Id}_{\mathbb{R}} \times P) \circ \psi^{-1})_\star \mu_0$*;*

(ii)

$$\int_{\mathbb{R}^n} \mathrm{d}\mu_0 = \int_{\mathcal{X}_T^{0t_c}} \rho_I(X^0) \mathrm{d}\lambda(X^0) = \int_{[t_0, t_0+T] \times S} (\rho_I \circ \psi)(t, s) \left| \det(J(\psi)(t, s)) \right| \mathrm{d}\lambda(t, s), \tag{13}$$

where $J(\psi)$ is the Jacobian matrix of the mapping ψ.

Proof.

(i) One notices that since ψ is 1-1, each point which achieves a collision, $X^0 \in \mathcal{X}_T^{0t_c} \subset \mathbb{R}^n$ is transported via $(\mathrm{Id}_{\mathbb{R}} \times P) \circ \psi^{-1}$ on the surface $\partial^c \mathcal{X}_R$ at a certain time $\tau(X^0) \in (t_0, t_0 + T]$ and reciprocally since:

$$\begin{array}{ccccc} \mathcal{X}_T^{0t_c} \subset \mathbb{R}^n & \xrightarrow{\psi^{-1}} & [t_0, t_0 + T] \times S & \xrightarrow{\mathrm{Id}_{\mathbb{R}} \times P} & [t_0, t_0 + T] \times \mathbb{R}^n, \\ X^0 & \longmapsto & (\tau(X^0), s(X^0)) & \longmapsto & (\tau(X^0), X(\tau(X^0)|X^0)). \end{array}$$

Therefore, we have that $h_\tau = ((\mathrm{Id}_{\mathbb{R}} \times P) \circ \psi^{-1})$ and by Theorem 5 in Appendix C,

$$\int_{[t_0, t_0+T] \times \mathbb{R}^n} 1_{A \times B}(t, X) \mathrm{d}\mu_F = \int_{\mathbb{R}^n} 1_{A \times B} \circ (\mathrm{Id}_{\mathbb{R}} \times P) \circ \psi^{-1}(X^0) \mathrm{d}\mu_0.$$

(ii) One uses the Jacobi's change of variables formula [69, Chapter 15], since ψ is a C^1-diffeomorphism. Note that this formula is obtained by applying (127) with $X = [t_0, t_0 + T] \times S$, $Y = \mathcal{X}_T^{0t}$,

$g(\psi) = \rho_I(\psi)\,|\det(J(\psi))|$, $\mu = \lambda$ and noting that $\mathrm{d}(\psi_\star\mu) = \mathrm{d}(\psi_\star\lambda) = \left|\det(J(\psi^{-1}))\right|\mathrm{d}\lambda$ [69, Remark 15.10]. Indeed,

$$\int_{[t_0,t_0+T]\times S}(\rho_I\circ\psi)(t,s)\,|\det(J(\psi)(t,s))|\,\mathrm{d}\lambda(t,s) = \int_{\mathcal{X}_T^{0t}}\rho_I(X^0)\left|\det(J(\psi)(\psi^{-1}(X^0)))\right|\mathrm{d}\psi_\star\lambda(X^0) =$$
$$\int_{\mathcal{X}_T^{0t}}\rho_I(X^0)\left|\det(J(\psi)(\psi^{-1}(X^0)))\right|\left|\det(J(\psi^{-1})(X^0))\right|\mathrm{d}\lambda(X^0) =$$
$$\int_{\mathcal{X}_T^{0t}}\rho_I(X^0)\left|\det(J(\psi)(\psi^{-1}(X^0)))\right|\left|\det(J(\psi)(\psi^{-1}(X^0)))\right|^{-1}\mathrm{d}\lambda(X^0) =$$
$$\int_{\mathcal{X}_T^{0t}}\rho_I(X^0)\mathrm{d}\lambda(X^0) = \int_{\mathcal{X}_T^{0t}}\mathrm{d}\mu(X^0).$$

Note that $J(\psi)(\psi^{-1}(X^0))J(\psi^{-1})(X^0) = I_n$. □

Example 3.

If the flow is linear, the function ψ is now defined as $\psi : [t_0, t_0+T]\times S \to \mathcal{X}_T^{0t_c}$, $\psi(t,s) = \Phi(t,t_0)^{-1}P(s)$.

Remark 2.
Assumption 2 is equivalent to the Assumptions (A1) and (A2) proposed in Coppola's article and reminded below.

(A1) Only one crossing.

(A2) Trajectories must cross.

For computing the Jacobian of ψ, one has:

$$\frac{\partial\psi}{\partial t}(t,s) = -\mathrm{D}\varphi_t^{t_0}(P(s))f(t,P(s)) \in \mathbb{R}^{12}.$$

This indeed follows from differentiating with respect to t the equality $P(s) = \varphi_{t_0}^t(\psi(t,s))$ by applying the chain rule:

$$\begin{aligned}
0 &= \frac{\partial}{\partial t}\left(\varphi_{t_0}^t(\psi(t,s))\right)\\
&= \frac{\partial\varphi_{t_0}^t}{\partial t}(\psi(t,s)) + \mathrm{D}\varphi_{t_0}^t(\psi(t,s))\frac{\partial\psi}{\partial t}(t,s)\\
&= f(t,\varphi_{t_0}^t(\psi(t,s))) + \mathrm{D}\varphi_{t_0}^t(\psi(t,s))\frac{\partial\psi}{\partial t}(t,s)\\
&= f(t,P(s)) + \left(\mathrm{D}\varphi_t^{t_0}(P(s))\right)^{-1}\frac{\partial\psi}{\partial t}(t,s).
\end{aligned}$$

In addition, we have that:

$$\frac{\partial\psi}{\partial s}(t,s) = \mathrm{D}\varphi_t^{t_0}(P(s))\frac{\partial P(s)}{\partial s} \in \mathbb{R}^{12\times 11}.$$

Hence

$$J(\psi)(t,s) = \mathrm{D}\varphi_t^{t_0}(P(s))\left[-f(t,P(s)) \;\middle|\; \frac{\partial P(s)}{\partial s}\right] \in \mathbb{R}^{12\times 12}. \tag{14}$$

Example 4.
In the case of linear dynamics, the computations above become

$$\frac{\partial \psi}{\partial t} = -\Phi^{-1}(t,t_0)\frac{\partial \Phi(t,t_0)}{\partial t}\Phi^{-1}(t,t_0)P(s) = -\Phi^{-1}(t,t_0)A(t)P(s),$$

since $\frac{\partial \Phi(t,t_0)}{\partial t} = A(t)\Phi(t,t_0)$. *Moreover, we have*

$$\frac{\partial \psi}{\partial s} = \Phi(t,t_0)^{-1}\frac{\partial P(s)}{\partial s},$$

and (14) *becomes*

$$J(\psi) = \Phi^{-1}(t,t_0)\left(-A(t)P(s) \;\middle|\; \frac{\partial P(s)}{\partial s}\right).$$

Practical computations for the Jacobian matrix in Coppola's case (Example 2(c)), are as follows:

$$\frac{\partial P(s)}{\partial s} = \left(\begin{array}{ccc|c} -R\sin(\theta)\sin(\phi) & R\cos(\theta)\cos(\phi) & & \\ R\cos(\theta)\sin(\phi) & R\sin(\theta)\cos(\phi) & & 0_{3,9} \\ 0 & -R\sin(\phi) & & \\ \hline & 0_{9,2} & & I_9 \end{array}\right).$$

Due to 0 blocks in the above matrix, to compute the determinant of $J(\psi)$, one only needs the first three coordinates of the $f(t,P(s))$ vector, and since $f(t,\cdot)$ is the dynamics, one has

$$f(t,P(s)) = (v_{r1}, v_{r2}, v_{r3}, \dot{v}_{r1}, \dot{v}_{r2}, \dot{v}_{r3}, v_{p1}, v_{p2}, \dot{v}_{p3}, \dot{v}_{p1}, \dot{v}_{p2}, \dot{v}_{p3})^T \in \mathbb{R}^{12}.$$

This gives:

$$\det(J(\psi)(t,s)) = \begin{vmatrix} -v_{r1} & -R\sin(\theta)\sin(\phi) & R\cos(\theta)\cos(\phi) \\ -v_{r2} & R\cos(\theta)\sin(\phi) & R\sin(\theta)\cos(\phi) \\ -v_{r3} & 0 & -R\sin(\phi) \end{vmatrix} \det\left(\mathrm{D}\varphi_t^{t_0}(P(s))\right),$$

which amounts to:

$$\begin{aligned} \det(J(\psi)) &= R^2\sin(\phi)\left(\cos(\theta)\sin(\phi)\,v_{r1} + \sin(\phi)\sin(\theta)\,v_{r2} + \cos(\phi)\,v_{r3}\right)\det\left(\mathrm{D}\varphi_t^{t_0}(P(s))\right) \\ &= R^2\sin(\phi)\,v_r\cdot\hat{n}\det\left(\mathrm{D}\varphi_t^{t_0}(P(s))\right), \end{aligned} \tag{15}$$

where $\hat{n} = [\cos(\theta)\sin(\phi) \;\; \sin(\phi)\sin(\theta) \;\; \cos(\phi)]^T$ is the unit vector normal to the sphere.

Example 5.
For linear dynamics, one may easily deduce that

$$\det(J(\psi)) = \begin{vmatrix} -v_{r1} & -R\sin(\theta)\sin(\phi) & R\cos(\theta)\cos(\phi) \\ -v_{r2} & R\cos(\theta)\sin(\phi) & R\sin(\theta)\cos(\phi) \\ -v_{r3} & 0 & -R\sin(\phi) \end{vmatrix} \det(\Phi^{-1}(t,t_0)),$$

and finally

$$\begin{aligned}\det(J(\psi)) &= R^2\sin(\phi)\left(\cos(\theta)\sin(\phi)\,v_{r1}+\sin(\phi)\sin(\theta)\,v_{r2}+\cos(\phi)\,v_{r3}\right)\det(\Phi^{-1}(t,t_0))\\ &= R^2\sin(\phi)\,v_r\cdot\hat{n}\det(\Phi^{-1}(t,t_0)).\end{aligned} \tag{16}$$

Now, since ψ is $1-1$, one can apply Equation (13) and get:

$$\int_{\mathbb{R}^n}\mathrm{d}\mu_0=\int_{t_0}^{t_0+T}\int_0^{2\pi}\int_0^{\pi}\int_{-\infty}^{\infty}\int_{-\infty}^{\infty}\int_{-\infty}^{\infty}\rho_I(\psi(t,\theta,\phi,v_r,r_p,v_p))\left|\det\left(\mathrm{D}\varphi_t^{t_0}(P(t,\theta,\phi,v_r,r_p,v_p))\right)\right| 1_{v_r\cdot\hat{n}\leqslant 0}(v_r)\left|R^2\sin(\phi)\,v_r\cdot\hat{n}\right|\mathrm{d}v_p\mathrm{d}r_p\mathrm{d}v_r\mathrm{d}\phi\mathrm{d}\theta\mathrm{d}t \tag{17}$$

Example 6.
For linear dynamics, we have

$$\int_{\mathbb{R}^n}\mathrm{d}\mu_0=\int_{t=t_0}^{t_0+T}\int_0^{2\pi}\int_0^{\pi}\int_{-\infty}^{\infty}\int_{-\infty}^{\infty}\int_{-\infty}^{\infty}\rho_I(\psi(t,\theta,\phi,v_r,r_p,v_p))\left|\det(\Phi^{-1}(t,t_0))\right| 1_{v_r\cdot\hat{n}\leqslant 0}(v_r)\left|R^2\sin(\phi)\,v_r\cdot\hat{n}\right|\mathrm{d}v_p\mathrm{d}r_p\mathrm{d}v_r\mathrm{d}\phi\mathrm{d}\theta\mathrm{d}t \tag{18}$$

Lemma 2.
Let a given random vector X with probability density ρ_X and another random vector Y related to X by the equation $y=g(x)$, and g bijective. The probability density ρ_Y for Y is:

$$\rho_Y(y)=\rho_X(g^{-1}(y))\ \left|\det(J(g^{-1})(y))\right|. \tag{19}$$

Proof. Let $\mathbb{P}(Y\in S)$ be the probability that Y takes a value in some particular subset S, so that we get:

$$\mathbb{P}(Y\in S)=\int_S\rho_Y(y)\,\mathrm{d}y.$$

Since Y takes a value in S whenever X takes a value in $g^{-1}(S)$, one has:

$$\mathbb{P}(Y\in S)=\int_{g^{-1}(S)}\rho_X(x)\,\mathrm{d}x.$$

Now, changing from variable x to y gives:

$$\mathbb{P}(Y\in S)=\int_{g^{-1}(S)}\rho_X(x)\ \mathrm{d}x=\int_S\rho_X(g^{-1}(y))\ \left|\det(J(g^{-1})(y))\right|\ \mathrm{d}y.$$

□

In our case, let g be the flow $\varphi_{t_0}^t$, and ρ_I be the probability density of the initial random state X^0, one obtains the probability density $\rho_t(X)$ of the random state X at a given fixed time t from Equation (19):

$$\rho_t(X)=\rho_I(\varphi_t^{t_0}(X))\ \left|\det\left(\mathrm{D}\varphi_t^{t_0}(X)\right)\right|. \tag{20}$$

Example 7.
In the linear case, the flow is given by $X^0 \mapsto \Phi(t, t_0)X^0$ *and then, we have that the probability density* $\rho_t(X)$ *of the random state* X *at a given fixed time* t *is given by*

$$\rho_t(X) = \rho_I(\Phi^{-1}(t, t_0)X) \ \left|\det(\Phi^{-1}(t, t_0))\right|. \tag{21}$$

From Equations (20) and (17), one has:

$$\mathcal{P}_I(T) = \int_{\mathbb{R}^n} \mathrm{d}\mu_0 = \int_{t=t_0}^{t_0+T} \int_{\theta=0}^{2\pi} \int_{\phi=0}^{\pi} \int_{v_r=-\infty}^{\infty} \int_{r_p=-\infty}^{\infty} \int_{v_p=-\infty}^{\infty} \rho_t(P(\theta, \phi, v_r, r_p, v_p)) 1_{v_r \cdot \hat{n} \leqslant 0}(v_r) \left|R^2 \sin(\phi)\, v_r \cdot \hat{n}\right| \mathrm{d}v_p \mathrm{d}r_p \mathrm{d}v_r \mathrm{d}\phi \mathrm{d}\theta \mathrm{d}t. \tag{22}$$

Remark 3.
Equation (22) *is similar to formula (15) in Coppola's article, with two differences. Firstly, the parametrization in spherical coordinates is different, but this does not affect the result in any way. Secondly, there is a slight abuse of notation in formula (15) of Coppola's article, concerning the probability density function* $\rho_t(X)$ *which appears instead of ours* $\rho_t(P(s))$*. More precisely, this means that* ρ_t *is the probability density of the state random variable* X *at each fixed time* t*, but this function should be applied to* $P(s)$ *(after the reparametrization).*
There is also a slight abuse of notations in this document regarding the definition of a probability density function $\rho_t(P(s))$ *as shown in Lemma 2 since the random vector and the variable of the density function coincide.*

We move on to the next assumption made in [28]:

Assumption 3. *Independence of the two random vectors* x_p *and* x_s*.*
The dynamic model and probability distribution function for one object are independent from the dynamic model and probability distribution function of the other object.

Keeping in mind the slight abuse of notations mentioned in Remark 3 and if $\rho_{tps}(x_p, x_s)$, $\rho_{tp}(x_p)$, $\rho_{ts}(x_s)$ denote respectively the joint density functions of the random vectors $X^T = \begin{bmatrix} x_p^T & x_s^T \end{bmatrix}$, x_p and x_s then Assumption 3 means that:

$$\rho_{tps}(x_p, x_s) = \rho_{tp}(x_p)\rho_{ts}(x_s). \tag{23}$$

This implies that the density $\rho_t(P(s)) = \rho_t(x_r(\theta, \phi, v_r), x_p)$ satisfies:

$$\rho_t(x_r, x_p) = \rho_{tps}(x_p, x_s) = \rho_{tp}(x_p)\rho_{ts}(x_p + x_r), \tag{24}$$

where $x_r = x_s - x_p$ is the relative state on the sphere of radius R. This may be proved by noting that $X_{rp} = \begin{bmatrix} x_r \\ x_p \end{bmatrix} = \begin{bmatrix} -I_6 & I_6 \\ I_6 & 0_{6,6} \end{bmatrix} \begin{bmatrix} x_p \\ x_s \end{bmatrix}$ and by applying Lemma 2. Therefore, Equation (17) becomes:

$$\mathcal{P}_I(T) = \int_{t_0}^{t_0+T} \int_0^{2\pi} \int_0^{\pi} |\sin(\phi)| \int_{-\infty}^{\infty} R^2 \left|v_r \cdot \hat{n}\right| 1_{v_r \cdot \hat{n} \leqslant 0}(v_r) \int_{-\infty}^{\infty} \int_{-\infty}^{\infty} \rho_{tp}(x_p)\rho_{ts}(x_p + x_r) \mathrm{d}v_p \mathrm{d}r_p \mathrm{d}v_r \mathrm{d}\phi \mathrm{d}\theta \mathrm{d}t. \tag{25}$$

The next assumption from [28] is related to the Gaussian nature of the two density functions of the random vectors x_p and x_s.

Assumption 4. *Gaussian distributions.*
The probability distribution functions $\rho_{tp} \sim \mathcal{N}(m_p(t), P_p(t))$ *and* $\rho_{ts} \sim \mathcal{N}(m_s(t), P_s(t))$ *remain Gaussian at each time* t*.*

It may be deduced that $x_r = x_s - x_p \sim \mathcal{N}(m_s(t) - m_p(t), \underbrace{P_p(t) + P_s(t)}_{P_r(t)})$.

Let us define the following matrices:

$$G^{-1} = P_p^{-1} + P_s^{-1}, \quad T = GP_s^{-1}, \tag{26}$$

where G is a symmetric positive semidefinite matrix. Let us define the random vector $w = x_p + Tx_r$. Keeping in mind that:

$$\begin{aligned} \rho_{tp}(x_p) &= \frac{1}{\sqrt{(2\pi)^6}\sqrt{\det(P_p)}} e^{-\frac{1}{2}(x_p - m_p)^T P_p^{-1}(x_p - m_p)}, \\ \rho_{ts}(x_s) &= \frac{1}{\sqrt{(2\pi)^6}\sqrt{\det(P_s)}} e^{-\frac{1}{2}(x_s - m_s)^T P_s^{-1}(x_s - m_s)}, \end{aligned} \tag{27}$$

then

$$\rho_t(x_r, x_p) = \rho_{tp}(x_p)\rho_{ts}(x_p + x_r) = \rho_t(w, x_r) = \rho_{tw}(w)\rho_{tr}(x_r), \tag{28}$$

is obtained after tedious algebraic manipulations for which the following identities are used:

$$\begin{aligned} TP_sT^T + (I_6 - T)P_p(I_6 - T)^T &= GT^T + G(I_6 - T)^T = G, \\ \det(P_p)\det(P_s) &= \det(P_pP_s) = \det(GP) = \det(G)\det(P), \end{aligned} \tag{29}$$

and:

$$\begin{aligned} &\rho_{tw} \sim \mathcal{N}(m_p(t) + T\underbrace{(m_s(t) - m_p(t))}_{m_r(t)}, G(t)), \\ &\rho_{tr} \sim \mathcal{N}(m_r(t), P_r(t)). \end{aligned} \tag{30}$$

Equation (28) shows that the random vectors $w = x_p + Tx_r$ and x_r are independent. Therefore, we get that:

$$\begin{aligned} \mathcal{P}_I(T) &= \int_{t_0}^{t_0+T}\int_0^{2\pi}\int_0^{\pi} |\sin(\phi)| \int_{-\infty}^{\infty} R^2 |v_r \cdot \hat{n}| \, 1_{v_r \cdot \hat{n} \leqslant 0}(v_r)\rho_{tr}(x_r) \underbrace{\int_{-\infty}^{\infty} \rho_{tw}(w)\mathrm{d}w}_{=1} \mathrm{d}v_r\mathrm{d}\phi\mathrm{d}\theta\mathrm{d}t \\ &= \int_{t_0}^{t_0+T}\int_0^{2\pi}\int_0^{\pi} |\sin(\phi)| \int_{-\infty}^{\infty} R^2 |v_r \cdot \hat{n}| \, 1_{v_r \cdot \hat{n} \leqslant 0}(v_r)\rho_{tr}(x_r(\theta, \phi, v_r))\mathrm{d}v_r\mathrm{d}\phi\mathrm{d}\theta\mathrm{d}t. \end{aligned} \tag{31}$$

The next step consists in partitioning the mean vector $m_r(t) = \begin{bmatrix} m_{r_r}(t) \\ m_{v_r}(t) \end{bmatrix}$ and the covariance matrix $P_r(t)$ as $P_r(t) = \begin{bmatrix} P_{11}(t) & P_{12}(t) \\ P_{12}^T(t) & P_{22}(t) \end{bmatrix}$ leading to:

$$\begin{aligned} P_r^{-1}(t) &= \begin{bmatrix} P_{11}^{-1}(t) + P_{11}^{-1}(t)P_{12}(t)\Delta^{-1}(t)P_{12}^T(t)P_{11}^{-1}(t) & -P_{11}^{-1}(t)P_{12}(t)\Delta^{-1}(t) \\ -\Delta^{-1}(t)P_{12}^T(t)P_{11}^{-1}(t) & \Delta^{-1}(t) \end{bmatrix}, \\ \Delta(t) &= P_{22}(t) - P_{12}^T(t)P_{11}^{-1}(t)P_{12}(t). \end{aligned}$$

Consequently, we get that:

$$\begin{aligned}
-\frac{1}{2}(x_r-m_r)^T P_r^{-1}(x_r-m_r) &= -\frac{1}{2}(r_r-m_{r_r})^T P_{11}^{-1}(r_r-m_{r_r})\cdots \\
&\quad -\frac{1}{2}(\cdot)^T\Delta^{-1}\underbrace{(\overbrace{v_r-P_{12}^TP_{11}^{-1}r_r}^{v'}-\overbrace{(m_{v_r}-P_{12}^TP_{11}^{-1}m_{r_r})}^{m'_v})}_{v'-m'_v}, \\
&= -\frac{1}{2}(r_r-m_{r_r})^T P_{11}^{-1}(r_r-m_{r_r})-\frac{1}{2}(v'-m'_v)^T\Delta^{-1}(v'-m'_v),
\end{aligned}$$

and $\rho_{tr}(x_r)=\rho_{tr}(r_r)\rho_{tv'}(v')$ with:

$$\begin{aligned}
&\rho_{tr}\sim\mathcal{N}(m_{r_r}(t),P_{11}(t)), \\
&\rho_{tv'}\sim\mathcal{N}(m'_v(t),\Delta(t)).
\end{aligned} \tag{32}$$

Moreover, $|v_r\cdot\hat{n}|=\left|v'(t)\cdot\hat{n}+R\hat{n}^TP_{11}^{-1}(t)P_{12}(t)\hat{n}\right|=\left|v'(t)\cdot\hat{n}+R\hat{n}^TP_{12}^T(t)P_{11}^{-1}(t)\hat{n}\right|=|v'(t)\cdot\hat{n}+\epsilon_0(\hat{n},t)|$, where $\epsilon_0(\hat{n},t)=R\hat{n}^TP_{12}^T(t)P_{11}^{-1}(t)\hat{n}$ and we get:

$$\begin{aligned}
\mathcal{P}_I(T) &= \int_{t_0}^{t_0+T}\int_0^{2\pi}\int_0^{\pi}R^2\left|\sin(\phi)\right|\rho_{tr}(r_r)\cdot \\
&\quad \underbrace{\int_{-\infty}^{\infty}\left|v'(t)\cdot\hat{n}+\epsilon_0(\hat{n},t)\right|1_{v'(t)\cdot\hat{n}+\epsilon_0(\hat{n},t)\leqslant 0}(v')\rho_{tv'}(v')\mathrm{d}v'}_{I(\hat{n},t)}\,\mathrm{d}\phi\mathrm{d}\theta\mathrm{d}t.
\end{aligned} \tag{33}$$

The unit vector normal to the sphere $\hat{n}$ is defined by $\hat{n}=[\cos(\theta)\sin(\phi)\ \ \sin(\phi)\sin(\theta)\ \ \cos(\phi)]^T$ and the orthogonal matrix $\overline{T}$ defined by:

$$\overline{T}=\begin{bmatrix}\cos(\theta)\sin(\phi) & \sin(\phi)\sin(\theta) & \cos(\phi)\\ -\sin(\theta) & \cos(\theta) & 0\\ -\cos(\theta)\cos(\phi) & -\sin(\theta)\cos(\phi) & \sin(\phi)\end{bmatrix}, \tag{34}$$

is such that $\vec{i}=\begin{bmatrix}1 & 0 & 0\end{bmatrix}^T=\overline{T}\hat{n}$. With the notations:

$$\begin{aligned}
v''(t) &= \overline{T}v'(t)=\begin{bmatrix}\epsilon(t)\\ \zeta(t)\end{bmatrix}, \\
m''_v(t) &= \overline{T}m'_v(t)=\begin{bmatrix}m_\epsilon(t)\\ m_\zeta(t)\end{bmatrix}, \\
\overline{\Delta}(\theta,\phi,t) &= \overline{T}\Delta(t)\overline{T}^T=\begin{bmatrix}\sigma^2(\theta,\phi,t) & \overline{\Delta}_{12}(t)\\ \overline{\Delta}_{12}^T(t) & \overline{\Delta}_{22}(t)\end{bmatrix}, \\
\sigma^2(\theta,\phi,t) &= \hat{n}^T(P_{22}(t)-P_{12}^T(t)P_{11}(t)^{-1}P_{12}(t))\hat{n},
\end{aligned} \tag{35}$$

we have that $\rho_{tv'}(v')=\rho_{tv''}(v'')$ with $v''\sim\mathcal{N}(m''_v(t),\overline{\Delta}(t))$ and simple algebraic computations lead to $\rho_{tv''}(v'')=\rho_{t\epsilon}(\epsilon)\rho_{t\overline{\zeta}}(\overline{\zeta})$ with:

$$\begin{aligned}
\epsilon &\sim \mathcal{N}(m_\epsilon,\sigma^2), \\
\overline{\zeta} &= \zeta-\frac{\epsilon\overline{\Delta}_{12}^T}{\sigma^2}\sim\mathcal{N}\left(m_\zeta-\frac{m_\epsilon\overline{\Delta}_{12}^T}{\sigma^2},\overline{\Delta}_{22}-\frac{\overline{\Delta}_{12}^T\overline{\Delta}_{12}}{\sigma^2}\right).
\end{aligned}$$

Note that $m_\epsilon(\theta,\phi,t) = \hat{n}^T(m_{v_r} - P_{12}^T(t)P_{11}^{-1}(t)m_{r_r}) = \vec{i}^{\,T} m_v''(t)$. Therefore,

$$\begin{aligned} I(\hat{n},t) &= \int_{-\infty}^{\infty} \left|v'(t)\cdot\hat{n} + \epsilon_0(\hat{n},t)\right| 1_{v'(t)\cdot\hat{n}+\epsilon_0(\hat{n},t)\leqslant 0}(v')\rho_{tv'}(v')\mathrm{d}v', \\ &= \int_{-\infty}^{\infty} \left|\epsilon(t) + \epsilon_0(\hat{n},t)\right| 1_{\epsilon+\epsilon_0(\hat{n},t)\leqslant 0}(\epsilon)\rho_{tv''}(v'')\mathrm{d}\overline{\zeta}\mathrm{d}\epsilon, \\ &= \int_{-\infty}^{\infty} \left|\epsilon(t) + \epsilon_0(\hat{n},t)\right| 1_{\epsilon+\epsilon_0(\hat{n},t)\leqslant 0}(\epsilon)\rho_{t\epsilon}(\epsilon) \underbrace{\int_{-\infty}^{\infty} \rho_{t\overline{\zeta}}(\overline{\zeta})\mathrm{d}\overline{\zeta}}_{1}\,\mathrm{d}\epsilon, \\ &= -\frac{1}{\sqrt{2\pi}\,\sigma}\int_{-\infty}^{-\epsilon_0(\hat{n},t)} \left(\epsilon(t) + \epsilon_0(\hat{n},t)\right) e^{-\dfrac{(\epsilon - m_\epsilon)^2}{2\sigma^2}}\,\mathrm{d}\epsilon, \end{aligned} \tag{36}$$

since $v'(t)\cdot\hat{n} = v''(t)\cdot\overline{T}\hat{n} = v''(t)\cdot\vec{i}$. Finally, remembering that the error function is given by:

$$\begin{aligned} \mathrm{erf}: \mathbb{R} &\to \mathbb{R} \\ x &\mapsto \mathrm{erf}(x) = \frac{1}{\sqrt{\pi}}\int_0^x e^{-t^2}\mathrm{d}t, \end{aligned} \tag{37}$$

the integral $I(\hat{n},t)$ may be readily computed as:

$$I(\hat{n},t) = \frac{\sigma}{\sqrt{2\pi}} e^{-\dfrac{(\epsilon_0(\hat{n},t)+m_\epsilon)^2}{2\sigma^2}} - \frac{(m_\epsilon + \epsilon_0(\hat{n},t))}{2}\left[1 - \mathrm{erf}\left(\frac{m_\epsilon + \epsilon_0(\hat{n},t)}{\sqrt{2}\,\sigma}\right)\right], \tag{38}$$

and the probability $\mathcal{P}_I(T)$ is finally obtained as:

$$\mathcal{P}_I(T) = \int_{t_0}^{t_0+T}\int_0^{2\pi}\int_0^{\pi} R^2 \left|\sin(\phi)\right| \rho_{tr}(r_r(\theta,\phi)) I(\hat{n},t)\mathrm{d}\phi\mathrm{d}\theta\mathrm{d}t. \tag{39}$$

2.4 Derivation of the classic short-term encounter formula

2.4.1 The 2D integral

The first subsequent assumption made to obtain the classic short-term encounter formula is the following:

Assumption 5. *No velocity uncertainty.*
At each time $t \in [t_0, t_0+T]$, the relative velocity vector $v_r(t)$ is precisely known and is a deterministic vector.

This assumption is clearly mathematically unrealistic since, even if the relative position vector at $t = t_0$, $r_r(t_0)$ is a random vector and the relative velocity vector at $t = t_0$ is a deterministic vector $v_r(t_0)$, the relative velocity vector at any time $t > t_0$ will be a random vector $v_r(t)$ due to the interconnections in the relative dynamics between r_r and v_r (unless the flow $\varphi_{t_0}^t$ has a particular structure). Nevertheless, one can expect that this propagated uncertainty affecting the relative velocity vector will be small enough to be considered as not significant.
Assumption 5 first implies that the matrix $P_{12} = 0$. This implies that $\epsilon_0(\hat{n}, t) = 0$ and therefore that $v_r = v'$ and $m_\epsilon = \hat{n} \cdot m_{v_r} = \hat{n} \cdot v_r$. From Equation (38), we get that:

$$I(\hat{n}, t) = \frac{\sigma}{\sqrt{2\pi}} e^{-\frac{m_\epsilon^2}{2\sigma^2}} - \frac{m_\epsilon}{2}\left[1 - \operatorname{erf}\left(\frac{m_\epsilon}{\sqrt{2}\,\sigma}\right)\right]. \tag{40}$$

If v_r is a deterministic vector, ϵ is a deterministic variable either since $\epsilon(t) = \hat{n} \cdot v'(t) = \hat{n} \cdot v_r(t)$ and its variance $\sigma \to 0^+$. In Equation (40), we have:

$$\lim_{\sigma \to 0^+} I(\hat{n}, t) = \begin{cases} -\hat{n} \cdot v_r & \text{if} \quad \hat{n} \cdot v_r \leqslant 0 \\ 0 & \text{if} \quad \hat{n} \cdot v_r > 0. \end{cases} \tag{41}$$

From Equation (39), the probability $\mathcal{P}_I(T)$ becomes:

$$\mathcal{P}_I(T) = -\int_{t_0}^{t_0+T} \int_0^{2\pi} \int_0^{\pi} R^2 \sin(\phi)\, \rho_{tr}(r_r(\theta, \phi)) 1_{\hat{n} \cdot v_r(t) \leqslant 0}(\theta, \phi, t)(\hat{n} \cdot v_r(t)) \mathrm{d}\phi \mathrm{d}\theta \mathrm{d}t. \tag{42}$$

To get rid of the function $1_{\hat{n} \cdot v_r(t) \leqslant 0}(\epsilon)$ in the integrand of (42), one may modify the integration limits to the hemisphere where $\hat{n} \cdot v_r(t) \leqslant 0$. By choosing τ-dependent axes for the spherical coordinates for which the x-axis is aligned with the vector $v_r(\tau)$ where τ is the first hitting time, we get the following formula:

$$\mathcal{P}_I(T) = -\int_{t_0}^{t_0+T} \int_{\frac{\pi}{2}}^{\frac{3\pi}{2}} \int_0^{\pi} R^2 \sin(\phi)\, \rho_{tr}(r_r(\theta, \phi))(\hat{n} \cdot v_r(t)) \mathrm{d}\phi \mathrm{d}\theta \mathrm{d}t. \tag{43}$$

It is important to note that $r_r(\theta, \phi)$ in (42) is expressed in the original basis while $r_r(\theta, \phi)$ is expressed in the new basis for which the x-axis is aligned with the vector $v_r(\tau)$. The 2D-geometry of the hemisphere domain of integration for encounters obeying to Assumptions 1-5 is illustrated by Figure 4.

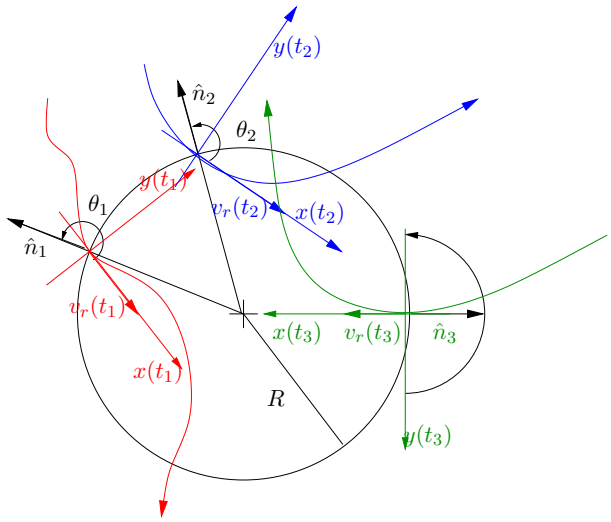

Figure 4: Illustration in 2D of three collisions at t_1, t_2 and t_3 with the hemisphere of integration for t_3.

As is clearly suggested by the terminology *short-term* encounter, the next set of assumptions relies on the assumed short duration of the encounter.

Assumption 6. *Short encounter time.*
The encounter time interval $[t_0, t_0 + T]$ *is small enough that the relative motion is a straight line.*

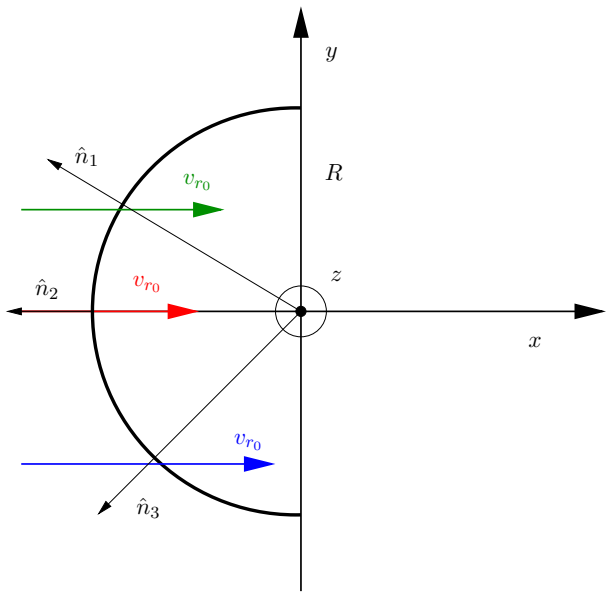

Figure 5: Three collisions in (x, y) plane with deterministic and rectilinear relative velocity v_{r_0}.

Assumption 6 has a strong impact on the structure of the relative vector field f_r which has to satisfy $f_r = \begin{bmatrix} v_{r_0} & 0 \end{bmatrix}^T$ when there is no uncertainty on the relative velocity. The relative state-space solution is therefore defined as :

$$\begin{array}{rcl} r_r(t) & = & v_{r_0}(t - t_0) + r_{r_0} \\ v_r(t) & = & v_{r_0}, \end{array} \tag{44}$$

where v_{r0} is a deterministic vector. It may be easily deduced that the relative trajectory is characterized by a mean vector $m_{r_r}(t) = E[r_r(t)] = mr_0 + v_{r_0}(t - t_0)$. This implies also that the relative trajectory has a constant covariance matrix $P_{11}(t) = E\left[(r_r(t) - mr_r(t))(r_r(t) - mr_r(t))^T\right] = P_{11}(t_0)$. It is to be noted that the time-invariant nature of the covariant matrix of the random vector $r_r(t)$ is deduced from the assumptions rather than part of the *a priori* assumptions themselves as improperly presented in the reference [28].
Keeping in mind that the encounter frame has been chosen such that $v_{r_0} = \|v_{r_0}\|\vec{i}$, we get that :

$$\begin{array}{rcl} mr_1(t) & = & mr_1(0) + \|v_{r_0}\|(t - t_0) \\ mr_2(t) & = & mr_2(0) \\ mr_3(t) & = & mr_3(0). \end{array} \tag{45}$$

In addition, the dot product in (43) may be readily calculated as $\hat{n}\cdot v_r(t) = \hat{n}\cdot v_{r_0} = \|v_{r_0}\|\cos(\theta)\sin(\phi)$. Applying Corollary 1 to (43) with $h : [0, \pi]\times[\pi/2, 3\pi/2] \to \overline{B}(0, R),\ (\phi, \theta) \mapsto (r_{r_2}, r_{r_3})$, $\det(\mathrm{D}h(\phi, \theta)) = R^2\sin^2(\phi)\cos(\theta)$ and $g = \rho_{tr}$, we get that :

$$\begin{array}{rcl} \mathcal{P}_I(T) & = & -\displaystyle\int_{t_0}^{t_0+T}\int_{\frac{\pi}{2}}^{\frac{3\pi}{2}}\int_0^{\pi} \|v_{r_0}\|R^2\sin^2(\phi)\cos(\theta)\rho_{tr}(r_r(\theta,\phi))\mathrm{d}\phi\mathrm{d}\theta\mathrm{d}t \\ & = & \displaystyle\int_{t_0}^{t_0+T}\int_{\frac{\pi}{2}}^{\frac{3\pi}{2}}\int_0^{\pi} \|v_{r_0}\|\rho_{tr}(r_r(\theta,\phi))|\det(\mathrm{D}h(\phi,\theta))|\mathrm{d}\phi\mathrm{d}\theta\mathrm{d}t \\ & = & \displaystyle\int_{t_0}^{t_0+T}\iint_{\overline{B}(0,R)} \|v_{r_0}\|\rho_{tr}(r_r(r_{r_2}, r_{r_3}))\mathrm{d}r_{r_2}\mathrm{d}r_{r_3}\mathrm{d}t, \end{array} \tag{46}$$

where $r_r(r_{r_2}, r_{r_3}) = \left[\begin{array}{ccc} r_{r_1}(r_{r_2}, r_{r_3}) & r_{r_2} & r_{r_3} \end{array}\right]^T$ and $r_{r_1}(r_{r_2}, r_{r_3}) = -\sqrt{R^2 - r_{r_2}^2 - r_{r_3}^2}$. Equation (46) is equivalent to Equation (28) in [1] with $T \to \infty$ and $t_0 \to -\infty$.
At this point, it is known that $r_r \sim \mathcal{N}(mr_r, P_{11}(t_0))$. Therefore, the trick already used above with P_r and consisting in building a linear transformation L from the partitioning of $P_{11}(t_0)$ may be applied. With the following partitioning of $P_{11}(t_0)$, the linear transformation L is given as:

$$L = \left[\begin{array}{cc} 1 & -\varpi^T P_{r_{r_2}r_{r_3}}^{-1} \\ 0_{2,1} & I_2 \end{array}\right] \quad \text{where} \quad P_{11}(t_0) = \left[\begin{array}{cc} \eta^2 & \varpi^T \\ \varpi & P_{r_{r_2}r_{r_3}} \end{array}\right].$$

Applying L to the random vector $r_r - mr_r$, we get:

$$L(r_r - mr_r) = \left[\begin{array}{c} r_{r_1} - \varpi^T P_{r_{r_2}r_{r_3}}^{-1}\left[\begin{array}{c} r_{r_2} \\ r_{r_3} \end{array}\right] - \left(mr_1 - \varpi^T P_{r_{r_2}r_{r_3}}^{-1}\left[\begin{array}{c} mr_2 \\ mr_3 \end{array}\right]\right) \\ \hline r_{r_2} - mr_2 \\ r_{r_3} - mr_3 \end{array}\right] := \left[\begin{array}{c} \bar{r}_{r_1} - \bar{m}r_1 \\ \hline \varsigma - m\varsigma \end{array}\right].$$

We also have:

$$LP_{11}(t_0)L^T = \left[\begin{array}{cc} \eta^2 - \varpi^T P_{r_{r_2}r_{r_3}}^{-1}\varpi & 0_{1,2} \\ 0_{2,1} & P_{r_{r_2}r_{r_3}} \end{array}\right] \tag{47}$$

and $\det(P_{11}(t_0)) = \eta^2\varpi^T P_{r_{r_2}r_{r_3}}^{-1}\varpi \cdot \det(P_{r_{r_2}r_{r_3}})$. The normal density ρ_{tr} may then be factorized as $\rho_{tr}(r_r) = \rho_{t\bar{r}_{r_1}}(\bar{r}_{r_1})\rho_\varsigma(\varsigma)$ where:

$$\rho_{t\bar{r}_{r_1}} \sim \mathcal{N}(\bar{m}r_1, \eta^2 - \varpi^T P_{r_{r_2}r_{r_3}}^{-1}\varpi), \quad \rho_\varsigma \sim \mathcal{N}(m\varsigma, P_{r_{r_2}r_{r_3}}). \tag{48}$$

Note that the normal density ρ_ς does not depend upon time since $m\varsigma$ (from (45)) and $P_{r_{r_2}r_{r_3}}$ are constant over time. Then, the probability $\mathcal{P}_I(T)$ becomes:

$$\mathcal{P}_I(T) = \int_{t_0}^{t_0+T} \iint_{\overline{B}(0,R)} \|v_{r_0}\| \rho_{tr}(r_r) \mathrm{d}r_{r_2} \mathrm{d}r_{r_3} \mathrm{d}t = \iint_{\overline{B}(0,R)} \rho_\varsigma(\varsigma) \int_{t_0}^{t_0+T} \|v_{r_0}\| \rho_{t\bar{r}_{r_1}}(\bar{r}_{r_1}(t)) \mathrm{d}t \mathrm{d}\varsigma. \quad (49)$$

In Formula (49), the variable r_{r_1} appearing in $\bar{r}_{r_1}$ must satisfy $r_{r_1} = -\sqrt{R^2 - r_{r_2}^2 - r_{r_3}^2}$ to comply with the hemisphere of integration depicted on Figure 5. The last step to obtain the classical 2D probability of collision formula (see [21], [1] or [72]) is a final change of variables $\chi = \bar{m}r_1 - \bar{r}_{r_1}$ for the inner integral with respect to time and extending the time of integration to infinity at both limits.

$$\int_{t_0}^{t_0+T} \|v_{r_0}\| \rho_{t\bar{r}_{r_1}}(\bar{r}_{r_1}(t)) \mathrm{d}t \simeq \int_{-\infty}^{+\infty} \|v_{r_0}\| \rho_{t\bar{r}_{r_1}}(\bar{r}_{r_1}(t)) \mathrm{d}t = \int_{-\infty}^{+\infty} \rho_\chi(\chi) \mathrm{d}\chi = 1, \quad (50)$$

where $\rho_\chi \sim \mathcal{N}(0, \eta^2 - \varpi^T P_{yz}^{-1} \varpi)$.
The last assumption related to the limits of integration is called *Time integrates out* and qualified as an odd one in [28]. We strongly agree with this feeling since the statement defining this assumption "the time integration interval is sufficiently long to approximate the time integral (50) as 1 but not so long as to violate the short-term encounter assumption" proves to be almost a contradiction in terms. Finally, the classical 2D probability of collision, computed as the double integral on a disk of a Gaussian function, is retrieved as:

$$\mathcal{P}_I(T) = \frac{1}{2\pi \det(P_\varsigma)} \iint_{\overline{B}(0,R)} \exp\left[-\frac{1}{2}(\varsigma - m\varsigma)^T P_\varsigma^{-1} (\varsigma - m\varsigma)\right] \mathrm{d}\varsigma. \quad (51)$$

Remark 4.
Note that M.R. Akella and K.T. Alfriend [1] are the first authors having given the relations between the 2D integral in (51) *and a 3D integral involving the full relative position covariance and a hidden time integration through the integration over the relative velocity vector (which direction is perpendicular to the encounter plane). This paper extends a preliminary result by Z.N. Khutorovsky [45] giving the collision probability as a function of time under the assumption that the size of the primary is much smaller compared to the position uncertainty of the secondary object.*

2.4.2 Validity of the 2D integral

The formula (51) has been widely studied in the literature and used in practice for risk assesment. Since the seminal work in [34], different numerical approaches have been conducted to compute the most efficiently the 2D integral (see for instance [61], [3], [21], [72]). Nevertheless, it is well-known that the assumptions 5 and 6 are not met for some conjunctions (events with long durations, with non negligible uncertainty on the relative velocity and/or satellite pairs orbiting in close proximity) and different ways to estimate conjunction duration and the validity of the 2D integral have been proposed.
First, K. Chan has proposed in [25] to analyze the extent of the encounter region for which the relative orbit can be considered to be a straight line to decide when is the above approximation of using Equation (51) instead of Equation (39) good enough. It is then proposed that if the path of the relative motion is a straight line over a length of 8.5 standard deviations along the integration direction, then the simplification is valid from a computational viewpoint.

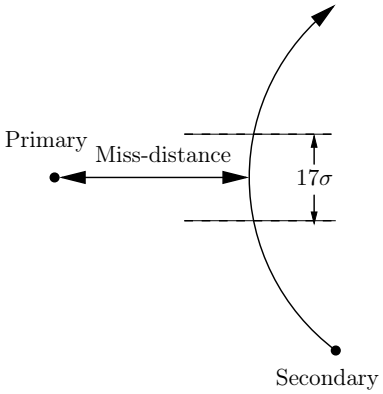

Figure 6: Path length for rectilinear approximation according to [25].

As has been demonstrated later, a key assumption for the validity of this simplification is that the relative velocity between the two objects is high in order to get a short encounter duration. In [36], a twofold study has been conducted on historical operational data and generated encounter geometries both in LEO and GEO orbit regimes to determine the relative velocity threshold below which the validity of the rectilinear assumption breaks down and a 3D alternative (developed by McKinley in this particular case [58]) has to be used instead of the 2D integral. In the first case, the study gathers 3680 conjunction events in LEO, between June of 2005 and June of 2007, and 12 events in the GEO orbit case. All in all, the results of [36] confirm that not only relative velocity, but also combined covariance, and miss distance have a decisive impact on the encounter duration and therefore on the discrepancy between the 2D integral and the 3D computation. In addition, the relative velocity threshold in itself can be set to 10 m/sec. Note also the linearity test developed in [5], where the objective is to get a minimum relative velocity at TCA to ensure that a user-specified fractional probability threshold will not be exceeded. This fractional probability threshold is computed as the absolute difference between the 2D and an alternative based on nonlinear relative motion divided by the 2D results. However, as previously mentioned, depending on the miss distance and covariance, the study also concludes that the 2D integral may still be sufficient for relative velocities as low as 1 m/sec and that a good metric for determining when the 2D integral may be validly computed and used is the encounter duration (for an encounter duration less than 500 s).
This notion of a short-term encounter validity time interval that provides a metric for assessing the acceptability of the short encounter assumptions is formally defined in [27]. To do so, it is necessary to get back to the time integral (50).

$$I(\varsigma) = \int_{t_0}^{t_0+T} \|v_{r_0}\| \rho_{t\bar{r}_{r_1}}(\bar{r}_{r_1}(t))\mathrm{d}t = \int_{\chi_0}^{\chi_T} \rho_\chi(\chi)\mathrm{d}\chi, \tag{52}$$

where $\|v_{r_0}\|$ is the relative velocity at TCA ($t_{TCA} = 0$) and

$$\begin{array}{lcl} \chi(t) & = & \bar{m}r_1 - \bar{r}_{r_1} = \|v_{r_0}\|t + \varpi^T P^{-1}_{r_{r_2}r_{r_3}}(\varsigma - m\varsigma_0) + \sqrt{R^2 - r_{r_2}^2 - r_{r_3}^2}, \\ m\chi & = & 0, \\ \sigma_\chi^2 & = & \eta^2 - \varpi^T P^{-1}_{r_{r_2}r_{r_3}}\varpi, \\ \rho_\chi(\chi) & \sim & \mathcal{N}_1(0,\sigma_\chi) = \dfrac{1}{\sqrt{2\pi}\,\sigma_\chi^2} e^{-\dfrac{\chi^2}{2\sigma_\chi^2}}, \end{array} \tag{53}$$

since $mr_1(t) = \|v_{r_0}\|t$. When deriving the 2D integral for the computation of the probability of collision under the short-term assumptions, the integral $I(\varsigma)$ in (52) is equal to 1 since it is computed

over all time. V.T. Coppola defines the short-term duration as the duration for which this integral $I(\varsigma)$ can be approximately but accurately considered to be equal to 1. Note that by using the definition of the normal cumulative distribution function, it is easy to compute that:

$$I(\varsigma) = \frac{1}{2}\left(\operatorname{erf}(\alpha_T) - \operatorname{erf}(\alpha_0)\right), \tag{54}$$

where $\alpha_T = \dfrac{\chi_T}{\sigma_\chi\sqrt{2}}$ and $\alpha_0 = \dfrac{\chi_0}{\sigma_\chi\sqrt{2}}$. Therefore, $\operatorname{erf}(\alpha_T) \to 1$ and $\operatorname{erf}(\alpha_0) \to -1$ is needed to get $I(\varsigma) \simeq 1$. Let γ be the absolute error with respect to 1 or -1 when computing respectively $\operatorname{erf}(\alpha_T)$ and $\operatorname{erf}(\alpha_0)$ and evaluating the integral $I(\varsigma)$ over a finite duration. The idea is, for a given absolute error γ to compute α_0 and α_T such that:

$$\alpha_0 \leqslant \operatorname{erf}^{-1}(-1+\gamma) \quad \text{and} \quad \alpha_T \geqslant \operatorname{erf}^{-1}(1-\gamma). \tag{55}$$

The first condition is satisfied for $t_0 \leqslant \tau_0 = \dfrac{-\sqrt{2}\,\alpha_c(\gamma)\sigma_\chi + \varpi^T m\varsigma_0 - \delta_{max}}{\|v_{r_0}\|}$ while the second condition leads to $\dfrac{-\sqrt{2}\,\alpha_c(\gamma)\sigma_\chi + \varpi^T m\varsigma_0 - \delta_{min}}{\|v_{r_0}\|} = \tau_1 \leqslant t_0 + T$ where δ_{min} and δ_{max} are computed as the minimum and maximum of $\varpi^T\varsigma + \sqrt{R^2 - \varsigma^T\varsigma}$ over the area of the circle $\|\varsigma\| \leqslant R$. A not so straightforward computation leads to :

$$\begin{aligned}
\delta_{max} &= \max_{\|\varsigma\|\leqslant R} \ \varpi^T\varsigma + \sqrt{R^2 - \varsigma^T\varsigma} = R\sqrt{1+\varpi^T\varpi} \quad \text{for} \quad \varsigma = \frac{R\varpi}{\sqrt{1+\varpi^T\varpi}},\\
\delta_{min} &= \min_{\|\varsigma\|\leqslant R} \ \varpi^T\varsigma + \sqrt{R^2 - \varsigma^T\varsigma} = -R\sqrt{\varpi^T\varpi} \qquad \text{for} \quad \varsigma = -\frac{R\varpi}{\sqrt{\varpi^T\varpi}}.
\end{aligned} \tag{56}$$

Let us give some additional details on how equations in (56) are obtained.
The derivation is quite the same for both min and max problems. The constraint set of both problems is the closed ball $\overline{B}(0,R)$. First, consider the min and max problems over the boundary $\partial\overline{B}(0,R)$:

$$\delta^1_{max} = \max_{\varsigma^T\varsigma = R^2} \ \varpi^T\varsigma \quad \text{and} \quad \delta^1_{min} = \min_{\varsigma^T\varsigma = R^2} \ \varpi^T\varsigma. \tag{57}$$

Introducing the Lagrangian $L(\varsigma;\lambda) = \varpi^T\varsigma + \lambda(\varsigma^T\varsigma - R^2)$ (where $\lambda \neq 0$ is a lagrangian parameter), the first necessary condition of optimality reads

$$\nabla L(\varsigma^*;\lambda^*) = \varpi + 2\lambda^*\varsigma^* = 0 \ \Leftrightarrow \ \varsigma^* = \frac{-\varpi}{2\lambda^*}. \tag{58}$$

As ${\varsigma^*}^T\varsigma^* = R^2$, we get that $\lambda^* = \pm\dfrac{\sqrt{\varpi^T\varpi}}{2R}$ and $\varsigma^* = \mp\dfrac{R\varpi}{\sqrt{\varpi^T\varpi}}$. The Hessian of the Lagrangian is given by $H[L](\varsigma^*,\lambda^*) = 2\lambda^* I_2$ and therefore, the second order sufficient condition gives a local maximum $\delta^1_{max} = R\sqrt{\varsigma^T\varsigma}$ for $\lambda^* = -\dfrac{\sqrt{\varpi^T\varpi}}{2R}$, $\varsigma^* = \dfrac{R\varpi}{\sqrt{\varpi^T\varpi}}$ and a local minimum $\delta^1_{min} = -R\sqrt{\varsigma^T\varsigma}$ for $\lambda^* = \dfrac{\sqrt{\varpi^T\varpi}}{2R}$, $\varsigma^* = -\dfrac{R\varpi}{\sqrt{\varpi^T\varpi}}$.
The next step consists in checking the global optimality of this solution over the ball $\overline{B}(0,R)$, i.e. check if there exists $\overline{\varsigma} \in B(0,R)$ such that $\delta_{max}(\overline{\varsigma}) > \delta^1_{max}$ and if there exists $\underline{\varsigma} \in B(0,R)$ such that $\delta_{min}(\underline{\varsigma}) < \delta^1_{min}$.
In the first case (maximum problem), it is necessary to compute the maximum of $\varpi^T\varsigma + \sqrt{R^2 - \varsigma^T\varsigma}$ over the open ball. It amounts to solve an unconstrained convex optimization problem and to verify

that the obtained solution is in the open ball since it is the maximization of a concave function over an open set. A first order necessary and sufficient condition is given by the vanishing of the gradient of the cost function, i.e. the equation of the critical point of the cost function:

$$\varpi - \frac{\overline{\varsigma}}{\sqrt{R^2 - \overline{\varsigma}^T\overline{\varsigma}}} = 0. \tag{59}$$

From (59), it is easy to compute that $\overline{\varsigma}^T\overline{\varsigma} = \dfrac{R^2\varpi^T\varpi}{1+\varpi^T\varpi}$ and $\overline{\varsigma} = \dfrac{R\varpi}{\sqrt{1+\varpi^T\varpi}} \in B(0,R)$ for an optimal cost of $\delta_{max}(\overline{\varsigma}) = R\sqrt{1+\varpi^T\varpi} > \delta^1_{max}$. The conclusion in (56) follows.
In the second case(minimum problem), a simple geometric argument, illustrated at Figure 7, may be used to show that $\delta_{min} = \delta^1_{min}$. Indeed, $\nexists\, \underline{\varsigma} \in B(0,R)$ such that $\varpi^T\underline{\varsigma} + \sqrt{R^2 - \underline{\varsigma}^T\underline{\varsigma}} < R\sqrt{\varpi^T\varpi} = \delta^1_{min}$ since $B(0,R) \subset \mathcal{H}^+$ where $\mathcal{H}^+$ is the positive half-space defined by the hyperplane $\varpi^T\varsigma^* = \delta^1_{min}$, i.e. $\forall\, \varsigma \in B(0,R),\ \varpi^T(\varsigma - \varsigma^*) > 0$ and therefore $\forall\, \varsigma \in B(0,R),\ \varpi^T\varsigma + \sqrt{R^2 - \varsigma^T\varsigma} > \varpi^T\varsigma^* = \delta^1_{min} = \delta_{min}$.

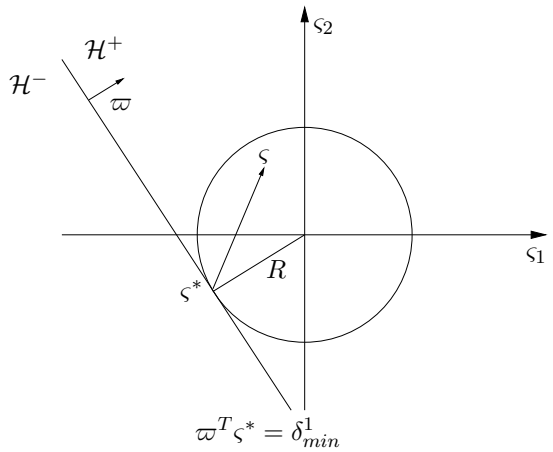

Figure 7: Ball $B(0,R) \subset \mathcal{H}^+$.

Finally, we get that:

$$\tau_0(\gamma) = \frac{-\sqrt{2}\,\alpha_c(\gamma)\sigma_\chi + \varpi^T m\varsigma_0 - R(\sqrt{1+\varpi^T\varpi}}{\|v_{r_0}\|}, \quad \tau_1(\gamma) = \frac{\sqrt{2}\,\alpha_c(\gamma)\sigma_\chi + \varpi^T m\varsigma_0 + R(\sqrt{\varpi^T\varpi}}{\|v_{r_0}\|}, \tag{60}$$

and

$$\Delta\tau(\gamma) = \tau_1(\gamma) - \tau_0(\gamma) = \frac{2\sqrt{2}\,\alpha_c(\gamma)\sigma_\chi + R(\sqrt{\varpi^T\varpi} + \sqrt{1+\varpi^T\varpi})}{\|v_{r_0}\|}. \tag{61}$$

Remark 5.
As shown in [27], the interval $[\tau_0, \tau]$ does not always include the origin ($t_{TCA} = 0$) and the duration $\Delta\tau$ may be smaller than the duration between τ_0 or τ_1 and $t = 0$.

Keeping in mind the last remark, the short-term encounter validity time interval is then defined in [27] by:

$$\Delta t(\gamma) = \max\{\Delta\tau(\gamma), \tau_0(\gamma), \tau_1(\gamma)\}. \tag{62}$$

This means that the rectilinear and constant-covariance assumptions must be satisfied during the time span $TCA \pm \Delta t(\gamma)$ ($\gamma = 10^{-16}$ for double-precision numerical processing). This appears to be

consistent with the index defined by Chan and converted in time span as $17\sigma\|v_{r_0}\|$ in [27]. Still, at our knowledge, there is no known absolute threshold for the time span that could indicate a clear separation between long-term and short-term encounters.
The usage of this time span has been reviewed in [40] and adapted to define bounds for the time integration in Coppola's formula.
for and refined in [39].

2.5 Three different implementations of the 3D PoC

In all the numerical implementations encountered in the literature, the time and sphere integrations are performed separately. In addition, the collision probability $\mathcal{P}_I(T)$ given in (39) may also be defined by introducing the *collision probability rate* $p_i(t)$.

Definition 4. *[Collision probability rate [32]]*
The collision probability rate $p_i(t)$ is the instantaneous increase in collision probability at t. We have therefore that

$$P_I(T) = \int_{t_0}^{t_0+T} p_i(t)\mathrm{d}t. \tag{63}$$

In addition, if Assumptions 1-4 are fulfilled then, following (31)*, the collision probability rate is nothing but*

$$p_i(t) = \int_0^{2\pi}\int_0^{\pi} |\sin(\phi)| \int_{-\infty}^{\infty} R^2 \, |v_r \cdot \hat{n}| \, 1_{v_r\cdot\hat{n}\leqslant 0}(v_r)\rho_{tr}(x_r(\theta,\phi,v_r))\, dv_r\, d\phi d\theta. \tag{64}$$

Remark 6.
Note that Equation (64) *is the definition of the collision rate as given in reference [32]. The subsequent developments of Coppola as given above may be used without loss of generality and Equation* (39) *may replace Equation* (31)*.*

$$p_i(t) = \int_0^{2\pi}\int_0^{\pi} R^2 \sin(\phi)\, \rho_{tr}(r_r(\theta,\phi))I(\hat{n},t)\, d\phi d\theta. \tag{65}$$

Remark 7.
The function $p_i(t)$ is also known as the probability density flux penetrating the HBR sphere at t in the reference [68] or as the collision probability flow in the reference [76].

In [7], S. Alfano published an analysis of twelve conjunctions and compared results obtained with two different Monte Carlo simulations and with several short-term and long-term collision probability computations. The three different implementations of Coppola's formulation have been evaluated on different subsets of these twelve cases. The results are summarized in each case below.

Remark 8.
It is important to notice that the notion of collision probability rate (or collision probability flow) has also been extensively used in air traffic control (see [76] and the references therein) and automotive applications (see [10] and the references therein) with results very similar to the one of Coppola for the formulation of the probability of collision. These references focus on upper bounds of the collision probability rate, integrated over a time period that are numerically tractable via usual quadratures. The first reference uses a relaxation of the set of trajectories that have not earlier entered the collision volume given by the set of all trajectories leading to a collision. The second reference derives a formulation of an upper bound of the probability of collision over a time period that may be found in the literature dedicated to the problem of level crossings of vector stochastic processes [14], [43]. This line of research originates in the twin papers [65, 66] with the Rice's formula and has found specific applications in reliability theory [42].

2.5.1 Coppola's implementation of the 3D PoC

The numerical implementation of the Formula (39) is quickly described in [28] in the section presenting the numerical results of the proposed method. Very few details are given except that the triple integration is performed in two steps: the outer time numerical integration is based on a Simpson's rule while a Lebedev quadrature is used for the integration over the sphere. The dynamical model used for the propagation of the Gaussian density is not detailed except that a grid of ephemeris (including the 6×6 covariance matrices is generated by STK (software available from Analytical Graphics Inc.) by numerically integrating the trajectory and the covariance matrix.

Numerical integration over the unit sphere The integral defining the collision probability rate in (65) is an integral over the unit sphere written into a standard form that may be generically defined as:

$$p_i(t) = \int_0^{2\pi} \int_0^{\pi} R^2 \sin(\phi)\, \rho_{tr}(r_r(\theta,\phi)) I(\hat{n},t) \mathrm{d}\phi \mathrm{d}\theta = I[f] = \int_0^{2\pi} \int_0^{\pi} f(\theta,\phi) \sin(\phi)\, \mathrm{d}\phi \mathrm{d}\theta, \tag{66}$$

where $f : [t_0, t_0+T] \times \mathbb{S}^2 \to \mathbb{R}$ and the dependency of the function f upon time has been omitted for simplification's sake since the objective is to present the principles of the Lebedev quadratures [52], [53], [54], [55]. Before exposing the basics of Lebedev quadratures, some preliminary facts about the expansion of square integrable functions over the sphere are given.
Following [13], a function which is square integrable on $\mathbb{S}^2$ has an expansion in terms of the spherical harmonics orthonormal basis on the unit sphere:

$$f(\theta,\phi) = \sum_{n=0}^{\infty} \sum_{m=_n}^{n} c_{mn} Y_n^m(\theta,\phi), \tag{67}$$

where the spherical harmonic functions $Y_n^m(\theta,\phi)$ are given by:

$$Y_n^m(\theta,\phi) = \frac{1}{\sqrt{2\pi}} P_n^m(\cos(\phi)) e^{im\theta}, \;\; -n \leqslant m \leqslant n, \;\; n,m \in \mathbb{N}. \tag{68}$$

P_n^m are the normalized Legendre functions, m is the order of the spherical harmonic, n is the degree, c_{mn} are the coefficients of the expansion that may be computed as the inner product of the function f with the basis functions:

$$c_{mn} = \int_0^{2\pi} \int_0^{\pi} f(\theta,\phi) \overline{Y}_n^m(\theta,\phi) \mathrm{d}\phi \mathrm{d}\theta. \tag{69}$$

Note that $\overline{Y}_n^m(\theta,\phi)$ is the conjugate of $Y_n^m(\theta,\phi)$. This class of spherical harmonics expansion is well-know in astrodynamics when expanding the gravity potential [79], [59].
A quadrature is a numerical scheme giving an approximation of the integral $I[f]$ by a weighted sum over a finite collection of points $\{x_i\} \subset \mathbb{S}^2$:

$$\int_0^{2\pi} \int_0^{\pi} f(\theta,\phi) \sin(\phi)\, \mathrm{d}\phi \mathrm{d}\theta \approx \sum_{i=1}^{N} w_i f(x_i) := Q_N[f], \tag{70}$$

where w_i are the weights and $Q_N[f]$ the quadrature of the integral. A quadrature scheme is therefore based on the choice of the distribution of nodes $\{x_i\}$ and on the choice of the weights w_i. Lebedev quadratures belong to the class of Gauss quadratures for which the weights are not fixed (Chebyshev quadratures) but computed with the nodes at the same time over the whole sphere.

The general Lebedev quadrature scheme may be written as [54]:

$$\begin{aligned} Q_N[f] &= A_1 \sum_{i=1}^{6} f(a_i^1) + A_2 \sum_{i=1}^{12} f(a_i^2) + A_3 \sum_{i=1}^{8} f(a_i^3) + \sum_{k=1}^{N_1} B_k \sum_{i=1}^{24} f(b_i^k) + \sum_{k=1}^{N_2} C_k \sum_{i=1}^{24} f(c_i^k) \\ &\quad + \sum_{k=1}^{N_3} D_k \sum_{i=1}^{48} f(d_i^k), \end{aligned} \tag{71}$$

where the typical nodes of each type have the form:

$$\begin{array}{lll} a_1^1 = (1,\ 0,\ 0), & & a_1^2 = (2^{-1/2},\ 2^{-1/2},\ 0), \quad a_1^3 = (3^{-1/2},\ 3^{-1/2},\ 3^{-1/2}), \\ b_1^k = (l_k,\ l_k,\ m_k), & 2l_k^2 + m_k^2 = 1, & \\ c_1^k = (p_k,\ q_k,\ 0), & p_k^2 + q_k^2 = 1, & \\ d_i^k = (r_k,\ s_k,\ t_k), & r_k^2 + s_k^2 + t_k^2 = 1. & \end{array} \tag{72}$$

The remaining points are obtained by permutation of coordinates or by change of their sign. The generic rationale behind the computation of the weights and the node is that the quadrature has to be exact for all spherical harmonics up to a given degree p while keeping symmetry under octahedral rotations and reflections. This problem is simplified by a theorem of S.L. Sobolev implying that this condition need be imposed only on those polynomials which are invariant under the octahedral rotation group with inversion. Imposing these conditions leads to solving a nonlinear system of equations which has been solved and tabulated up to order 131 [55]. The number of samples is then given by $N = 26 + 24(N_1 + N_2) + 48N_3$.

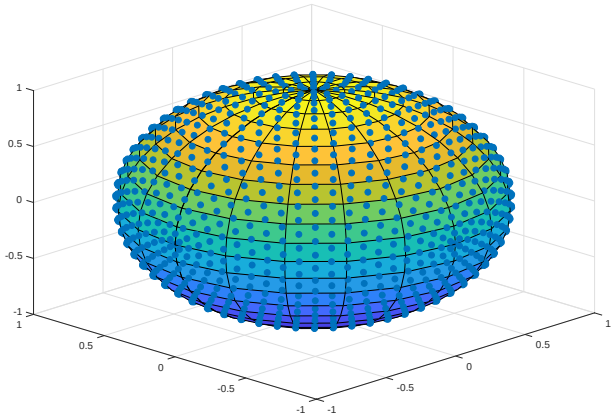

Figure 8: Lebedev's quadrature with $N = 1454$ samples for integration over the sphere.

Numerical integration over time The time integration used in [28] is a composite Simpson'rule. Here is recalled the composite Simpson rule for $2M$ subintervals for the numerical integration of $\int_{t_0}^{t_0+T} f(t)\mathrm{d}t$.

Theorem 1. *[Composite Simpson rule [57]]*
If the interval $[t_0, t_0 + T]$ is subdivided into $2M$ subintervals $[t_k, t_{k+1}]$ of equal width $h = T/2M$ by using $t_k = t_0 + kh$ for $k = 0,\ 1, \cdots,\ 2M$. The composite Simpson rule for $2M$ subintervals is given by the following expression:

$$\int_{t_0}^{t_0+T} f(t)\mathrm{d}t \approx \frac{h}{3} \sum_{k=1}^{M} [f(t_{2k-2}) + 4f(t_{2k-1}) + f(t_{2k})]. \tag{73}$$

Summary of numerical results Coppola has evaluated his formulation on five cases from [7] (cases 3, 4, 8, 10 and 11). The first one case 3 falls within the category of short-term encounters and was mainly meant to study the adequacy between the 3D PoC and the 2D Poc as well as to study the impact of the time integration bounds on the accuracy of the 3D PoC. The four last cases involve long-term conjunctions for which some of the simplifying assumptions of the 2D PoC formulation are not fulfilled. The comparisons of the results obtained with this implementation and the results obtained by the voxels method of Alfano appear to be satisfactory and consistent.

2.5.2 CARA implementation of the 3D PoC

The CARA implementation of the 3D PoC formulation is given in the reference [40] and at first, has been validated using Monte Carlo simulations of several well-studied conjunctions. Since then, the opinion of CARA about the usefulness of this formulation seems to be different. One of the objective of the paper [40] was to show that the usual 2D PoC integral may provide inaccurate computations or at least significant differences when compared to the 3D PoC estimate. In particular, the relative dynamical model used to propagate the uncertainty may be more realistic in the 3D PoC computations than the one on which relies the 2D Poc.

Uncertainty propagation Computing the collision probability as defined by Equation (39), where $\rho_{tr} \sim \mathcal{N}(m_{r_r}(t), P_{11}(t))$ implies that $m_{r_r}(t)$ and $P_{11}(t)$ are available on the grid of points defined on the interval $[t_0, t_0 + T]$ for numerical integration and therefore a specific care must be taken to define the uncertainty propagation on this interval. At CARA, the implementation described in [40] is built on the Keplerian two-body dynamical model to propagate $m_{r_r}(t)$ from TCA and the analytically-derived state transition matrix Φ_{sh} given in [75] to linearly propagate the covariances expressed in the ECI-frame:

$$P_{11}(t) = \Phi_{sh}(t, t_{TCA}) P(t_{TCA}) \Phi_{sh}^T(t, t_{TCA}). \tag{74}$$

Choice of time integration limits Based on the formulation of Coppola in [27], for the estimation of short-term conjunction durations (see subsection on the validity of the 2D integral above), conjunction bounds are defined as:

$$t_0 = \tau_m - E\frac{\tau_1 - \tau_2}{2}, \quad t_0 + T = \tau_m + E\frac{\tau_1 - \tau_2}{2}, \tag{75}$$

where $\tau_m = \frac{\tau_1 + \tau_0}{2}$ is the conjunction midpoint and E is a user-specified factor used to expand the conjunctions bounds in order for all peaks in $p_i(t)$ to be included in the conjunction time interval. The choice for E is dependent upon the dynamical model used for the uncertainty propagation. For instance, when using 3D PoC formulation with the simplified dynamical model and propagation summarized by Equation (44) under the assumptions that the covariance remains constant during the encounter with no uncertainty on the relative velocity ($P_r(t) = \begin{bmatrix} P_{11}(t_{TCA}) & 0_{3\times3} \\ 0_{3\times3} & 0_{3\times3} \end{bmatrix}$, Hall recommends to set $E = 1$. When the Keplerian two-body dynamical model is used, the factor E may vary from 2 to 5 with an apparent maximum of 10.

Numerical integration over time In order to remedy the problem of possible numerical instabilities caused by Simpson's rule for time integration, CARA's software relies on the trapezoidal scheme of the closed Newton-Cotes quadrature formulas for time integration.

Theorem 2. *[Trapezoidal rule [57]]*
If the interval $[t_0, t_0 + T]$ *is subdivided into* M *subintervals* $[t_k, t_{k+1}]$ *of equal width* $h = T/M$ *by using* $t_k = t_0 + kh$ *for* $k = 0,\ 1, \cdots,\ M$*. The trapezoidal rule for* M *subintervals is given by the following expression:*

$$\int_{t_0}^{t_0+T} f(t)\mathrm{d}t \approx \frac{h}{2}\sum_{k=0}^{M}(f(t_k) + f(t_{k-1})). \tag{76}$$

Numerical integration over the unit sphere The CARA's implementation uses a Lebedev quadrature for the integration over the unit sphere with the maximum available Lebedev algebraic order of 131, which implies to compute a weighted sum over 5810 points.

Summary of numerical results Only two cases (case 3 and case 10) from [7] are used to validate the CARA's implementation of the 3D PoC.
The first (a short-term encounter) confirms the results given in [28] and allows also to study the step-by-step relaxation of the 2D PoC assumptions (rectilinear relative motion, no uncertainty on the relative velocity and a time-invariant covariance matrix).
For the second test case (case 10), an identical analysis (step-by-step relaxation of simplifying assumptions) shows that the four relaxation schemes produce distinctly different results for example exhibiting two peaks for $p_i(t)$ and the result from the complete Coppola's implementation (Kepler two-body propagation with a time-varying complete covariance matrix) in line with Alfano's Monte Carlo simulations.
In a second step, the authors of [40] analyze a set of 80,827 archived OCMs, representing historical actual conjunctions that occurred between 2016-04-01 and 2016-06-1. This analysis reveals various types of conjunctions events:

- Repeating and/or blended conjunction events: such events occur when two satellites persistently operate in close proximity and this may be detected by the presence of multiple (possibly blending) peaks of the curve of the flux $p_i(t)$. On a purely empirical basis (no clear theoretical justification is given in [40]), the CARA team proposes the following index in order to identify the extended, repeating of blended events which lead the Coppola's formulation to break down.

  $$\frac{\Delta\tau}{T^o_{min}} > 0.01, \tag{77}$$

  where T^o_{min} is the minimum orbital period between the two objects concerned by the conjunction.

- Isolated conjunction events for which noteworthy differences between the 2D PoC and the 3D PoC have to be noticed since they may induce false alarms or misdetections. A further empirical analysis of the CARA team would tend to induce a correlation between these discrepancies and some features of the data used for the computation ($[\tau_0, \tau_1]$ does not bracket t_{TCA}, the peak in probability flux is sharp and relatively far from the conjunction midpoint, $[\tau_0, \tau_1]$ does not bracket the peak of flux, the covariance matrix of one of the obect is of a poor quality).

2.5.3 CNES implementation of the 3D PoC

The implementation of Coppola's formulation of the CNES team is known from the references [70] and [68]. Unfortunately, though the reference [70] is the most detailed one with respect to

the implementation, it is not the most up-to-date versions since some variations have been made recently. The second reference [68] is more focused on the results obtained than on numerical details.

Uncertainty propagation The propagation of the uncertainty is the same as the one used by the team CARA i.e. the Kepler two body dynamical model for the mean vectors and Equation (74) for the covariance matrices.

Choice of time integration limits The time integration limits are τ_0 and τ_2 computed from Equation (60) with $\sqrt{2}\,\alpha_c = 15$.

Numerical integration over time An adaptive Simpson rule is used and described in the reference [70]. The rationale behind the adaptive Simpson rule is briefly recalled. Suppose that the interval $[t_0, t_0+T]$ has been subdivided into $2M$ subintervals $[t_k, t_{k+1}]$ of equal width $h = T/2M$ by using $t_k = t_0 + kh$ for $k = 0,\ 1, \cdots,\ 2M$ nodes. On each subinterval $[t_k, t_{k+1}]$, a tolerance $\epsilon_k > 0$ is defined as well as two subintervals $[t_k^1, t_{k+1}^1]$ and $[t_k^2, t_{k+1}^2]$ with $t_k^1 = t_k$ and $t_{k+1} = t_{k+1}^2$. the composite Simpson rule (73) is applied on such subinterval to get:

$$\begin{aligned} S(t_k^1, t_{k+1}^1) + S(t_k^2, t_{k+1}^2) \quad = \quad & \frac{h}{6}[f(t_{2k-2}^1) + 4f((t_{2k-2}^1 + t_{2k}^1)/2) + f(t_{2k}^1)] \\ & + \frac{h}{6}[f(t_{2k-2}^2) + 4f((t_{2k-2}^2 + t_{2k}^2)/2) + f(t_{2k}^2)]. \end{aligned} \tag{78}$$

Then, if $|S(t_k^1, t_{k+1}^1) + S(t_k^2, t_{k+1}^2) - S(t_k, t_{k+1})| < \epsilon_k$ then $\displaystyle\int_{t_k}^{t_{k+1}} f(t)\mathrm{d}t \approx S(t_k^1, t_{k+1}^1) + S(t_k^2, t_{k+1}^2)$. If the accuracy test fails, new tolerances $\epsilon_k^1 = \epsilon_k/2$ and $\epsilon_k^2 = \epsilon_k/2$ are defined for each subinterval for further refinement and testing. It may be shown that the process will terminate after a finite number of steps [57].

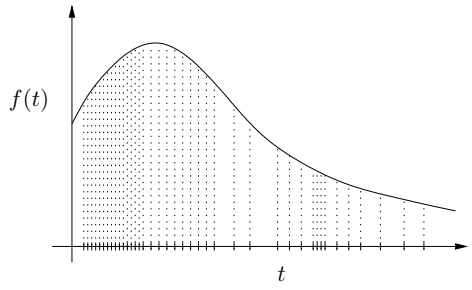

Figure 9: Subintervals used in adaptive Simpson quadrature.

Numerical integration over the unit sphere A classic Lebedev quadrature with 1454 nodes or 5810 nodes is mentioned in the reference [68] as well as a converged (θ, ϕ) discretization which is a combined adaptive Simpson scheme on θ and ϕ (this last one seems to be useful in some pathological cases where the covariance in the orthogonal plane to the relative velocity is very small compared to the combined hard body radius). At our knowledge, this is what is used in the latest version of the implementation of the method.

Summary of numerical results In [70], the implementation of Coppola is computed with and without uncertainty on the velocity and compared to the 2D PoC, the Monte Carlo reference results given in [7] and two alternatives given as the method of adjoining cylinders and the method of

bundled parallelepipeds [58], [5] on the twelve examples proposed by S. Alfano in [7]. Except for the test cases 11 and 12, the implementation of the Coppola's formulation and the reference Monte-Carlo as defined by the report conform with each other. Cases 11 and 12 are quite peculiar and should deserve a particular attention as has been done by Alfano for test case 11 (see [28]).
In [68], 28512 collision risks have been generated in order to evaluate the Coppola's formulation and to compare it to the 2D PoC formulation. Even if the two agree for most high-velocity encounters, important discrepancies remain in some cases pointing in particular the inadequacy of the 2D PoC result in those cases. For the long-term encounters (low relative velocity), the paper concludes that two issues have to be carefully addressed: the definition of the time span for the numerical integration and the fulfillment of the three assumptions involved in the Coppola's formulation.

2.6 The 3D PoC: Chan's counter-examples

In 2015, K. Chan has challanged Coppola's result in two twin papers [22], [23] in which four counter-examples pertaining to the long-term encounter setting are given. The main point raised by the Author in these references is quite not clearly formulated in its full generality: *"Even though it may be meaningful to consider the pdfs with their Cartesian positions and relative Cartesian positions as random variables* ***at a specific instant of time****, it is no longer meaningful to consider these quantities* ***over an extended period of time*** *for computing the probability between the two objects"*. Rephrased in [40] as *"Coppola's integration of the flux of a time-dependent probability distribution function (PDF) through a hemi-spherical surface is not consistent with the basic tenets of probability theory"*, the comment remains quite general and not exactly sustained by a rigorous theoretical analysis. We have therefore favoured a more thorough analysis of the proposed counter-examples in order to find the hidden catch in Coppola's formulation or in Chan's examples (if they don't comply with the assumptions set-up clearly presented in [28]). Unfortunately, Chan's papers have not been written with all the necessary details, particularly concerning the exact assumptions made at each step.
The counter-examples presented in [22] and [23] are built under the assumption that the relative motion of the secondary object with respect to the primary object may be well approximated by the first order linearized relative dynamic equations known as the Hill-Clohessy-Wiltshire (HCW) equations [26]. This clearly implies that the linearized model of the relative motion is derived with a circular orbit as the reference (the primary in this case) and under Keplerian assumptions.

Assumption Chan's counter-examples 1 (Circular reference orbit)**.**
The primary object is moving in a circular orbit under Keplerian assumptions.

Another induced assumption is that the primary and the secondary are sufficiently close to each other (proximity assumption) during the encounter time interval.

Assumption Chan's counter-examples 2 (Proximity assumption)**.**
The distance between the primary object and the secondary object is small with respect to the radius of the circular orbit of the primary for all $t \in [t_0, t_0 + T]$*.*

In the next paragraph, the HCW equations and their solution are briefly recalled.

2.6.1 Hill-Clohessy-Wiltshire relative equations of motion

Defining the state vector of the relative dynamics by $X_r(t) = [r_r(t)^T,\ v_r(t)^T]^T = [r_{r_1},\ r_{r_2},\ r_{r_3},\ v_{r_1},\ v_{r_2},\ v_{r_3}]^T$, the autonomous relative motion of the secondary has the following Linear Time-Invariant (LTI) state space representation [8]:

$$\frac{dX_r}{dt}(t) = \begin{bmatrix} 0 & 0 & 0 & 1 & 0 & 0 \\ 0 & 0 & 0 & 0 & 1 & 0 \\ 0 & 0 & 0 & 0 & 0 & 1 \\ 0 & 0 & 0 & 0 & 0 & 2n \\ 0 & -n^2 & 0 & 0 & 0 & 0 \\ 0 & 0 & 3n^2 & -2n & 0 & 0 \end{bmatrix} X_r(t), \tag{79}$$

where n is the mean motion of the reference (primary) orbit. It is well-known and it may be observed from Equation (79) that the in-plane motion ($\vec{X}_{LVLH}$ - $\vec{Z}_{LVLH}$) and the out-of-track motion ($\vec{Y}_{LVLH}$ direction) are decoupled. The transition matrix $\Phi_{HCW}(t, t_0)$ of (79) is readily available (using the Laplace transform for instance) such that $X_r(t) = \Phi_{HCW}(t, t_0)X_r(t_0)$ for $t \geqslant t_0$ where:

$$\Phi_{HCW}(t, t_0) = \left[\begin{array}{ccc|ccc} 1 & 0 & 6(\delta t - s_t) & (4s_t - 3\delta t)/n & 0 & 2(1 - c_t)/n \\ 0 & c_t & 0 & 0 & s_t/n & 0 \\ 0 & 0 & 4 - 3c_t & 2(c_t - 1)/n & 0 & s_t/n \\ \hline 0 & 0 & 6n(1 - c_t) & 4c_t - 3 & 0 & 2s_t \\ 0 & -ns_t & 0 & 0 & c_t & 0 \\ 0 & 0 & 3ns_t & -2s_t & 0 & c_t \end{array}\right] \tag{80}$$

where $\delta t = n(t - t_0)$, $c_t = \cos(n(t - t_0))$ and $s_t = \sin(n(t - t_0))$. The solution of the circular linearized relative equations are therefore given by:

$$\begin{array}{rcl} r_{r_1}(t) & = & r_{r_{10}} + 6(\delta t - s_t)r_{r_{30}} + (4s_t - 3\delta t)v_{r_{10}}/n + 2(1 - c_t)v_{r_{30}}/n \\ r_{r_2}(t) & = & c_t r_{r_{20}} + s_t v_{r_{20}}/n \\ r_{r_3}(t) & = & (4 - 3c_t)r_{r_{30}} + 2(c_t - 1)v_{r_{10}}/n + s_t v_{r_{30}}/n \\ v_{r_1}(t) & = & 6n(1 - c_t)r_{r_{30}} + (4c_t - 3)v_{r_{10}} + 2s_t v_{r_{30}} \\ v_{r_2}(t) & = & -ns_t r_{r_{20}} + c_t v_{r_{20}} \\ v_{r_3}(t) & = & 3ns_t r_{r_{30}} - 2s_t v_{r_{10}} + c_t v_{r_{30}}. \end{array} \tag{81}$$

The HCW relative motion is composed of an oscillatory mode along the $\vec{Y}_{LVLH}$ axis (out-of-plane motion) and a drifting ellipse for the in-plane motion (see the geometry of the drifting ellipse in $\vec{X}_{LVLH}$ - $\vec{Z}_{LVLH}$ plane as depicted by Figure 10). This latter is the combination of a stationary mode, an oscillation mode and a drifting mode.

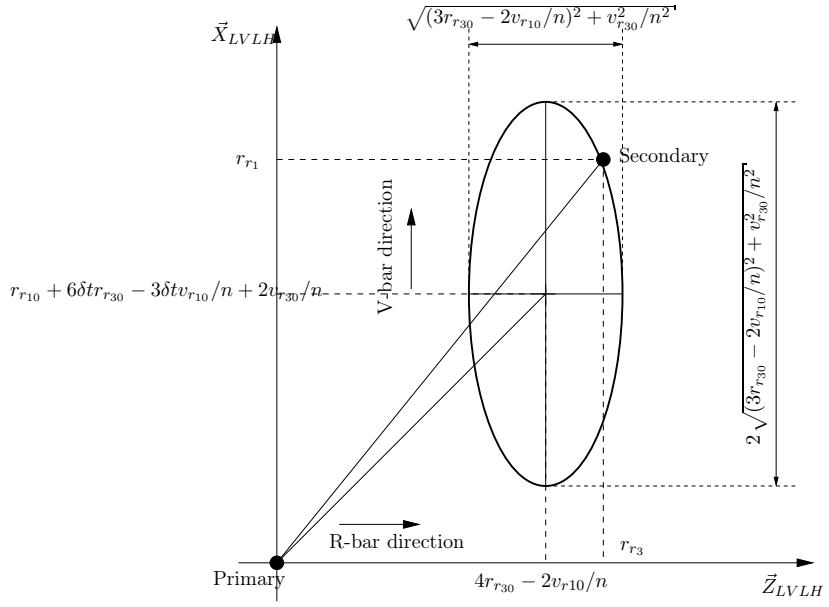

Figure 10: Drifting ellipse of the HCW relative motion

At this point, due to the linearity properties of the relative motion, if the state vector X_{r_0} at time t_0 is uncertain and distributed according to the density $\rho_{tX_{r_0}}$, the dynamic evolution of the two first moments, i.e. the mean $\mathrm{E}[X_r(t)] = m_r(t)$ and the covariance matrix $P_r(t,t) = P_r(t) = \mathrm{E}[(X_r(t) - m_r(t))(X_r(t) - m_r(t))^T])$ of the state vector $X_r(t)$ (which is a Gaussian stochastic process) can be computed as [44]:

$$m_r(t) = \Phi_{HCW}(t,t_0)m_r(t_0) \quad P_r(t) = \Phi_{HCW}(t,t_0)P_r(t_0)\Phi_{HCW}(t,t_0)^T. \tag{82}$$

2.6.2 Stationary hovering collision probability

In this example, the relative mean (nominal according to Chan's terminology) motion is assumed to be stationary i.e. $m_r(t_0) = \left[\begin{array}{cccccc} \bar{r}_{r_{10}} & 0 & 0 & 0 & 0 & 0 \end{array}\right]^T$. The exposition of the example is confusing in [22] and [23] so that it is necessary to rebuild the example and guess what the Author intends to prove by assuming explicitly what is implicitly suggested in the papers.
First of all, it seems that there is no uncertainty on the velocity vector at $t = t_0$ if we look at the isotropic 3D Gaussian pdf given in Equation (14) of [22] or Equation (1) of [23] and we have the mean vector and the covariance matrix at $t = t_0$ defined by:

$$m_r(t_0) = \left[\begin{array}{cccccc} m_{r_{r_{10}}} & 0 & 0 & 0 & 0 & 0 \end{array}\right]^T, \quad P_r(t_0) = \left[\begin{array}{cc} P_{11}(t_0) & 0_{3\times3} \\ 0_{3\times3} & 0_{3\times3} \end{array}\right]. \tag{83}$$

If the HCW transition matrix is partitioned as $\Phi_{HCW}(t,t_0) = \left[\begin{array}{cc} \Phi_{11}(t,t_0) & \Phi_{12}(t,t_0) \\ \Phi_{21}(t,t_0) & \Phi_{22}(t,t_0) \end{array}\right]$ according to the partitioning of the covariance matrix, by (80) and (82),we get that:

$$m_r(t) = \left[\begin{array}{cccccc} m_{r_{r_{10}}} & 0 & 0 & 0 & 0 & 0 \end{array}\right]^T, \quad P_r(t) = \left[\begin{array}{cc} \Phi_{11}(t,t_0)P_{11}(t_0)\Phi_{11}(t,t_0)^T & \Phi_{11}(t,t_0)P_{11}(t_0)\Phi_{21}(t,t_0)^T \\ \Phi_{21}(t,t_0)P_{11}(t_0)\Phi_{11}(t,t_0)^T & \Phi_{21}(t,t_0)P_{11}(t_0)\Phi_{21}(t,t_0)^T \end{array}\right]. \tag{84}$$

The initial isotropic Gaussian pdf of the relative position has a covariance $P_{11}(t_0) = \bar{\sigma}^2 I_{3\times 3}$ and therefore:

$$P_r(t) = \bar{\sigma}^2 \left[\begin{array}{cc} \Phi_{11}(t,t_0)\Phi_{11}(t,t_0)^T & \Phi_{11}(t,t_0)\Phi_{21}(t,t_0)^T \\ \Phi_{21}(t,t_0)\Phi_{11}(t,t_0)^T & \Phi_{21}(t,t_0)\Phi_{21}(t,t_0)^T \end{array} \right].$$

Due to the form of this covariance matrix, it is to be noted that the variances of the random variables r_r are not likely to be affine function of t as is claimed and enforced in references [22] and [23].
Let see what are the consequences of these choices on the computations involved in the derivation of the collision probability (39) and in particular in the calculation of the integral $I(\hat{n},t)$. First, if $m_r(t) = m_r(t_0)$ and in particular, $m_{v_r}(t) = 0_{3\times 1}$ and considering the HCW transition matrix then:

$$\begin{array}{rcl} m_\epsilon(\theta,\phi,t) & = & \hat{n}^T(m_{v_r} - P_{12}^T(t)P_{11}^{-1}(t)m_{r_r}) = -\hat{n}^T P_{12}^T(t)P_{11}^{-1}(t)m_{r_r}(t) \\ & = & -\hat{n}^T\Phi_{21}(t,t_0)\Phi_{11}(t,t_0)^{-1}m_{r_r}(t) = 0 \end{array} \tag{85}$$

Note that we need the invertibility of $\Phi_{11}(t,t_0)$, $\forall\ t \in [t_0, t_0+T]$ which is ensured by assuming that $n(t-t_0) \neq \pi/2 + k\pi$, $\forall\ t \in [t_0, t_0+T]$. The function $\epsilon_0(\hat{n},t) = R\hat{n}^T P_{12}^T(t)P_{11}^{-1}(t)\hat{n} = R\hat{n}^T\Phi_{21}(t,t_0)\Phi_{11}(t,t_0)^{-1}\hat{n}$ which is given by:

$$\epsilon_0(\hat{n},t) = R\hat{n}^T \left[\begin{array}{ccc} 0 & 0 & \frac{6n(1-c_t)}{4-3c_t} \\ 0 & -\frac{ns_t}{c_t} & 0 \\ 0 & 0 & \frac{3ns_t}{4-3c_t} \end{array} \right] \hat{n}. \tag{86}$$

The function $\epsilon_0(\hat{n},t)$ is a quadratic form which may be 0, positive or negative when the vector $\hat{n}$ covers the whole surface of a 3D unit sphere.

1- If $\epsilon_0(\hat{n},t) = 0$ then

$$I(\hat{n},t) = \frac{\sigma}{\sqrt{2\pi}}. \tag{87}$$

2- If $\epsilon_0(\hat{n},t) \neq 0$ then

$$I(\hat{n},t) = \frac{\sigma}{\sqrt{2\pi}} e^{-\frac{\epsilon_0^2(\hat{n},t)}{2\sigma^2}} - \frac{\epsilon_0(\hat{n},t)}{2}\left[1 - \mathrm{erf}\left(\frac{\epsilon_0(\hat{n},t)}{\sqrt{2}\,\sigma}\right)\right]. \tag{88}$$

Similarly, the variance σ of ϵ may be obtained as:

$$\sigma^2(\theta,\phi,t) = \hat{n}^T(P_{22}(t) - P_{12}^T(t)P_{11}(t)^{-1}P_{12}(t))\hat{n} = 0. \tag{89}$$

Thus, the rationale behind the derivation of (41) may be used here to compute the actual integral $I(\hat{n},t)$.

$$\lim_{\sigma\to 0^+} I(\hat{n},t) = \left\{ \begin{array}{cc} -\epsilon_0(\hat{n},t) & \text{if} \quad \epsilon_0(\hat{n},t) < 0 \\ 0 & \text{if} \quad \epsilon_0(\hat{n},t) \geqslant 0. \end{array} \right. \tag{90}$$

Finally, the collision probability $\mathcal{P}_I(T)$ must be computed as:

$$\mathcal{P}_I(T) = -\int_{t_0}^{t_0+T}\int_0^{2\pi}\int_0^{\pi} R^2 \sin(\phi)\,\rho_{tr}(r_r(\theta,\phi))1_{\epsilon_0(\hat{n},t)<0}(\theta,\phi,t)\epsilon_0(\hat{n},t)\mathrm{d}\phi\mathrm{d}\theta\mathrm{d}t. \tag{91}$$

The reference [22] uses Equation (43) to compute $\mathcal{P}_I(T)$ which is not the right thing to do considering the previous developments. The computation that is used in the companion paper [23] is nevertheless interesting and will prove to useful for the derivation of a new methodology (see Section 3). With the assumptions of [23], the situation may be summarized and illustrated by Figure 11

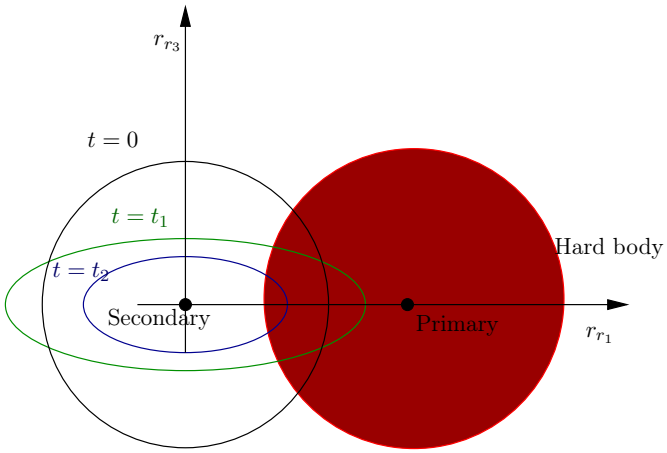

Figure 11: $1-\sigma$ sphere at $t = 0$ (black), $1-\sigma$ ellipses for $t = t_1$ (green) anf for $t = t_2$ (blue) with the hardbody collision sphere (red).

The local frame has its origin at the secondary object so that the σ-ellipses (or spheres) are centered at this point. The combined hard body sphere is centered at the primary which mean motion is considered to be stationary at the abscissa $m_{r_{r_{10}}}$. At $t = 0$, the pdf for the uncertainty relative state (defined in the plane (r_{r_1}, r_{r_2})) is an isotropic Gaussian 2D pdf defined as:

$$\rho_{r_{r_1} r_{r_3}} \sim \mathcal{N}(\begin{bmatrix} m_{r_{r_{10}}} & 0 \end{bmatrix}^T, \overline{\sigma}_0^2 I_2). \tag{92}$$

In each direction, the uncertainty at time t is supposed to remain Gaussian but characterized by a time-varying standard deviation $\sigma_{r_1}(t) = \overline{\sigma}_0 + \alpha t$ and $\sigma_{r_2}(t) = \overline{\sigma}_0 + \beta t$ respectively, with $\alpha > \beta > 0$ which means that the time-dependent pdf at time t is no more isotropic. The Author proposes then to make a change of variables on the relative position to render isotropic the time-dependent pdf at each time t. This implies to scale the hard body sphere to get a different ellipse at each time t. Figuring out the analytical equation of the envelope of the volume swept by the hard body during the encounter duration, it is then proposed to integrate the isotropic density over this volume to get the probability of collision. This approach is quite appealing and a new approach will be based on the idea of the integration of the initial pdf over the swept volume of the hard body sphere during the encounter duration. Unfortunately, apart the theoretical approximations of the exposition, this idea is quite misleading in the particular case analyzed by Chan. Indeed, all the samples drawn from the pdf and belonging to the hard body sphere at time $t = 0$ are initial conditions leading to a collision at $t = 0$. As the hard body is stationary since the hovering is stationary, these samples will lead to a collision at any time $t \geqslant t_1$. This means that the possible collisions issuing from these initial conditions will counted several times for the computation of the probability of collision and it is clear that the Assumption 2 (only one entering crossing) is violated here. This particular example cannot be used to show that the Coppola's formulation breaks down since the method has not been intended to work on such cases. In this particular case, the probability of collision should be computed as $\mathcal{P}_0 = \mu_I(\mathcal{X}_T^{00})$.

2.6.3 Elliptical relative motion with small drift and/or with high eccentricity

These two examples are simultaneously dealt with since the argument used by the Author of [22] is the same for both examples. K. Chan shows that under specific assumptions about the relative

motions (mainly an elliptic relative motion with none (but high eccentricity) or a small drift of the secondary around the primary), the two objects may experience multiple high-risk close approach events over the time interval of interest $[t_0, t_0+T]$. This is clearly in contradiction with Assumption 2 of only one entering crossing in the forbidden region $\mathcal{X}_R$ used to derive the 3D PoC formula. Therefore, this formula should not be used in such a context and the flaws pointed out by K. Chan in [22] are not fair as in the previous example.

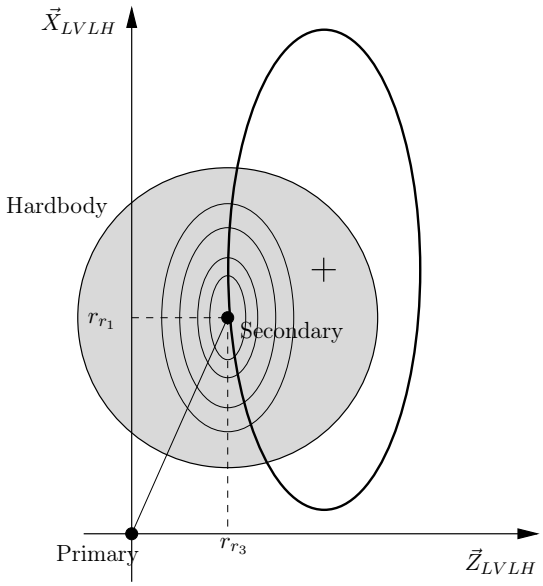

Figure 12: Encounter definition for Chan's examples 1 and 2 from [22].

2.6.4 Expanding spherical pdf

This last example is even poorly presented than the three previous one. The position of the secondary is not defined and what is known for sure is that the primary mean motion is assumed to be rectilinear with a constant velocity in the local orbital frame. At $t = 0$, the primary object is located at the origin of the frame and so is the hard body sphere which is attached to the mean position of the primary object. One may deduce (or assume) that the mean relative free motion, following the HCW equations (81), is given as:

$$\begin{array}{rcl} m_{r_{r_1}}(t) & = & 3(2m_{r_{r_{30}}} - m_{v_{r_{10}}}/n)\delta t, \\ m_{r_{r_2}}(t) & = & 0, \\ m_{r_{r_3}}(t) & = & 2(2m_{r_{r_{30}}} - m_{v_{r_{10}}}/n), \\ m_{v_{r_1}}(t) & = & 3(2nm_{r_{r_{30}}} - m_{v_{r_{10}}}), \\ m_{v_{r_2}}(t) & = & 0, \\ m_{v_{r_3}}(t) & = & 0, \end{array} \tag{93}$$

under the conditions $3nm_{r_{r_{30}}} - 2m_{v_{r_{10}}}$ and $m_{r_{r_{10}}} = m_{r_{r_{10}}} = m_{v_{r_{20}}} = m_{v_{r_{30}}} = 0$. It is then assumed that the initial Gaussian isotropic pdf at time $t = 0$, $\rho_{r_{r_0}} \sim \mathcal{N}(m_{r_0}, \overline{\sigma}_0^2 I_3)$, will be such that the $1-\sigma$ will expand with the same constant velocity $m_{v_{r_1}}(t) = m_{v_{r_1}}$ (see Figure 13), meaning that $\rho_{tr_r} \sim \mathcal{N}(m_{r_r}(t), \overline{\sigma}(t)^2 I_3)$ with $\overline{\sigma}(t) = R + 3(2nm_{r_{r_{30}}} - m_{v_{r_{10}}})t$, which is not consistent with the propagation of the covariance matrix as given by Equation (84).

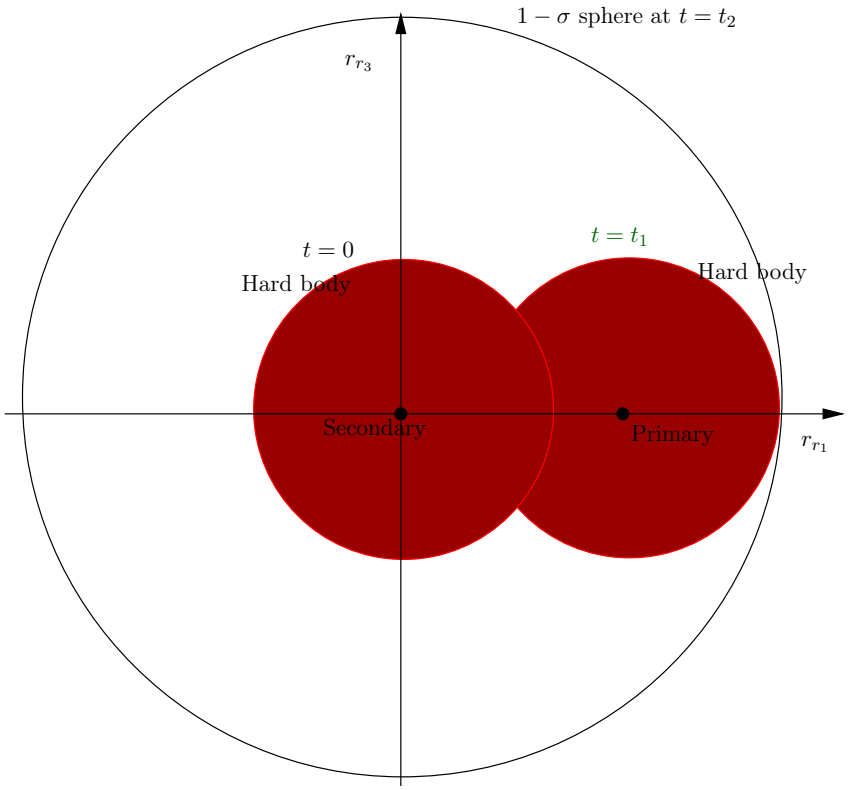

Figure 13: Expanding $1-\sigma$ sphere at $t=t_1$ (black) and drifting hardbody collision sphere (red).

Since the hard body sphere remains tangent to the time-varying $1-\sigma$ sphere of the pdf at time t, the Author seems to deduce that the cumulative probability is constant i.e. the probability rate is zero though the Coppola's formulation given in Equation (43) cannot be zero since the relative velocity is not zero. Once again, K. Chan should have been more careful when analyzing Coppola's formulation and should have made the preliminary analysis of the Coppola's formulation, starting from (39) and evaluating precisely the inner integral as it has been done for the first counter-example presented in this report. Note that all samples drawn in the $1-\sigma$ sphere of the pdf at time $t=0$ will lead to a collision at $t=0$ since it is included in the hard body sphere at $t=0$. Note also that any point of the hard body sphere defined at $t=t_1$ (corresponding to collision at that time) will be retro-propagated to the hard-body sphere at $t=0$ to produce a collision domain $\mathcal{X}_t^0$ which is exactly the initial hard body collision sphere. Once again, the Coppola's formulation cannot be used here for the very same argument as before and the probability of collision is given as $\mathcal{P}_0=\mu_I(\mathcal{X}_T^{00})\simeq 0.3935$.

3 An alternative method for long-term encounters

3.1 Introduction

Remember first from (5) that the probability of collision is given as follows:

$$\mathcal{P}_c([t_0,t_0+T])=\mathcal{P}_c(T,t_0)=\mathbb{P}(X_{ps}^0\in\mathcal{X}_T^0)=\mu_I(\mathcal{X}_T^0)=\int_{\mathcal{X}_T^0}\mathrm{d}\mu_I, \tag{94}$$

where $\mathcal{X}_T^0$ is the set of all the relative initial conditions which generate collisions on the time interval $t \in [t_0, t_0 + T]$. If the distribution of these relative initial conditions is assumed to be Gaussian with a density $\rho_I \sim \mathcal{N}(m_I, P_I)$ then the computation of the collision probability $\mathcal{P}_c([t_0, t_0 + T])$ boils down to the computation of the integral formula:

$$\mathcal{P}_c([t_0, t_0 + T]) := \frac{1}{\sqrt{(2\pi)^n \det(P_I)}} \int_{\mathcal{X}_T^0} e^{-\frac{1}{2}(X-m_I)^T P_I^{-1}(X-m_I)} \mathrm{d}X. \tag{95}$$

First, it is necessary to characterize more precisely the set $\mathcal{X}_T^0$ on which the integration is performed. Keeping in mind the definitions given in Section 2 of this report, a simple illustration of the points making up this set is given at Figure 14.

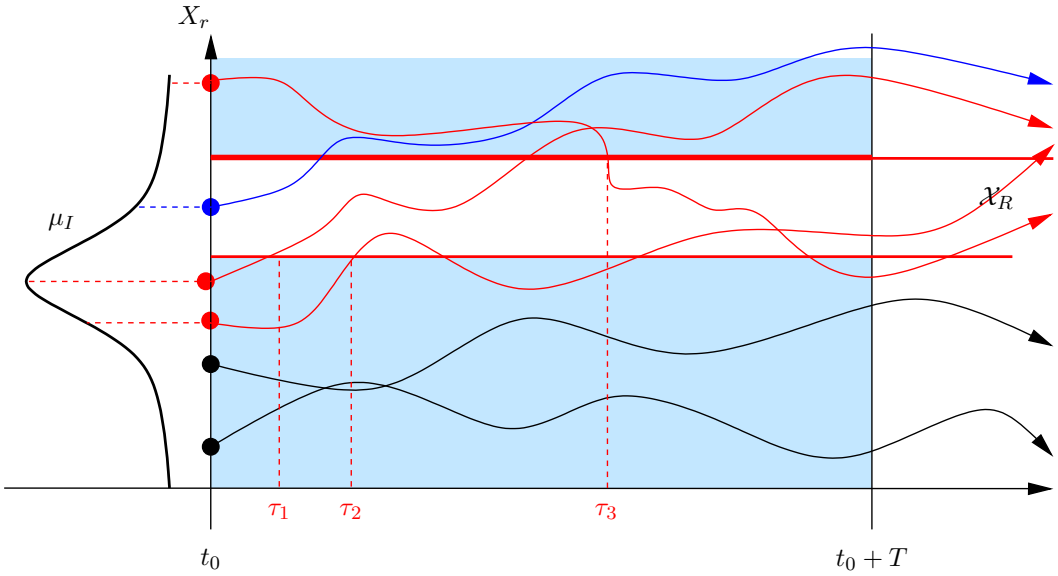

Figure 14: $1 - D$ illustration of the construction of $\mathcal{X}_T^0$ for $t_{TCA} = t_0$ - blue point: $\tau = t_{TCA}$, red points: $\tau > t_{TCA}$, black points: $\nexists\, \tau \in [t_0, t_0 + T] \mid X_r(\tau | X_r^0) \in \mathcal{X}_T^0$.

Obviously, these points are given by $X_r^0 = \varphi_t^{t_0}(X_r(\tau | X_r^0))$ where $\varphi_t^{t_0}$ is the inverse flow of the relative dynamics and τ is the first hitting time (i.e. $X(\tau | X_r^0) \in \partial\mathcal{X}_R$). The idea is then to build the set $\mathcal{X}_T^0$ by propagating backward and forward (if needed depending on the chosen time $t_{TCA} \in [t_0, t_0 + t_{TCA}]$) all the relative states $X_r(t | X_r^0)$ of the set $\mathcal{X}_R$ for each time $t \in [t_0, t_0 + t_{TCA}]$. The Figure 15 depicts an example of the building of the set $\mathcal{X}_T^0$ for a spherical hard body $\mathcal{X}_R$ and linear relative dynamics.

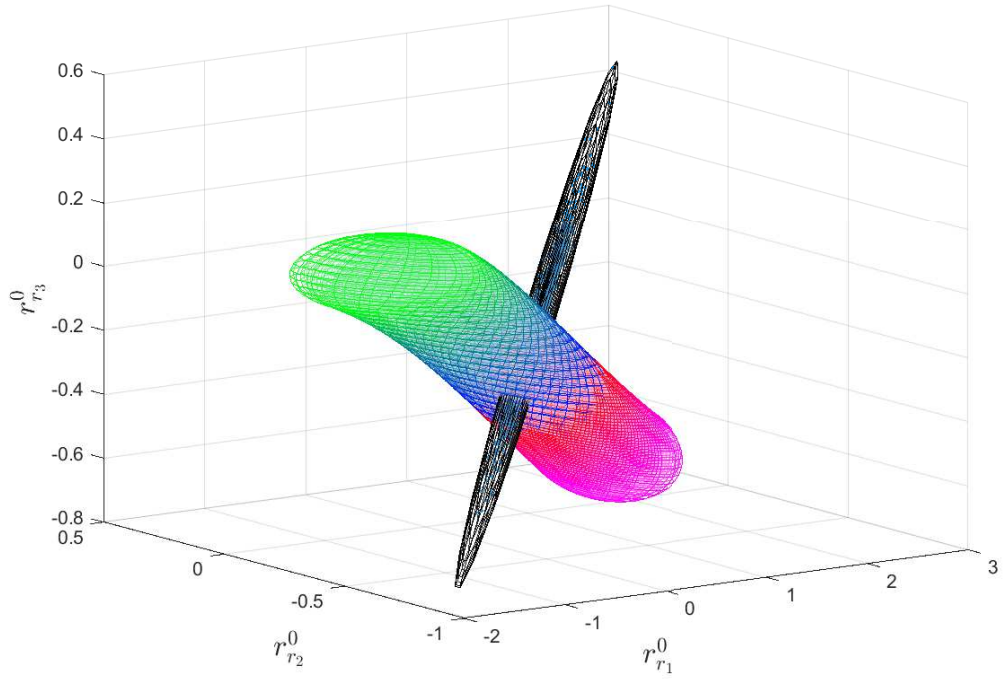

Figure 15: $4-\sigma$ ellipsoid of the Gaussian density (black) and $\mathcal{X}_T^0$ at TCA: red ($t_0 \leqslant t \leqslant t_{TCA}$) - blue ($t = t_{TCA}$) - red ($t_{TCA} < t \leqslant t_0 + T$).

In practice, the set on which the integration must be calculated is very difficult to determine analytically, so various simplifications have been made in literature as shown in the previous sections. Let us detail the ones necessary for the purpose of this work:

- The forbidden region $\mathcal{X}_R$ has a simple form. For instance, in the case of two objects, this describes the fact that the relative distance between them is less than a certain given radius threshold R. It is thus assumed that $\mathcal{X}_R$ is a basic real semi-algebraic set (described by a finite sequence of polynomial inequalities).

- As it has been seen previously, the relative dynamics are usually simplified. In what follows, we consider two objects, whose *relative dynamics flow is linear and invertible* and the solution of the relative dynamics equation is known via a given state transition matrix $\Phi(\cdot, t_0) : [t_0, t_0 + T] \to \mathbb{R}^6$, such that
$$X(t|x_0) = \Phi(t, t_0)X_0, \text{ for } t \in [t_0, t_0 + T].$$

Within this frame and using the two previous assumptions, we propose to tackle the integral (95) in two main steps:

1. ***Implicit representation of the integration domain by a polynomial superlevel set.*** The domain of integration $\mathcal{X}_T^0$ (see Equation (4)) is approximated by so-called polynomial superlevel sets (PSS) [30] (see also [41, 51] for similar works and [17, Chap. 3,p. 75] for the definition of superlevel set). More precisely, suppose that $\mathcal{X}_T^0$ can be outer-bounded by a hyper-rectangle $\mathcal{B} \supseteq \mathcal{X}_T^0$, with
$$\mathcal{B} = [a, b] := \{x \in \mathbb{R}^n, a_i \leqslant x_i \leqslant b_i, \text{ for } i = 1, 2, \ldots, n\}, \ a, b \in \mathbb{R}^n. \tag{96}$$

Definition 5 (polynomial superlevel set)**.**

A polynomial superlevel set (PSS) for $\mathcal{X}_T^0$ is defined by a polynomial $p_d \in \mathbb{R}[x]_d$, such that

$$\mathcal{X}_T^0 \subseteq \mathrm{PSS}_{p_d} := \{x \in \mathcal{B} : \, p_d(x) \geqslant 1\}. \tag{97}$$

Note that in this definition, the usual notation x for the indeterminate of the polynomial is used (as it is also used in Section 3.2 while when necessary, it will be denoted by X for the relative state. We believe that the context will clear enough to prevent any confusion.

The polynomial p_d defining the PSS approximation can be seen as an approximation of the indicator function $1_{\mathcal{X}_T^0}$ of the set $\mathcal{X}_T^0$. As shown in [30], such suitable approximations can be obtained by solving a convex optimization problem whose constraints are linear matrix inequalities (LMIs). Moreover, as the degree of the approximation d increases, the sequence $(p_d)_{d\geqslant 1}$ converges in $\mathcal{L}^1$-norm, almost uniformly and almost everywhere to the indicator function of the set $\mathcal{X}_T^0$ of interest. The set approximations provided by the method of [30] can be thought as a direct generalization of classical ellipsoidal set approximations, in the sense that if second degree approximations are used, we exactly recover well-known semi-definite optimization-based approaches (see for example [17, Chap. 8, pp. 410-414] and [16, Section 3.7]).

2. ***High-order quadrature for volumes implicitly defined by a polynomial superlevel set.*** For a fixed p_d, the integral (95) is approximated by:

$$\mathcal{P}_c([t_0, t_0+T]) \leqslant \frac{1}{\sqrt{(2\pi)^n \det(P_I)}} \int\limits_{\mathrm{PSS}_{p_d}} e^{-\frac{1}{2}(X-m_I)^T P_I^{-1}(X-m_I)} \mathrm{d}X. \tag{98}$$

Several methods exist for computing this integral of an n-variate Gaussian density, where the integration domain is implicitly defined by a polynomial [47, 41, 50]. However, a good complexity vs. accuracy trade-off analysis is more challenging to obtain, especially since, in practice, the ambient space dimension n is at least 3. To this end, for $n = 3$, we considered building an adaptive Gauss quadrature integration scheme based on the work presented in [67]. By converting the implicitly defined geometry into the graph of an implicitly defined height function, it leads to a recursive algorithm on the number of spatial dimensions which requires only one-dimensional root finding and one-dimensional Gaussian quadrature. The computed quadrature scheme yields strictly positive quadrature weights and inherits the high-order accuracy of Gaussian quadrature. Currently, for $n = 6$, blunt Monte-Carlo sampling is used, but more involved methods are to be studied and tested.

K. Chan formulated the need to find a suitable description of the volume of initial states (at a fixed time t_0) which lead to collisions during a given time interval $[t_0, T + t_0]$ in a series of works [23, 24]. He understood that the hard-body sphere (with radius R equal to the combined radius of the two spherical satellites) is mapped to a non-spherical volume at every instant of time t, which results in a union of non-spherical and non-disjoint volumes, known as the *"derived ellipsoid"*, since roughly speaking, for linearized dynamics with no velocity uncertainty, the hard-body sphere is mapped to an ellipsoid each time t (see Section 3.3.2 for more details). This is also sometimes called the *swept-volume*, a definition which was coined mainly in the case of rectilinear relative motion, when the hard-body sphere sweeps out a volume looking like a long circular cylinder extending along the direction of relative velocity.

Thus, for simplicity, we also call *swept-volume* the set $\mathcal{X}_T^0$, even in the general case of a non-rectilinear motion, when this volume is non-convex or in the higher-dimensional case (when for instance, both the relative positions and velocities are uncertain and hence the volume is 6 dimensional and not necessarily compact). In the works of Chan and also more recently in [77], a swept-volume defined by a union of ellipsoids is characterized by its envelope. This is computed numerically in the 3-dimensional case, or in an *ad-hoc* manner, with various trivial simplifications for lower dimensional cases. However, a general method relying both on an effective characterization of the swept-volume (when its shape is not trivially reduced to a cylinder) and on the computation of the subsequent integral of the Gaussian density over such a volume is missing in literature.
Note also that a different class of methods exists, which intends to deal with the highly complex shape of $\mathcal{X}_T^0$ by a different strategy: instead of considering at t_0 the image of the hard-body through the inverse flow, one propagates the initial uncertainty i.e., one considers the pushforward measure by the flow of the Gaussian measure at t_0. Roughly speaking this corresponds to performing a change of variable in the integral (95). The forward propagation of uncertainty is employed by Coppola's method [28] or the so-called methods of adjoining cylinders/parallelepipeds [5, 7]. Without entering the details, it is important to note that these methods work only under the assumption that a bijective map can be found between the set $\mathcal{X}_T^0$ and its image through the flow, during the time interval $[t_0, t_0 + T]$. In particular it implies that repeated encounters (when t in Equation (4) is not unique)) can not be correctly treated.
The present formulation, taking place in the framework of polynomial optimization, has the advantage of providing approximate closed-form descriptions of the collision-prone states $\mathcal{X}_T^0$ which can be effectively used for long-term and repeated conjunctions. Actually, even a visual accurate outer-approximation of $\mathcal{X}_T^0$ can provide an important insight on the practical type of encounter. For instance, a straight cylinder form can confirm some of the fast encounter assumptions. The PSS approximation allows for highly non-convex shapes to be represented, which in turn allows for further analysis of so-called long-term encounters. Another important advantage is that providing a PSS approximation of $\mathcal{X}_T^0$ allows for an implicit representation of *all* collision prone-states and in turn, for evaluating directly the integral (98), without introducing additional assumptions regarding uncertainty propagation or repeated conjunctions. This method allows for handling practical cases without the paramount Assumption 2 that *each initial condition enters the forbidden region at only one unique specific time*, which was required by previous methods like those of Coppola [28], or the adjoining cylinders/bundled parallelepipeds of Alfano [5].
Let us firstly recall the theoretical mathematical modeling and numerical solution as developed in [30, 41, 51]. In a second time, this is to be adapted to our setting of approximating the so-called *swept-volume*. Note that $t_{TCA} = t_0$ in the following without loss of generality. The proposed algorithms are easily tunable for a different case $t_0 < t_{TCA} < t_0 + T$.

3.2 PSS approximations of bounded semi-algebraic sets

Let a semi-algebraic set $\mathcal{K}$ be described by given real multivariate polynomials $g_i \in \mathbb{R}[x]_{d_i}$:

$$\mathcal{K} = \{x \in \mathbb{R}^n \, : g_i(x) \geqslant 0, i = 1, 2, \ldots, m\}\,, \tag{99}$$

and a bounding set $\mathcal{B} \supseteq \mathcal{K}$ as in Equation (96). We are interested in computing the coefficients of a sequence $(p_d)_{d \geqslant 1}$ of good polynomial outer-approximations $p_d \in \mathbb{R}[x]_d$, to the indicator function $1_{\mathcal{K}}$, in the sense that the polynomial superlevel set (PSS)

$$\mathrm{PSS}_{p_d} := \{x \in \mathcal{B} : \, p_d(x) \geqslant 1\},$$

converges strongly to $\mathcal{K}$ when $d \to \infty$.

3.2.1 Formulation as a polynomial optimization problem

Such a sequence can be found considering the following optimization problem, for each fixed d:

$$\begin{aligned} w_d^* = \quad & \inf_{p \in K[x]_d} \|p\|_1, \\ & \text{s.t.} \quad p \geqslant 0 \,\text{on}\, \mathcal{B}, \\ & \qquad p \geqslant 1 \,\text{on}\, \mathcal{K}. \end{aligned} \tag{100}$$

For completeness, note that this problem is closely related to the one of computing the volume of the semi-algebraic set $\mathcal{K}$. More precisely, one can consider the following infinite-dimensional linear programming problem in the cone of positive measures:

$$\begin{aligned} v^* = \quad & \sup_{\mu_0, \hat{\mu}_0} \mu_0(\mathcal{B}), \\ & \qquad \mu_0 + \hat{\mu}_0 = \lambda_{\mathcal{B}}, \\ & \text{s.t.} \quad \text{supp}(\mu_0) \subseteq \mathcal{K}, \\ & \qquad \text{supp}(\hat{\mu}_0) \subseteq \mathcal{B}, \\ & \qquad \mu_0, \hat{\mu}_0 \geqslant 0. \end{aligned} \tag{101}$$

where $\lambda_A = \text{vol}(A)$ is the Lebesgue measure of the set $A \subset \mathcal{B}$. This can be interpreted as: one searches to maximize the mass of a positive measure μ_0 whose support is included in $\mathcal{K}$ and which is dominated by the Lebesgue measure $\lambda_{\mathcal{B}}$ on $\mathcal{B}$. This translates to an equality constraint by introducing the slack variable $\widehat{\mu}_0$ such that $\mu_0 + \hat{\mu}_0 = \lambda_{\mathcal{B}}$. The second and third constraints ensure that the support of the respective measures is in the admissible domain $\mathcal{K}$ and respectively $\mathcal{B}$. The last constraints ensure that μ_0 and $\hat{\mu}_0$ are nonnegative measures (see [12] for very similar developments and additional details).
It is proven in [30, 41] that the supremum of Problem (101) is attained and $v^* = \text{vol}(\mathcal{K})$. Moreover, the infimum of Problem (100) is attained for a polynomial $p_d^* \in \mathbb{R}[x]_d$, with $\text{PSS}_{p_d^*} \supseteq \mathcal{K}$, $w_{d+1}^* \leqslant w_d^*$ and $\lim_{d \to \infty} w_d^* = \text{vol}(\mathcal{K})$.

3.2.2 LMI hierarchy to compute the PSS

In this section, we provide the basic details on the numerical computation of the solution of Problem (100) (or its dual Problem (101)), which is now more or less standard in the field of *Polynomial Optimization* [49].
Note that in Problem (100), we aim at finding a polynomial $p \in \mathbb{R}[x]_d$ such that

- p is positive on $\mathcal{B}$,
- $p - 1$ is positive on $\mathcal{K}$.

In order to obtain a numerically solvable problem, one enforces positivity by requiring the polynomial to be sum-of-squares (SOS). Let us denote the convex cone of real polynomials that are SOS by $\Sigma^2[x] \subset \mathbb{R}[x]$ and respectively, $\Sigma^2[x]_{2k} \subset \mathbb{R}[x]_{2k}$, its subcone of SOS polynomials of degree at most $2k$. Using Putinar's Positivstellensatz [48, 64, 49], Problem (100) becomes, when fixing $r \in \mathbb{N}$:

$$
\begin{aligned}
w*_{2r,d} = \quad & \inf_{p\in\mathbb{R}[x]_d} \int_{\mathcal{B}} p(x)\mathrm{d}x, \\
& \text{s.t.} \\
& \left.\begin{array}{l} p - \sigma_{0,\mathcal{B}} - \sum\limits_{1\leqslant j\leqslant n} (x_j - a_j)(b_j - x_j)\sigma_{j,\mathcal{B}} = 0 \\ \sigma_{0,\mathcal{B}} \in \Sigma^2[x]_{2r}, \\ \sigma_{j,\mathcal{B}} \in \Sigma^2[x]_{2(r-1)},\ \forall j = 1,\cdots,n, \end{array}\right\} p \geqslant 0 \,\text{on}\, \mathcal{B} \\
& \left.\begin{array}{l} p - \sigma_{0,\mathcal{K}} - \sum\limits_{1\leqslant j\leqslant m} g_j\sigma_{j,\mathcal{K}} = 1 \\ \sigma_{0,\mathcal{K}} \in \Sigma^2[x]_{2r}, \\ \sigma_{j,\mathcal{K}} \in \Sigma^2[x]_{2(r-\lceil d_j/2\rceil)},\ \forall j = 1,\cdots,m, \end{array}\right\} p \geqslant 1 \,\text{on}\, \mathcal{K},
\end{aligned}
\tag{102}
$$

Problem (102) is now tractable in software:

- its objective function $\int_{\mathcal{B}} p(x)\mathrm{d}x = \sum_{0\leqslant|i|\leqslant d} p_i \int_{\mathcal{B}} x^i \mathrm{d}x$ is a linear function of the coefficients p_i of the polynomial p, while the involved integrals on the bounding box $\mathcal{B}$ can be effectively computed and correspond to moments up to degree d of the Lebesgue measure on $\mathcal{B}$.
- The constraints can be recast in terms of Linear Matrix Inequalities (LMIs); this is already a classical strategy and several software tools are available to model problems of the form above, like for instance the Matlab Toolbox YALMIP [56].
- This boils down to solving only a semi-definite programming problem (whenever the degrees d and r are fixed).

One can prove that when $r \to \infty$, the value of Problem (102) converges to w^*_d and moreover, for any $2r \geqslant d$, the solution $p^*_{2r,d}$ of Problem (102) satisfies the constraints of Problem (100) i.e., $\mathrm{PSS}_{p^*_{2r,d}}$ is a PSS approximation of $\mathcal{K}$.

Remark 9 (Numerical Solving and Possible Improvements)**.**
For each fixed d and r, Problem (102) *can be written as a semidefinite program (SDP), which is a conic convex optimization problem that can be solved efficiently (in time polynomial in its input size) up to arbitrary precision fixed in advance. Numerical solvers like Mosek SDP solver [60] can be employed. However, when the whole hierarchy of relaxations is solved i.e., d is increased, the observed convergence is slow, mainly due to the Gibbs phenomenon, since the polynomial $p^*_{2r,d}$ approximates the indicator function $1_{\mathcal{K}}$, which is discontinuous. The works [41, 51] further improve on this issue and the implementation can be adjusted to include them.*

Let us now describe how we can compute PSS approximations of the so-called *swept-volume*.

3.3 PSS approximations of the swept-volume in relative dynamics

Recall that the swept-volume is defined as the set of *all initial conditions $X^0_r \in \mathbb{R}^n$ which lead to at least a collision during the time span $[t_0, t_0 + T]$*. When considering two objects and the fact that the solution of the relative dynamics equation is known via a given state transition matrix $\Phi(t, t_0)$, one has:

- The relative position and velocity are given at any time t by $X_r(t|X^0_r) = \Phi(t, t_0)X^0_r$, with $X^0_r \in \mathbb{R}^6$;

- The collision region is defined simply by $\mathcal{X}_R := \{r_r \in \mathbb{R}^3 : R^2 - r_r^T r_r \geqslant 0\}$;

Thus, equation (4) defining the swept-volume $\mathcal{X}_T^0$ becomes:

$$\mathcal{X}_T^0 = \left\{ X_r^0 \in \mathbb{R}^6 : \exists t \in [t_0, t_0 + T] \,\text{s.t.}\, R^2 - {X_r^0}^T \Phi(t, t_0)^T I_{11} \Phi(t, t_0) X_r^0 \geqslant 0 \right\}, \tag{103}$$

where the matrix $I_{11} \in \mathbb{R}^{6\times 6}$ is defined by $I_{11} := \begin{pmatrix} I_3 & 0 \\ 0 & 0 \end{pmatrix}$. Note that this appears in the formula simply because only the positions (first 3 coordinates of $X_r(t|X_r^0)$) at each time t are constrained to belong to $\mathcal{X}_R$.
The main idea is to describe the *swept-volume* $\mathcal{X}_T^0$ by semi-algebraic constraints, which can then be approximated by PSS, as we have shown in Section 3.2. Since $\mathcal{X}_R$ is a basic semi-algebraic set, several options are possible for keeping this setting: (1) obtain an *approximate* polynomial transition matrix $\Phi(t, t_0)$ – this is a univariate approximation in t, which means that $X_r(t|X_r^0)$ is a vector of polynomials in the variables t, X_r^0; or (2) consider a sufficiently fine discretization of size N, $\tau_N := \{t_0 \leqslant t_1 \leqslant \cdots \leqslant t_i \leqslant \cdots \leqslant t_0 + T\}$, which implies that $X_r(t_i|X_r^0)$ is linear in X_r^0 for each fixed grid value t_i. We consider the second option, for simplicity of implementation, in what follows.

3.3.1 PSS approximations of discretizations of the swept-volume

When considering a discretization on time, the constraint describing a subset $\mathcal{K}_i \subseteq \mathcal{X}_T^0$ corresponding to each t_i is:

$$\mathcal{K}_i := \{X_r^0 \in \mathbb{R}^6 : R^2 - {X_r^0}^T \Phi(t_i, t_0)^T I_{11} \Phi(t_i, t_0) X_r^0 \geqslant 0\}, \tag{104}$$

This discretization provides an approximate description of $\mathcal{X}_T^0$ as a union of basic semi-algebraic sets:

$$\bigcup_{i=1,\ldots,N} \mathcal{K}_i \subseteq \mathcal{X}_T^0. \tag{105}$$

Two observations are important: in general, the sets $\mathcal{K}_i$ are not disjoint and moreover, they are not compact.
The fact that they are not disjoint does not constitute an issue for the PSS-like method to be described in what follows. Let us stress that this also implies that imposing *only one crossing* i.e., there is only one t_i corresponding to each X_r^0 is not necessary for this method.
However, the fact that $\mathcal{K}_i$ are not compact, needs to be handled.

Computing the Bounding Box $\mathcal{B}$. A straightforward solution is to rely on the fact that a PPS computed for $\bigcup_{i=1,\ldots,N} \mathcal{K}_i$ is the volume on which the multivariate Gaussian density is to be integrated afterwards. Hence, one can consider, function of the numerical requirements, a suitable $\ell-\sigma$ ellipsoid corresponding to the given covariance matrix P_I (say $\ell = 6$ in practice maybe add some bound from other papers) and bound it by a hyper-rectangle $\mathcal{B}$. Then, each of the sets $\overline{\mathcal{K}}_i = \mathcal{K}_i \cap \mathcal{B}$ for $i = 1, \ldots, N$ is compact.

PSS for the 6-dimensional swept-volume. We are now ready to state the optimization problem to be solved:

Problem 2 (Approximate PSS Computation for the swept-volume)**.**

Let the semi-algebraic set $\overline{\mathcal{K}} = \bigcup_{i=1,\ldots,N} \overline{\mathcal{K}}_i$ *be given by the union of* N *basic compact semi-algebraic sets* $\overline{\mathcal{K}}_i$*, a given bounding hyper-rectangle* $\mathcal{B} \supseteq \overline{\mathcal{K}}$ *and also a fixed degree* d*. Solve the optimization problem*

$$\begin{aligned} w^*_{d,\overline{\mathcal{K}}} = \quad & \inf_{p \in K[X^0_r]_d} \|p\|_1, \\ & p \geqslant 0 \,\text{on}\, \mathcal{B}, \\ \text{s.t.} \quad & p \geqslant 1 \,\text{on}\, \overline{\mathcal{K}}_1, \\ & \ldots, \\ & p \geqslant 1 \,\text{on}\, \overline{\mathcal{K}}_N. \end{aligned} \tag{106}$$

The main result is the following.

Theorem 3. *The infimum in Problem* (106) *is attained for a polynomial* $p^*_{d,\overline{\mathcal{K}}} \in \mathbb{R}[X^0_r]_d$*. Moreover,* $\mathrm{PSS}_{p^*_{d,\overline{\mathcal{K}}}} \supseteq \overline{\mathcal{K}}$*,* $w^*_{d+1,\overline{\mathcal{K}}} \leqslant w^*_{d,\overline{\mathcal{K}}}$ *and* $\lim_{d\to\infty} w^*_{d,\overline{\mathcal{K}}} = \mathrm{vol}(\overline{\mathcal{K}})$*.*

Proof. The proof is similar to the one given in [30, Thm. 2]. Note also another similar proof in [51], which considers the dual problem in the space of positive measures, which can be formulated as:

$$\begin{aligned} v^*_{d,\overline{\mathcal{K}}} = \quad & \sup_{\mu_1,\ldots,\mu_N} \sum_{i=1}^{N} \mu_i(\mathcal{B}), \\ & \sum_{i=1}^{N} \mu_i \leqslant \lambda_{\mathcal{B}}, \\ \text{s.t.} \quad & \mathrm{supp}(\mu_i) \subseteq \overline{\mathcal{K}}_i,\ i = 1,\ldots,N \\ & \mu_i \geqslant 0,\ i = 1,\ldots,N. \end{aligned} \tag{107}$$

□

Formulation as an SOS. We proceed similarly to Section 3.2.2. Regarding the constraints defining the sets $\overline{\mathcal{K}}_i$:

$$\overline{\mathcal{K}}_i := \{X^0_r \in \mathbb{R}^6 : g_i(X^0_r) \geqslant 0, g_{j,\mathcal{B}} \geqslant 0,\ j = 1,\ldots,6\},\ i = 1,\ldots,N, \tag{108}$$

the polynomial g_i is obtained from Equation (104),

$$g_i(X^0_r) := R^2 - {X^0_r}^T \Phi(t_i, t_0)^T I_{11} \Phi(t_i, t_0) X^0_r,\ i = 1,\ldots,N, \tag{109}$$

and $g_{j,\mathcal{B}}$ are the constraints defining the hyper-rectangle $\mathcal{B}$,

$$g_{j,\mathcal{B}}(X^0_r) := (X^0_{r\,j} - a_j)(b_j - X^0_{r\,j}), j = 1,\ldots,6. \tag{110}$$

It follows that Problem (106) can be numerically solved by the following SOS formulation:

$$
\begin{aligned}
w*_{2r,d,\overline{\mathcal{K}}} = \quad & \inf_{p\in\mathbb{R}[X_r^0]_d} \int_{\mathcal{B}} p(X_r^0)\mathrm{dX_r^0}, \\
& \text{s.t.} \\
& \left.\begin{array}{l} p-\sigma_{0,\mathcal{B}}-\sum\limits_{1\leqslant j\leqslant 6} g_{j,\mathcal{B}}\sigma_{j,\mathcal{B}}=0 \\ \sigma_{0,\mathcal{B}}\in\Sigma^2[X_r^0]_{2r}, \\ \sigma_{j,\mathcal{B}}\in\Sigma^2[X_r^0]_{2(r-1)},\ \forall j=1,\cdots,6, \end{array}\right\} p\geqslant 0 \,\text{on}\, \mathcal{B} \\
& \left.\begin{array}{l} p-\sigma_{0,\mathcal{K}_1}-g_1\sigma_{1,\mathcal{K}_1}-\sum\limits_{1\leqslant j\leqslant 6} g_{j,\mathcal{B}}\sigma_{1,j,\mathcal{B}}=1 \\ \sigma_{0,\mathcal{K}_1}\in\Sigma^2[X_r^0]_{2r}, \\ \sigma_{1,\mathcal{K}_1}\in\Sigma^2[X_r^0]_{2(r-1)}, \\ \sigma_{1,j,\mathcal{B}}\in\Sigma^2[X_r^0]_{2(r-1)},\ \forall j=1,\cdots,6, \end{array}\right\} p\geqslant 1 \,\text{on}\, \overline{\mathcal{K}}_1, \qquad (111) \\
& \cdots \\
& \left.\begin{array}{l} p-\sigma_{0,\mathcal{K}_N}-g_N\sigma_{N,\mathcal{K}_N}-\sum\limits_{1\leqslant j\leqslant 6} g_{j,\mathcal{B}}\sigma_{N,j,\mathcal{B}}=1 \\ \sigma_{0,\mathcal{K}_N}\in\Sigma^2[X_r^0]_{2r}, \\ \sigma_{N,\mathcal{K}_N}\in\Sigma^2[X_r^0]_{2(r-1)}, \\ \sigma_{N,j,\mathcal{B}}\in\Sigma^2[X_r^0]_{2(r-1)},\ \forall j=1,\cdots,6, \end{array}\right\} p\geqslant 1 \,\text{on}\, \overline{\mathcal{K}}_N.
\end{aligned}
$$

Proposition 1 (Convergence of LMI hierarchy)**.**
For each fixed $d\in\mathbb{N}$, the value of Problem (111) *converges to $w^*_{d,\overline{\mathcal{K}}}$, as $r\to\infty$ and moreover, for any $2r\geqslant d$, the solution $p^*_{2r,d,\overline{\mathcal{K}}}$ of Problem* (102) *satisfies the constraints of Problem* (106) *i.e.,* $\mathrm{PSS}_{p^*_{2r,d,\overline{\mathcal{K}}}}$ *is a PSS approximation of $\overline{\mathcal{K}}$.*

Proof. The proof can be found in [51]. □

Before entering into more implementation details regarding Problem (111), let us discuss an important simplification which occurs in practice, when one considers that in the six dimensional relative dynamics (position, velocity), the Gaussian uncertainty on the velocity can be neglected during the encounter time interval $[t_0, t_0+T]$.

3.3.2 No velocity uncertainty

The case of no velocity uncertainty involves the following simplifications:

- The integral in Equation (95) becomes three-dimensional.
- The swept-volume $\mathcal{X}_T^0$ contains only relative positions, since the relative velocities are supposed to be exactly known. Consequently, straightforward calculations lead to the following characterization of the swept-volume.

Proposition 2 (Swept-volume in linear relative dynamics and no velocity uncertainty)**.**
Denote the state vector $X_r^0\in\mathbb{R}^6$ by $X_r^0 := (r_r^{0^T}, v_r^{0^T})^T$, where $v_r^0\in\mathbb{R}^3$ is given and not a random vector. Let the relative dynamics transition matrix $\Phi(t,t_0)$ be given and denoted by blocks by $\Phi := \begin{pmatrix}\Phi_{11} & \Phi_{12}\\ \Phi_{21} & \Phi_{22}\end{pmatrix}$.

Assume that $\Phi_{11}(t,t_0)$ is invertible for each $t \in [t_0, t_0+T]$. The swept-volume containing all the relative positions $r_r^0 \in \mathbb{R}^3$, which lead to collisions during the time interval $[t_0, t_0+T]$, is described by a union of ellipsoids,

$$\mathcal{X}_{rT}^0 = \bigcup_{t\in[t_0,t_0+T]} \mathcal{E}_{t,t_0},$$

with

$$\mathcal{E}_{t,t_0} := \left\{ r_r^0 \in \mathbb{R}^3 : R^2 - (r_r^0 - c(t,t_0))^T Q(t,t_0)^{-1} (r_r^0 - c(t,t_0)) \geqslant 0 \right\}, \tag{112}$$

where

$$\begin{array}{ll} c(t,t_0) & = -\Phi_{11}(t,t_0)^{-1}\Phi_{12}(t,t_0)v_r^0, \\ Q(t,t_0) & = \Phi_{11}(t,t_0)^{-1}\Phi_{11}(t,t_0)^{-T}. \end{array} \tag{113}$$

Proof. It is sufficient to plug-in the known terms in Equation (103). □

Remark 10 (The swept-volume as a compact set)**.**
Note that provided that the matrix $\Phi_{11}(t,t_0)$ is invertible for each $t \in [t_0, t_0+T]$, each ellipsoid $\mathcal{E}_{t,t_0}$ is proper ($Q(t,t_0)$ has full rank) and thus their union is compact. Otherwise, the swept-volume can still be described by the union of non-necessary proper quadratic forms.

Compared to the general case, a compact swept-volume is an advantage, in the sense that it can be directly bounded, without resorting to further intersections with the $\ell-\sigma$-ellipsoids of the Gaussian distribution.

Proposition 3 (Direct computation of a bounding box)**.**
Assume that $\Phi_{11}(t,t_0)$ is invertible for each $t \in [t_0, t_0+T]$. Then, $\mathcal{X}_{rT}^0$ in Proposition 2 is enclosed in the box $\mathcal{B}_r^0 \subset \mathbb{R}^3$:

$$\mathcal{B}_r^0 = \left[\min_{t\in[t_0,t_0+T]} (c(t,t_0) - \delta(t,t_0)), \max_{t\in[t_0,t_0+T]} (c(t,t_0) + \delta(t,t_0)) \right], \tag{114}$$

where $\delta(t,t_0)$, is the vector generated by the square roots of the diagonal elements of the matrix $\frac{1}{R^2}Q(t,t_0)$ and the min *and* max *are to be taken component-wise.*

Proof. Each ellipsoid in Equation (112) can be seen as an affine transformation of the unit ball, hence for each $t \in [t_0, t_0+T]$, one has:

$$r_r^0(t,t_0) - c(t,t_0) = \frac{1}{R}\Phi_{11}(t,t_0)^{-1} y, \text{ with } y \in \mathbb{R}^3,\ \|y\|_2 \leqslant 1,$$

from which one has a component-wise enclosure by taking the 2-norm of each row of the matrix $\frac{1}{R}\Phi_{11}(t,t_0)^{-1}$. □

In this simplified setting, we describe in Algorithm 1 how to compute a PSS approximation for the swept-volume. Its correctness follows directly from Propositions 2, 3 and 1.
For the general 6-dimensional case a similar algorithm can be designed, which solves Problem 111, with the additional requirement (and approximation) that a compact bounding box needs to be provided as input. As already mentioned, this may come from the covariance level sets of the Gaussian distribution in Equation (95).

Algorithm 1 PSSAPPROX3D$(\tau_N, \Phi(t,t_0), v_r^0, R, d, r)$

Input: time grid τ_N, $\Phi(t,t_0)$ with invertible upper-left block for $t \in \tau_N$, known initial velocities $v_r^0 \in \mathbb{R}^3$, radius R, degrees $2r \geqslant d$, $d \geqslant 1$.

Output: $p_d \in \mathbb{R}[x]_d$ is a PSS approx of the discretized collision set i.e.,
$\{x \in \mathbb{R}^3 : p_d(x) \geqslant 1\} \supseteq \{r_r^0 \in \mathbb{R}^3 : \exists t \in \tau_N, \text{s.t. } X_r^0 = [r_r^{0^T}\ v_r^{0^T}]^T,$
$X_r^{0^T} \Phi(t,t_0)^T I_{11} \Phi(t,t_0) X_r^0 \leqslant R^2\}$.

▷ *Define ellipsoids* $\mathcal{E}_{t_i,t_0} := \left\{r_r^0 \in \mathbb{R}^3 : R^2 - (r_r^0 - c(t_i,t_0))^T Q(t_i,t_0)^{-1}(r_r^0 - c(t_i,t_0)) \geqslant 0\right\}$

1: $c(t_i,t_0) \leftarrow -\Phi_{11}(t_i,t_0)^{-1}\Phi_{12}(t_i,t_0)v_r^0$, for $t_i \in \tau_N$;
2: $Q(t_i,t_0) \leftarrow \Phi_{11}(t_i,t_0)^{-1}\Phi_{11}(t_i,t_0)^{-T}$, for $t_i \in \tau_N$;

▷ *Find a bounding box* $\mathcal{B}_r := \{x \in \mathbb{R}^3 : a \leqslant x \leqslant b\}$

3: $\delta(t_i,t_0) \leftarrow \sqrt{\text{diag}\left(\frac{1}{R^2}Q(t_i,t_0)\right)}$, for $t_i \in \tau_N$;
4: $[a,b] \leftarrow \left[\min_{t_i \in \tau_N}(c(t_i,t_0) - \delta(t_i,t_0)),\ \max_{t_i \in \tau_N}(c(t_i,t_0) + \delta(t_i,t_0))\right]$;

▷ *Solve the optimization problem*
5: $g_{t_i} \leftarrow R^2 - (x - c(t_i,t_0))^T Q(t_i,t_0)^{-1}(x - c(t_i,t_0))$ for $t_i \in \tau_N$;
6: $g_{j,\mathcal{B}_r^0} \leftarrow (x_j - a_j)(b_j - x_j)$, for $j = 1,2,3$;

$$
\begin{aligned}
w*_{2r,d} = \quad & \min_{p \in \mathbb{R}[x]_d} \int_{\mathcal{B}_r^0} p(x)\mathrm{dx}, \\
& \text{s.t.} \\
& \left.\begin{array}{l} p - \sigma_{0,\mathcal{B}_r^0} - \sum\limits_{1 \leqslant j \leqslant 3} g_{j,\mathcal{B}_r^0}\sigma_{j,\mathcal{B}_r^0} = 0 \\ \sigma_{0,\mathcal{B}_r^0} \in \Sigma^2[X_r^0]_{2r}, \\ \sigma_{j,\mathcal{B}_r^0} \in \Sigma^2[X_r^0]_{2(r-1)},\ \forall j = 1,2,3, \end{array}\right\} p \geqslant 0 \,\text{on}\, \mathcal{B}_r^0 \\
& \left.\begin{array}{l} p - \sigma_{0,t_i} - g_{t_i}\sigma_{1,t_i} = 1 \\ \sigma_{0,t_i} \in \Sigma^2[X_r^0]_{2r}, \\ \sigma_{1,t_i} \in \Sigma^2[X_r^0]_{2(r-1)}, \end{array}\right\} p \geqslant 1 \ \text{on each ellipsoid}\ \mathcal{E}_{t_i,t_0},\ \text{for}\ t_i \in \tau_N.
\end{aligned}
\tag{115}
$$

7: **return** $p_{2r,d}^* = \text{Argmin}\ (115)$

3.4 Integration of a Gaussian on a volume implicitly defined by a polynomial

We already mentioned in Section 3.2.1 that the problem of finding a PSS is closely related to the one of computing the volume of a semi-algebraic set. In fact Problem 101 (and similarly Problem 107) can be adapted such that their optimal value is the volume with respect to a Gaussian measure denoted by μ_0 in Equation (95), instead of the classical Lebesgue one, cf. [51]:

$$
\begin{aligned}
v_{\text{Gauss}}^* = \quad & \sup_{\mu_0, \hat{\mu}_0} \mu_0(\mathcal{K}), \\
& \mu_0 + \hat{\mu}_0 = \mu_g, \\
& \text{s.t. } \text{supp}(\mu_0) \subseteq \mathcal{K}, \\
& \mu_0, \hat{\mu}_0 \geqslant 0.
\end{aligned}
\tag{116}
$$

Compared to Problem 101, this formulation requires the computation of the moments of a Gaussian measure, while the Lebesgue measure moments on a given hyper-rectangle were required before. In practice, we have however observed more numerical issues when directly solving Problem 116 instead of Problem 101, hence we decided to stick with Problem 107 for computing a PSS and then,

to employ other methods for the computation of the restriction of the Gaussian to the obtained PSS.
Two strategies have been developed so far:

- ***The 3D case:*** After Algorithm 1 is executed, the obtained polynomial $p^*_{2r,d}$ provides an implicit representation of the approximated volume. This is used as input for [67, Algorithm 3], which automatically determines a high-order accurate numerical quadrature for the evaluation of integrals over volumes, whose geometry is defined implicitly via a fixed level set of a smooth function $\phi : \mathbb{R}^3 \to \mathbb{R}$. Obviously in our case, $\phi = p^*_{2r,d}$.

- ***The 6D case:*** Similarly, after Problem 111 is solved for an optimal $p^*_{2r,d}$, the integral of a Gaussian distribution over the volume $\mathrm{PSS}_{p^*_{2r,d}}$ is evaluated by a Monte Carlo sampling, namely evaluating $\dfrac{\sum_{i=1}^{N_\mathrm{s}} 1_{\mathrm{PSS}_{p^*_{2r,d}}}(X_{\mathrm{s},i})}{N_\mathrm{s}}$, which consists in simply checking whether $p^*_{2r,d}(X_{\mathrm{s},i}) \geqslant 1$ for each sample $X_{\mathrm{s},i}$.

3.5 Detailed numerical implementation

For the 6D case, which is more general, some implementation details are given in Algorithms 2, 3 and 4. Specifically, all the constraints are scaled to the unit cube $[-1,1]^6$, in Algorithms 2 and 3, which ensures a much better numerical quality of the results. This rather tedious, but necessary step is documented for completeness of this report. A proof of correctness is given below.

Algorithm 2 FindPosBoundBox($\tau_N, \Phi(t,t_0), m^0_{v_r}, Q^0_{v_r}, R$)

Input: time grid τ_N, $\Phi(t,t_0)$ with invertible upper-left and upper-right block for $t \in \tau_N$, given mean initial velocities $m^0_{v_r} \in \mathbb{R}^3$ and 6-σ ellipsoid matrix $Q^0_{v_r}$, radius R.
Output: $[a^0_r, b^0_r] := \{r^0_r \in \mathbb{R}^3 : a \leqslant r^0_r \leqslant b\} \supseteq \{r^0_r \in \mathbb{R}^3 : \exists t \in \tau_N, \text{s.t.}$
$X^0_r := [r^{0^T}_r \ v^{0^T}_r]^T \in \mathbb{R}^6$, $(v^0_r - m^0_{v_r})^T Q^{0^{-1}}_{v_r}(v^0_r - m^0_{v_r}) \leqslant 1$,
$X^{0^T}_r \Phi(t,t_0)^T I_{11} \Phi(t,t_0) X^0_r \leqslant R^2\}$.

$c(t_i,t_0) \leftarrow -\Phi_{11}(t_i,t_0)^{-1}\Phi_{12}(t_i,t_0)m^0_{v_r}$, for $t_i \in \tau_N$;
$Q(t_i,t_0) \leftarrow \Phi_{11}(t_i,t_0)^{-1}\Phi_{11}(t_i,t_0)^{-1^T}$, for $t_i \in \tau_N$;
$\delta_1(t_i,t_0) \leftarrow \sqrt{\mathrm{diag2vec}\left(\frac{1}{R^2}Q(t_i,t_0)\right)}$, for $t_i \in \tau_N$;
if $Q^0_{v_r} \neq 0$ **then**
  $q(t_i,t_0) \leftarrow \Phi_{11}(t_i,t_0)^{-1}\Phi_{12}(t_i,t_0)Q^0_{v_r}\Phi_{12}(t_i,t_0)^T\Phi_{11}(t_i,t_0)^{-T}$, for $t_i \in \tau_N$;
  $\delta_2(t_i,t_0) \leftarrow \sqrt{\mathrm{diag2vec}\left(q(t_i,t_0)\right)}$, for $t_i \in \tau_N$;
else
▷ *No velocity uncertainty*
  $q(t_i,t_0) \leftarrow 0$;
  $\delta_2(t_i,t_0) \leftarrow 0$;
end if
$[a^0_r, b^0_r] \leftarrow \left[\min_{t_i \in \tau_N}\left(c(t_i,t_0) - \delta_1(t_i,t_0) - \delta_2(t_i,t_0)\right), \max_{t_i \in \tau_N}\left(c(t_i,t_0) + \delta_1(t_i,t_0) + \delta_2(t_i,t_0)\right)\right]$;
return $[a^0_r, b^0_r]$.

Algorithm 3 ScaleConstrainsUnitCube($\tau_N, \Phi(t,t_0), m^0_{v_r}, Q^0_{v_r}, R$)

Input: time grid τ_N, $\Phi(t,t_0)$ with invertible upper-left and upper-right block for $t \in \tau_N$, given mean initial velocities $m^0_{v_r} \in \mathbb{R}^3$ and 6-σ ellipsoid matrix $Q^0_{v_r}$, radius R.

Output: Polynomial constraints for the set $\{X^0_r = [r^{0^T}_r \ v^{0^T}_r]^T \in \mathbb{R}^6 : \exists t \in \tau_N, \text{s.t.}$ $X^{0^T}_r \Phi(t,t_0)^T I_{11} \Phi(t,t_0) X^0_r \leqslant R^2,\ (v^0_r - m^0_{v_r})^T Q^{0^{-1}}_{v_r} (v^0_r - m^0_{v_r}) \leqslant 1\}$ rescaled in the unit box $[-1,1]^6$.

▷ *Find a bounding box for positions* $[a^0_r, b^0_r] := \{r^0_r \in \mathbb{R}^3 : a \leqslant r^0_r \leqslant b\}$

$[a^0_r, b^0_r] \leftarrow$ FindPosBoundBox($\tau_N, \Phi(t,t_0), m^0_{v_r}, Q^0_{v_r}, R$);

▷ *Rescale variables* $[r^0_r; v^0_r]$ *to* $[-1;1]^3 \times [-1;1]^3$

$c(t_i,t_0) \leftarrow -\Phi_{11}(t_i,t_0)^{-1}\Phi_{12}(t_i,t_0) m^0_{v_r}$, for $t_i \in \tau_N$;

$Q(t_i,t_0) \leftarrow \Phi_{11}(t_i,t_0)^{-1}\Phi_{11}(t_i,t_0)^{-T}$, for $t_i \in \tau_N$;

$\tilde{c}(t_i,t_0) \leftarrow \text{vec2diag}\left(\frac{b^0_r - a^0_r}{2}\right)^{-1}\left(c(t_i,t_0) - \frac{b^0_r + a^0_r}{2}\right)$, for $t_i \in \tau_N$;

$\tilde{Q}(t_i,t_0) \leftarrow \frac{1}{R^2}\text{vec2diag}\left(\frac{b^0_r - a^0_r}{2}\right)^{-1} Q(t_i,t_0) \text{vec2diag}\left(\frac{b^0_r - a^0_r}{2}\right)^{-1}$, for $t_i \in \tau_N$;

if $Q^0_{v_r} \neq 0$ **then**

  $\delta_3 \leftarrow \sqrt{\text{diag2vec}\left(Q^0_{v_r}\right)}$;

  $[a^0_v, b^0_v] \leftarrow [-\delta_3,\ \delta_3]$;

  $\Delta(t_i,t_0) \leftarrow -\text{vec2diag}\left(\frac{b^0_r - a^0_r}{2}\right)^{-1} \Phi_{11}(t_i,t_0)^{-1}\Phi_{12}(t_i,t_0)\text{vec2diag}\left(\frac{b^0_v - a^0_v}{2}\right)$;

  $\tilde{Q}^0_{v_r} \leftarrow \text{vec2diag}\left(\frac{b^0_v - a^0_v}{2}\right) Q^0_{v_r} \text{vec2diag}\left(\frac{b^0_{v_r} - a^0_{v_r}}{2}\right)$;

else

  $\Delta(t_i,t_0) \leftarrow 0$;

end if

▷ *Define polynomial constraints*

▷ *Position constraints*

$g_{t_i} \leftarrow 1 - \left(\tilde{r}^0_r - \tilde{c}(t_i,t_0) - \Delta(t_i,t_0)\tilde{v}^0_r\right)^T \tilde{Q}(t_i,t_0)^{-1}\left(\tilde{r}^0_r - \tilde{c}(t_i,t_0) - \Delta(t_i,t_0)\tilde{v}^0_r\right)$ for $t_i \in \tau_N$;

if $Q^0_{v_r} \neq 0$ **then**

▷ *Velocity constraints*

  $h_{v_r{}^0} \leftarrow 1 - \tilde{v}^{0^T}_r \tilde{Q}^{0^{-1}}_{v_r} \tilde{v}^0_r$;

else

  $h_{v_r{}^0} \leftarrow 0$;

end if

return $\{g_{t_i} \geqslant 0, t_i \in \tau_N\}, \{h_{v_r{}^0} \geqslant 0\}$

Algorithm 4 PSSApprox6D$(\tau_N, \Phi(t,t_0), m^0_{v_r}, Q^0_{v_r}, R, d, l)$

Input: time grid τ_N, $\Phi(t,t_0)$ with invertible upper-left and upper-right block for $t \in \tau_N$, given mean initial velocities $m^0_{v_r} \in \mathbb{R}^3$ and 6-σ ellipsoid matrix $Q^0_{v_r}$, radius R, degrees $2l \geqslant d$, $d \geqslant 1$.

Output: $p_d \in \mathbb{R}[x]_d$ is a PSS approx of the discretized collision set i.e.,
$\{x \in \mathbb{R}^6 : p_d(x) \geqslant 1\} \supseteq \{X^0_r = [r^{0^T}_r \ v^{0^T}_r]^T \in \mathbb{R}^6 : \exists t \in \tau_N, \text{s.t.}$
$X^{0^T}_r \Phi(t,t_0)^T I_{11} \Phi(t,t_0) X^0_r \leqslant R^2,\ (v^0_r - m^0_{v_r})^T Q^{0^{-1}}_{v_r} (v^0_r - m^0_{v_r}) \leqslant 1\}$.

▷ *Rescale variables* $[r^{0^T}_r \ v^{0^T}_r]^T$ *to* $[-1;1]^3 \times [-1;1]^3$

1: $\{g_{t_i} \geqslant 0, t_i \in \tau_N\}, \{h^0_{v_r} \geqslant 0\} \leftarrow$ScaleConstrainsUnitCube$(\tau_N, \Phi(t,t_0), m^0_{v_r}, Q^0_{v_r}, R)$

▷ *Solve optimization problem*

2: **if** $Q^0_{v_r} = 0$ **then**

3: $g_{r0,j} \leftarrow 1 - \tilde{r}^{0^2}_{r,j}$, for $j = 1,2,3$;

$$
\begin{aligned}
w*_{2l,d} = \ & \min_{p \in \mathbb{R}[\tilde{r}^0_r]_d} \int_{[-1;1]^3} p(\tilde{r}^0_r) \mathrm{d}\tilde{r}^0_r, \\
& \text{s.t.} \\
& \left.\begin{array}{l} p - \sigma_{r0,0} - \sum\limits_{1 \leqslant j \leqslant 3} g_{r0,j}\sigma_{r0,j} = 0 \\ \sigma_{r0,0} \in \Sigma^2[\tilde{r}^0_r]_{2l}, \\ \sigma_{r0,j} \in \Sigma^2[\tilde{r}^0_r]_{2(l-1)},\ \forall j = 1,2,3, \end{array}\right\} p \geqslant 0 \,\text{on}\, [-1;1]^3 \\
& \left.\begin{array}{l} p - \sigma_{t_i,0} - g_{t_i}\sigma_{t_i,1} = 1 \\ \sigma_{t_i,0} \in \Sigma^2[\tilde{r}^0_r]_{2l}, \\ \sigma_{t_i,1} \in \Sigma^2[\tilde{r}^0_r]_{2(l-1)}, \end{array}\right\} p \geqslant 1 \ \text{on each set}\ \{\tilde{r}^0_r \in \mathbb{R}^3 : g_{t_i}(\tilde{r}^0_r) \geqslant 0\},\ \text{for}\ t_i \in \tau_N.
\end{aligned} \tag{117}
$$

4: **return** $p^*_{2l,d} =$ Argmin (117)

5: **else**

6: $g_{r0,j} \leftarrow 1 - \tilde{r}^{0^2}_{r,j}$, and $g_{v0,j} \leftarrow 1 - \tilde{v}^{0^2}_{r,j}$, for $j = 1,2,3$;

$$
\begin{aligned}
w*_{2l,d} = \ & \min_{p \in \mathbb{R}[\tilde{X}^0_r]_d} \int_{[-1;1]^6} p(\tilde{X}^0_r) \mathrm{d}\tilde{X}^0_r, \\
& \text{s.t.} \\
& \left.\begin{array}{l} p - \sigma_0 - \sum\limits_{1 \leqslant j \leqslant 3} g_{r0,j}\sigma_{r0,j} - \sum\limits_{1 \leqslant j \leqslant 3} g_{v0,j}\sigma_{v0,j} = 0 \\ \sigma_0 \in \Sigma^2[\tilde{X}^0_r]_{2l}, \\ \sigma_{r0,j}, \sigma_{v0,j} \in \Sigma^2[\tilde{X}^0_r]_{2(l-1)},\ \forall j = 1,2,3, \end{array}\right\} p \geqslant 0 \,\text{on}\, [-1;1]^6 \\
& \left.\begin{array}{l} p - \sigma_{t_i,0} - g_{t_i}\sigma_{t_i,1} - h^0_{v_r}\sigma_{v_0,t_i} = 1 \\ \sigma_{t_i,0} \in \Sigma^2[\tilde{X}^0_r]_{2l}, \\ \sigma_{t_i,1}, \sigma_{v_0,t_i} \in \Sigma^2[\tilde{X}^0_r]_{2(l-1)}, \end{array}\right\} p \geqslant 1 \ \text{on each set} \\
& \qquad \{\tilde{X}^0_r \in \mathbb{R}^6 : g_{t_i}(\tilde{X}^0_r) \geqslant 0, h^0_{v_r}(\tilde{X}^0_r) \geqslant 0\},\ \text{for}\ t_i \in \tau_N.
\end{aligned} \tag{118}
$$

7: **return** $p^*_{2l,d} =$ Argmin (118)

8: **end if**

Proposition 4. *Algorithm 4 is correct.*

Proof. Note that the $3D$ case proved above is directly obtained when the matrix input $Q^0_{v_r}$ is zero. Otherwise, the velocities are uncertain, so to obtain a compact constraint, the 6-σ covariance ellipsoid is used, so $(v^0_r - m^0_{v_r})^T Q^{0^{-1}}_{v_r} (v^0_r - m^0_{v_r}) \leqslant 1$. Hence, Equation (112) becomes, for each fixed

t:

$$\begin{array}{l}\hat{\mathcal{E}}_{t,t_0} := \left\{ r_r^0 \in \mathbb{R}^3 : R^2 - (r_r^0 - c_{v0}(t,t_0))^T Q(t,t_0)^{-1} (r_r^0 - c_{v0}(t,t_0)) \geqslant 0, \right. \\ \left. 1 - (v_r^0 - m_{v_r}^0))^T Q_{v_r}^{0^{-1}} (v_r^0 - m_{v_r}^0) \geqslant 0 \right\},\end{array} \tag{119}$$

where

$$\begin{array}{ll} c_{v0}(t,t_0) & = -\Phi_{11}(t,t_0)^{-1}\Phi_{12}(t,t_0) r_r^0, \\ Q(t,t_0) & = \Phi_{11}(t,t_0)^{-1}\Phi_{11}(t,t_0)^{-T}. \end{array} \tag{120}$$

If moreover,$\Phi_{12}(t,t_0)$ has full rank, the set $\hat{\mathcal{E}}_{t,t_0}$ can be enclosed in the box returned by Algorithm 2, by seeing each ellipsoid as an affine transformation of the unit ball. Specifically, this transformation is:

$$v_r^0 = A_{v0} u_{v0} + m_{v_r}^0, \text{ with } \|u_{v0}\|_2 \leqslant 1, \text{ and } A_{v0} A_{v0}^T = Q_{v_r}^0, \tag{121}$$

which gives:

$$\begin{array}{ll} c_{v0}(t,t_0) & = -\Phi_{11}(t,t_0)^{-1}\Phi_{12}(t,t_0) m_{v_r}^0 \\ & \quad -\Phi_{11}(t,t_0)^{-1}\Phi_{12}(t,t_0) A_{v0} u_{v0}, \text{with } \|u_{v0}\|_2 \leqslant 1. \end{array} \tag{122}$$

One finally has:

$$\begin{array}{ll} r_r^0(t|t_0) & = \frac{1}{R}\Phi_{11}(t,t_0)^{-1} u_{r0} \\ & \quad -\Phi_{11}(t,t_0)^{-1}\Phi_{12}(t,t_0) m_{v_r}^0 \\ & \quad -\Phi_{11}(t,t_0)^{-1}\Phi_{12}(t,t_0) A_{v0} u_{v0}, \text{with } \|u_{v0}\|_2 \leqslant 1,\ \|u_{r0}\|_2 \leqslant 1, \end{array} \tag{123}$$

which gives the proposed bounding. Next, the rescaling of the variables $[r_r^{0^T}\ v_r^{0^T}]^T$ to the box $[-1;1]^6$ is important for the numerical quality of the results, although from a theoretical point of view it is not necessary. Substituting the simple scaling formula $\tilde{x} = \frac{2x}{b-a} - \frac{b+a}{b-a}$ to be applied component-wise in the above equations, one obtains the equations defined in lines 4, 5, 9, 10 of Algorithm 3, which directly translates to the polynomial constraints in lines 14 and 16 of Algorithm 3. These constraints, now concern the rescaled variables $\tilde{X}_r^0 = [\tilde{r}_r^{0^T}\ \tilde{v}_r^{0^T}]^T \in [-1;1]^6$. Following the theoretical developments in Section 3.3.1, Problem 118 or respectively 117 provide a PSS solution for the input set. □

3.6 Numerical Implementation and Examples

Example 8.

Appendix
This appendix quickly summarizes the main definitions from measure theory and integration that are needed for the developments presented in this report. The material here in is mainly borrowed from the references [15], [11] and [69].

A Basic definitions, results and facts from measure theory

Definition 6 (Indicator Function)**.** *Let $B \subset A$. The indicator function 1_B of B is defined as:*

$$1_B : \begin{array}{ccc} A & \to & \{0,1\}, \\ x & \mapsto & \begin{cases} 0 & \text{if } x \notin B, \\ 1 & \text{if } x \in B. \end{cases} \end{array}$$

Definition 7 (σ-algebra)**.** *Let A be a set. A σ-algebra of subsets of A (sometimes called a σ-field) is a family $\mathcal{A}$ of subsets of A such that:*

1. $\emptyset \in \mathcal{A}$,
2. $\forall E \in \mathcal{A}$, $A \backslash E \in \mathcal{A}$,
3. *for every sequence* $(E_n)_{n\in\mathbb{N}} \in \mathcal{A}$, $\bigcup_{n\in\mathbb{N}} E_n \in \mathcal{A}$.

Example 9.

- *$\mathcal{P}(A)$ is a (the maximal) σ-algebra on A.*
- *$\{\emptyset, A\}$ is a (the minimal) σ-algebra on A.*
- *For $B \subset A$, $\{\emptyset, B, A\backslash B, A\}$ is a σ-algebra on A.*
- *If $B \neq \emptyset$ and $B \neq A$ then $\{\emptyset, B, A\}$ is not a σ-algebra on A.*

Definition 8. *For every system of sets $\mathcal{G} \in \mathcal{P}(A)$, there exists a smallest σ-algebra containing $\mathcal{G}$. This σ-algebra, denoted by $\sigma(\mathcal{G})$ is the σ-algebra generated by $\mathcal{G}$.*

Definition 9 (Borel σ-algebra or topological σ-algebra)**.** *The σ-algebra $\sigma(\mathcal{O}^n)$, denoted $\mathcal{B}(\mathbb{R}^n)$, generated by the system $\mathcal{O}^n$ of all open sets of $\mathbb{R}^n$ is called the Borel σ-algebra on $\mathbb{R}^n$ and its members are the Borel sets or Borel measurable sets.*

Note that the Borel σ-algebra $\mathcal{B}(\mathbb{R}^n)$ may be generated by the family of half-open rectangles in $\mathbb{R}^n$, i.e. $\mathcal{B}(\mathbb{R}^n) = \mathcal{I}$ where $\mathcal{I} = \mathcal{I}(\mathbb{R}^n) = \{[a_1, b_1) \times \cdots \times [a_n, b_n) : \ a_j, b_j \in \mathbb{R}\}$.

Definition 10 (Measurable Space)**.** *A measurable space is a pair $(A, \mathcal{A})$ where A is a set and $\mathcal{A}$ is a σ-algebra of subsets of A.*

Definition 11 (Measure)**.** *Let $(A, \mathcal{A})$ be a measurable space (see Definition 10). A positive measure on A (or, more precisely, on $(A, \mathcal{A})$) is a mapping $\mu : \mathcal{A} \to [0, +\infty]$ satisfying:*

1. $\mu(\emptyset) = 0$,

2. *for every sequence* $(E_n)_{n\in\mathbb{N}}$ *of pairwise disjoint sets in* $\mathcal{A}$, $\mu\left(\bigcup_{n\in\mathbb{N}} E_n\right) = \sum_{n\in\mathbb{N}} \mu(E_n)$.

Example 10.

- *Borel measure : A measure defined on the Borel* σ*-algebra* $\mathcal{B}(\mathbb{R}^n)$ *is called a Borel measure.*

- *Dirac Measure at* a *: Let* $(A, \mathcal{A})$ *be any measurable space and let* $a \in A$. *Then* $\delta_a : \mathcal{A} \to \{0, 1\}$, *defined for* $A \in \mathcal{A}$ *by:*

$$\delta_a(A) = \begin{cases} 0 & \text{if} \quad a \notin A, \\ 1 & \text{if} \quad a \in A, \end{cases}$$

  is called the Dirac measure at the point a.

- *Lebesgue measure: The set-function* λ^n *on* $(\mathbb{R}^n, \mathcal{B}(\mathbb{R}^n))$ *that assigns the value :*

$$\lambda^n([a_1, b_1) \times \cdots \times [a_n, b_n)) = \prod_{j=1}^{n} (b_j - a_j)$$

  to every half-open rectangle $[a_1, b_1) \times \cdots \times [a_n, b_n) \in \mathcal{I}$, *is called the n-dimensional Lebesgue measure. If* $A \subset \mathbb{R}^n$ *then*

$$\lambda^n(A) = \inf_{A \subset \bigcup_{i=1}^{\infty} R_i} \sum (b_1^i - a_1^i) \cdot \cdots \cdot (b_n^i - a_n^i),$$

  where the R_i*'s are half-open rectangles, i.e.* $R_i = [a_1^i, b_1^i) \times \cdots \times [a_n^i, b_n^i)$.
  The 1-dimensional-Lebesgue measure represents the conventional "length" of a segment:

$$\forall\, (a, b) \in \mathbb{R}^2 \ \text{s.t.}\ a < b, \ \ \lambda([a, b]) = b - a.$$

  Remark that, for $a \in \mathbb{R}$, $\lambda(\{a\}) = 0$. *From the second point of Definition 11:*

$$\forall\, (a, b) \in \mathbb{R}^2 \ \text{s.t.}\ a < b, \ \ \lambda([a, b]) = \lambda(\{a\}) + \lambda(]a, b[) + \lambda(\{b\}) = \lambda(]a, b[)\,.$$

Definition 12 (Measure Space)**.** *A measure space is a triplet* $(A, \mathcal{A}, \mu)$ *where* A *is a set,* $\mathcal{A}$ *is a* σ*-algebra of subsets of* A, *and* μ *is a positive measure on* $(A, \mathcal{A})$.

Property 1. *Let* $(A, \mathcal{A}, \mu)$ *be a measure space and* $B, C \in \mathcal{A}$. *Then,* $C \subset B \Rightarrow \mu(C) \leqslant \mu(B)$.

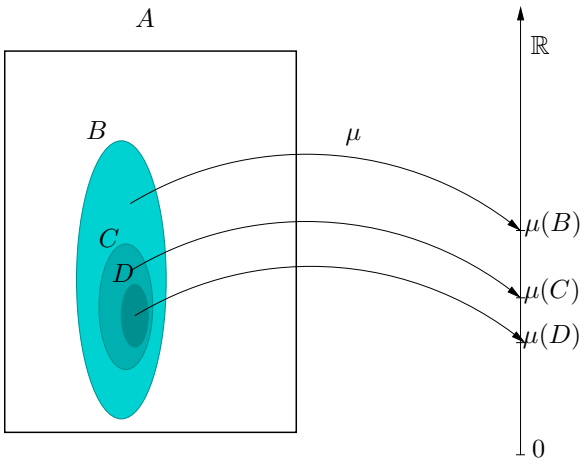

Figure 16: Monotonicity of positive measures.

Definition 13 (σ-finite measure)**.** *A measure μ defined on $(A, \mathcal{A})$ is said to be σ-finite and $(A, \mathcal{A}, \mu)$ is called a σ-finite measure space if $\mathcal{A}$ contains an increasing sequence $(A_j)_{j\in\mathbb{N}} \subset \mathcal{A}$ of sets $A_1 \subset A_2 \subset \cdots$ such that $\cup_{j\in\mathbb{N}} A_j = A$ (exhausting sequence) verifying $\mu(A_j) < \infty$ for all $j \in \mathbb{N}$.*

Definition 14 (Support of a Measure)**.** *Let $(A, \mathcal{A}, \mu)$ be a measure space.*
The support of the positive measure μ is the smallest closed set defined as:

$$\operatorname{supp}(\mu) = \{x \in A \text{ s.t. } \mu(U) > 0 \text{ for every open neighborhood } U \text{ of } x\}.$$

Example 11.

- *The support of the Dirac measure at 0 is the singleton $\{0\}$.*
- *Let $(\mathbb{R}, \mathcal{B}(\mathbb{R}))$. The support of the Lebesgue measure λ is $\mathbb{R}$. Note that every single point has Lebesgue measure zero and so has every countable union of points.*

Definition 15 (Product Measure)**.** *Let $(A_1, \mathcal{A}_1, \mu_1)$ and $(A_2, \mathcal{A}_2, \mu_2)$ be two σ-finite measure spaces. Then the set-function*

$$\begin{array}{rccc} \rho: & \mathcal{A}_1 \times \mathcal{A}_2 & \to & [0, \infty], \\ & A_1 \times A_2 & \mapsto & \mu_1(A_1)\mu_2(A_2) \end{array}$$

is the unique measure called product measure, denoted by $\rho = \mu_1 \otimes \mu_2$ and defined on the measurable space $(A_1 \times A_2, \mathcal{A}_1 \otimes \mathcal{A}_2)$ where $\mathcal{A}_1 \otimes \mathcal{A}_2 = \sigma(\mathcal{A}_1 \times \mathcal{A}_2)$ is a product σ-algebra. $(A_1 \times A_2, \mathcal{A}_1 \otimes \mathcal{A}_2, \mu_1 \otimes \mu_2)$ is called the product measure space.
The product measure ρ is a σ-finite measure on $(A_1 \times A_2, \mathcal{A}_1 \otimes \mathcal{A}_2)$ such that

$$\rho(E) = \int\int 1_E(x, y)\mu_1(\mathrm{d}x)\mu_2(\mathrm{d}y) = \int\int 1_E(x, y)\mu_2(\mathrm{d}y)\mu_1(\mathrm{d}x),$$

holds for all $E \in \mathcal{A}_1 \otimes \mathcal{A}_2$.

Example 12.
The n-dimensional Lebesgue measure λ^n *on* $(\mathbb{R}^n, \mathcal{B}(\mathbb{R}^n))$ *may be defined as a product measure, i.e.*

$$(\mathbb{R}^n, \mathcal{B}(\mathbb{R}^n), \lambda^n) = (\mathbb{R}^d \times \mathbb{R}^{n-d}, \mathcal{B}(\mathbb{R}^d) \otimes \mathcal{B}(\mathbb{R}^{n-d}), \lambda^d \otimes \lambda^{n-d}), \ \forall\ n > d \geqslant 1.$$

B Measurable functions and integration

Definition 16 ($(\mathcal{A}_1, \mathcal{A}_2)$-measurable mapping)**.** *Let* $(A_1, \mathcal{A}_1)$ *and* $(A_2, \mathcal{A}_2)$ *be two measurable spaces. A mapping* $f : A_1 \to A_2$ *is* $(\mathcal{A}_1, \mathcal{A}_2)$*-measurable if*

$$f^{-1}(B) \in \mathcal{A}_1, \ \forall\ B \in \mathcal{A}_2.$$

Definition 17 (Measurable function)**.** *Let* $(A, \mathcal{A})$ *be a measurable space. A function* $f : A \to \mathbb{R}$ *is* $\mathcal{A}$*-measurable (or measurable in short) if* $\{x : f(x) < c\} \in \mathcal{A}$ *for every* $c \in \mathbb{R}$ *or equivalently*

$$f^{-1}(B) \in \mathcal{A}, \ \forall\ B \in \mathcal{B}(\mathbb{R}^n).$$

A measurable function $f : A \to \mathbb{R}$ is a $(\mathcal{A}_1, \mathcal{B}(\mathbb{R}))$-measurable mapping.

Example 13.
Let $(X, \mathcal{A})$ *be a measurable space. The indicator function* $f(x) = 1_A(x)$ *is measurable if and only if* $A \in \mathcal{A}$*. Indeed, for a set* $A \in \mathcal{A}$

$$\begin{array}{lcll} \{x : 1_A(x) < c\} & = & \emptyset \in \mathcal{A} & \text{if} \quad c \leqslant 0, \\ \{x : 1_A(x) < c\} & = & X \backslash A \in \mathcal{A} & \text{if} \quad c \in (0, 1], \\ \{x : 1_A(x) < c\} & = & X \in \mathcal{A} & \text{if} \quad c > 1. \end{array}$$

Definition 18 (Simple function)**.** *A simple function* $g : A \to \mathbb{R}$ *on a measurable space* $(A, \mathcal{A})$ *is a function of the form:*

$$g(x) = \sum_{j=1}^{M} y_j 1_{A_j}(x),$$

with finitely many disjoint sets $A_1, \cdots, A_M \in \mathcal{A}$ *and* $y_1, \cdots, y_M \in \mathbb{R}$*.*
If $y_i \geqslant 0$ *for all* i*, the function* g *is called a positive simple function.*

Definition 19. *Suppose* μ *is a positive measure on the measurable space* $(A, \mathcal{A})$ *and* f *is measurable*

- *If* $f = \sum_{j=1}^{M} y_j 1_{A_j}$ *is a positive simple function then*

$$\int f \mathrm{d}\mu = \sum_{i=1}^{M} y_i \mu(A_i).$$

- *If* $f \geqslant 0$ *then*

$$\int f \mathrm{d}\mu = \sup \left\{ \int g \mathrm{d}g : \ g \leqslant f, \ g \text{ is positive simple} \right\}.$$

- *For arbitrary f,*

$$\int f \mathrm{d}\mu = \int f^+ \mathrm{d}\mu - \int f^- \mathrm{d}\mu,$$

where $f^+ = \max\{f, 0\}$ and $f^+ = -\min\{f, 0\}$.

If $(B, \mathcal{B})$ is measurable, the integral of f over B is defined by:

$$\int_B f \mathrm{d}\mu = \int f 1_B \mathrm{d}\mu.$$

Theorem 4 (Fubini)**.** *Let $(A_1, \mathcal{A}_1, \mu_1)$ and $(A_2, \mathcal{A}_2, \mu_2)$ be σ-finite measure spaces and let $f: A_1 \times A_2 \to \mathbb{R}$ be $\mathcal{A}_1 \otimes \mathcal{A}_2$-measurable. If at least one of the following is finite*

$$\int_{A_1 \times A_2} |f| \mathrm{d}(\mu_1 \otimes \mu_2), \quad \int_{A_2} \int_{A_1} |f(x,y)| \mu_1(\mathrm{d}x) \mu_2(\mathrm{d}y), \quad \int_{A_1} \int_{A_2} |f(x,y)| \mu_2(\mathrm{d}y) \mu_1(\mathrm{d}x)$$

then

$$\int_{A_1 \times A_2} f \mathrm{d}(\mu_1 \otimes \mu_2) = \int_{A_2} \int_{A_1} f(x,y) \mu_1(\mathrm{d}x) \mu_2(\mathrm{d}y) = \int_{A_1} \int_{A_2} f(x,y) \mu_2(\mathrm{d}y) \mu_1(\mathrm{d}x).$$

Definition 20 (Density)**.** *Let $(A, \mathcal{A}, \mu)$ be a measure space and ρ a positive real $\mathcal{A}$-measurable function, the set-function*

$$\mu_\rho: \ A \mapsto \int_A \rho \mathrm{d}\mu = \int 1_A \rho \mathrm{d}\mu = \int 1_A(x) \rho(x) \mu(\mathrm{d}x),$$

is a measure on $(A, \mathcal{A})$ called the measure with density function ρ with respect to μ and denoted $\mu_\rho = \rho\mu$. Traditionally, the density is denoted $\rho = \dfrac{d\mu_\rho}{d\mu}$.

For instance, if the measure μ_I is Gaussian ($\mu_I = \mu_g$), with mean $m \in \mathbb{R}^n$, and covariance matrix Σ, given by:

$$\mu_I(A) := \frac{1}{\sqrt{(2\pi \mathrm{det}(\Sigma))^n}} \int_A \exp\left(-\frac{(X-m)^T \Sigma^{-1} (X-m)}{2}\right) \mathrm{d}X, \tag{124}$$

where $A \in \mathcal{B}(\mathbb{R}^n)$, and $\mathcal{B}(\mathbb{R}^n)$ denotes the completion of the Borel σ-algebra on $\mathbb{R}^n$ and the integral in (124) is with respect to the standard n-dimensional Lebesgue measure. The density of the measure μ_I is a function $\rho_I : \mathbb{R}^n \to \mathbb{R}$ defined by:

$$\rho_I(X) = \frac{1}{\sqrt{(2\pi \mathrm{det}(\Sigma))^n}} \exp\left(-\frac{(X-m)^T \Sigma^{-1} (X-m)}{2}\right). \tag{125}$$

Using the notation of Definition 20, one has $\rho_I = \dfrac{d\mu_I}{d\lambda}$.

C Image of a measure

Let us denote by $M(S)_+$ the cone of all nonnegative Borel measures on the subset S of a measurable space. For completeness, let us recall the classical notions related to the *pushforward measure*, which is roughly speaking *the image of a given measure under a given mapping*:

Definition 21. *[78, Theorem 1.44] (Pushforward measure) Let two measurable spaces $(X, \mathcal{A})$ and $(Y, \mathcal{B})$, a $(\mathcal{A}, \mathcal{B})$-measurable mapping $h : X \to Y$ and a measure $\mu \in M(X)_+$. The pushforward measure (or image measure under the mapping h) $\mu_h = h_\star \mu \in M(Y)_+$ defined on $\mathcal{B}$ is given by:*

$$\mu_h(B) = h_\star \mu(B) = \mu(h^{-1}(B)), \tag{126}$$

for all Borel measurable sets $B \subseteq Y$.

For an arbitrary set $B \subseteq Y$, $h^{-1}(B)$ is *the preimage* of B under the mapping h, i.e.

$$h^{-1}(B) = \{x \in X \ : \ h(x) \in B\}.$$

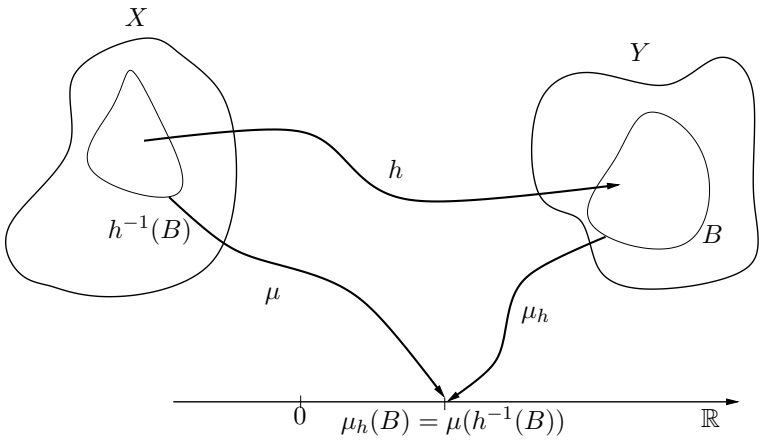

Figure 17: Pushforward measure or image measure μ_h.

Theorem 5. *[15, Theorem 3.6.1] (Change of variables) Let $\mu \in M(X)_+$. A measurable function g on Y is integrable with respect to the pushforward measure $h_\star \mu \in M(Y)_+$ if and only if the composition $g \circ h$ is integrable with respect to the measure $\mu \in M(X)_+$. In that case:*

$$\int_Y g \ \mathrm{d}(h_\star \mu) = \int_X g \circ h \mathrm{d}\mu. \tag{127}$$

A useful corollary may be easily deduced from Theorem 5.

Corollary 1. *[69, Corollary 15.8] (General transformation theorem)*
Let $h : X \to Y$ be a C^1-diffeomorphism. A measurable function g on Y is integrable with respect to λ^n if and only if, the function $g \circ h \cdot |\det \mathrm{D}h| : X \to \overline{\mathbb{R}}$ is integrable with respect to λ^n. In this case,

$$\int_Y g(y)\lambda^n(\mathrm{d}y) = \int_X g(h(x))|\det \mathrm{D}h(x)|\lambda^n(\mathrm{d}x). \tag{128}$$

D Local frame for relative motion modelling

When modelling the relative motion of two space objects in close proximity, it is usual to define a moving Local-Vertical-Local-Horizontal (LVLH) frame R_{LVLH} located at the center of gravity of a reference object (here the primary object to be consistent with Chan's rules) and which rotates with its angular velocity. The precise definition of $R_{LVLH} = \left(O_S, \vec{X}_{LVLH}, \vec{Y}_{LVLH}, \vec{Z}_{LVLH}\right)$ may vary in the literature and in this document, the choice is to define it with its origin O_S, as the centre of mass of the reference satellite and its axes by the vectors:

- $\vec{Z}_{LVLH}$ is radial inward, oriented from primary to the centre of the Earth ;
- $\vec{Y}_{LVLH}$ is normal to the orbital plane in the opposite direction of the angular momentum ;
- $\vec{X}_{LVLH} = \vec{Y}_{LVLH} \wedge \vec{Z}_{LVLH}$ $[\vec{X}_{LVLH}, \vec{Y}_{LVLH}, \vec{Z}_{LVLH}]$ completes the orthogonal right-handed frame.

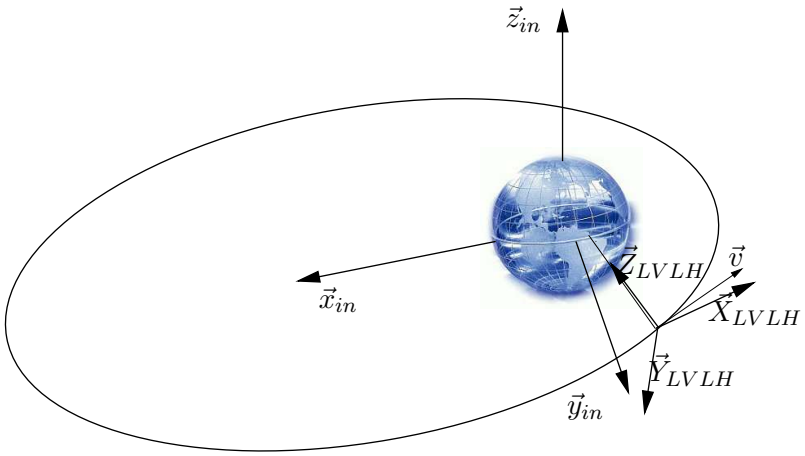

Figure 18: *LVLH frame*

Note also the usual English designation for these three axes:

- Axis of $\vec{Z}_{LVLH}$ is **R-bar** ;
- Axis of $\vec{Y}_{LVLH}$ is **H-bar** ;
- Axis $\vec{X}_{LVLH} = \vec{Y}_{LVLH} \wedge \vec{Z}_{LVLH}$ is **V-bar**.

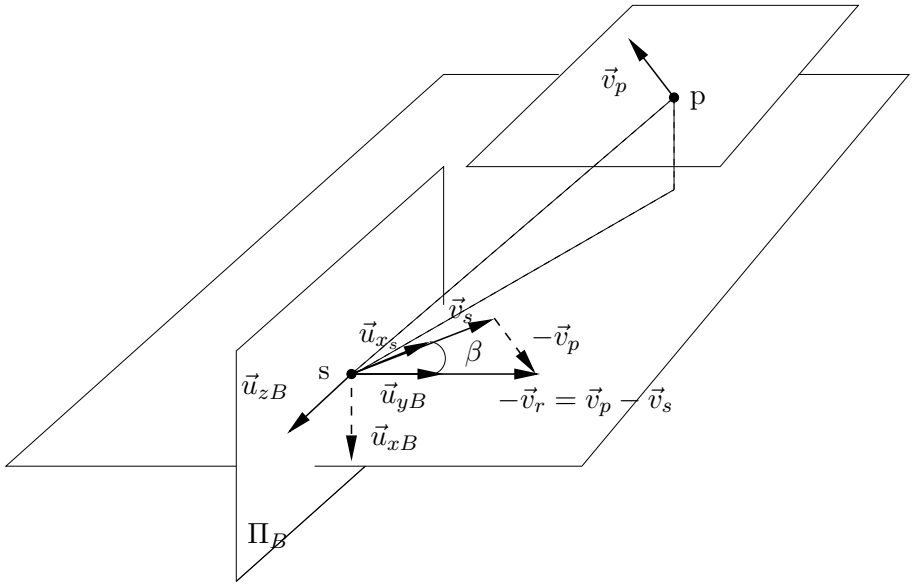
$\vec{v}_p$
p
$\vec{v}_s$
$\vec{u}_{x_s}$
$-\vec{v}_p$
β
s
$\vec{u}_{zB}$
$\vec{u}_{yB}$
$-\vec{v}_r = \vec{v}_p - \vec{v}_s$
$\vec{u}_{xB}$
Π_B

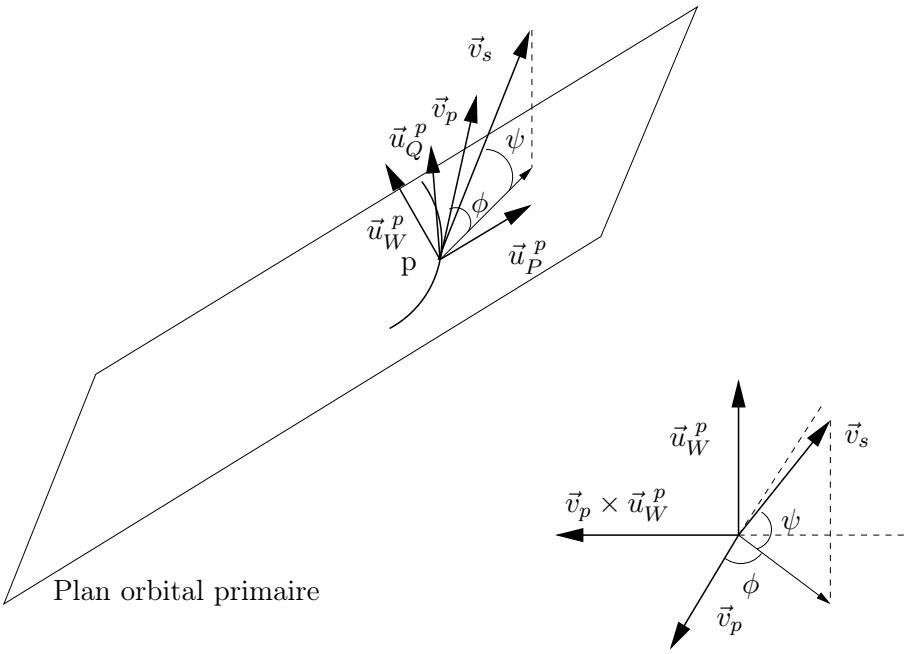
$\vec{v}_s$
$\vec{v}_p$
$\vec{u}_Q^{\,p}$
ψ
ϕ
$\vec{u}_W^{\,p}$
p
$\vec{u}_P^{\,p}$
Plan orbital primaire
$\vec{u}_W^{\,p}$
$\vec{v}_s$
$\vec{v}_p \times \vec{u}_W^{\,p}$
ψ
ϕ
$\vec{v}_p$

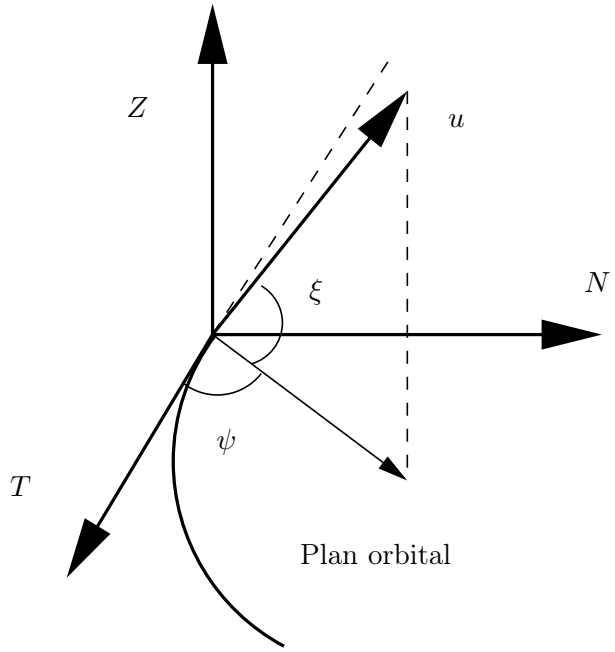
Z
u
N
ξ
ψ
T
Plan orbital

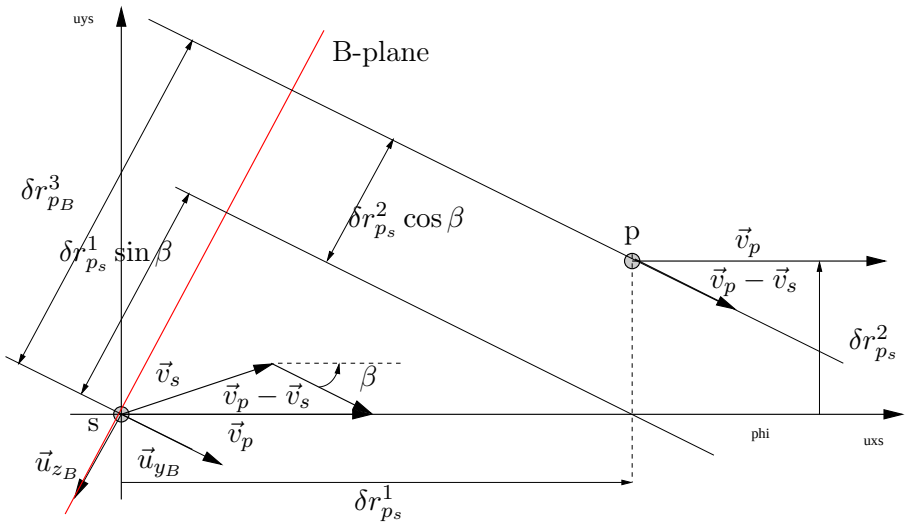
uys
B-plane
$\delta r^3_{p_B}$
$\delta r^1_{p_s} \sin\beta$
$\delta r^2_{p_s} \cos\beta$
p
$\vec{v}_p$
$\vec{v}_p - \vec{v}_s$
$\delta r^2_{p_s}$
$\vec{v}_s$
$\vec{v}_p - \vec{v}_s$
β
s
$\vec{v}_p$
phi
uxs
$\vec{u}_{z_B}$
$\vec{u}_{y_B}$
$\delta r^1_{p_s}$

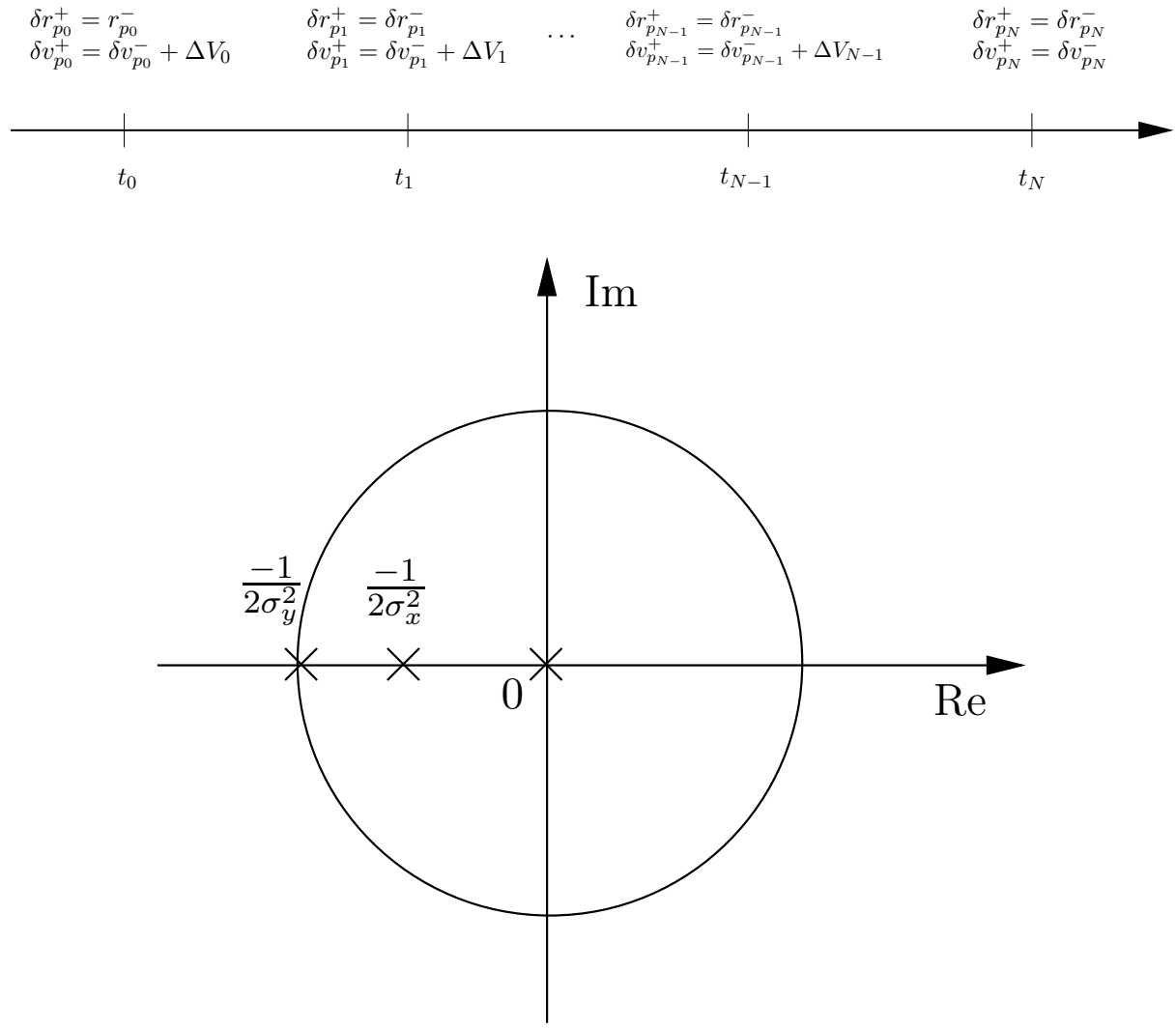

References

[1] M.R. Akella and K.T. Alfriend. Probability of collision between space objects. *Journal of Guidance, Control and Dynamics*, 23(5):769–772, 2000.

[2] A. Alfano. Aerospace Support to Space Situation Awareness. *Applicationes Mathematicae*, oct 2002.

[3] S. Alfano. A numerical implementation of spherical objet collision probability. *Journal of Astronautical Sciences*, 53(1), Janvier-Mars 2005.

[4] S. Alfano. Satellite collision probability enhancements. *Journal of Guidance Control and Dynamics*, 29(3):588–592, 2006.

[5] S. Alfano. Beta conjunction analysis tool. In *Proceedings of AAS/AIAA Astrodynamics Specialist Conference*, number AAS 07-393, Mackinac Island, MI, USA, August 2007.

[6] S. Alfano. Review of conjunction probability methods for short-term encounters (aas 07-148). *Advances in the Astronautical Sciences*, 127(1):719, 2007.

[7] S. Alfano. Satellite conjunction Monte Carlo analysis. *Advances in the Astronautical Sciences*, 134:2007–2024, jan 2009.

[8] K.T. Alfriend, editor. *Spacecraft Formation Flying: Dynamics, Control and Navigation.* Astrodynamics Series. Elsevier, Burlington, USA, 2010.

[9] K.T Alfriend, M.R. Akella, J. Frisbee, J.L. Foster, D.-J. Lee, and M. Wilkins. Probability of collision error analysis. *Space Debris*, 1(1):21–35, 1999.

[10] R. Altendorfer and C. Wilkmann. A new approach to estimate the collision probability for automotive applications. *arXiv: Systems and Control*, 2019.

[11] L. Ambrosio. *Calculus of variations and nonlinear partial differential equations. Lecture Notes in Mathematics*, volume 1927, chapter Transport equation and Cauchy problem for non-smooth vector fields. Springer-Verlag, 2008.

[12] D. Arzelier, F. Bréhard, M. Joldeş, J.B. Lasserre, L. Martire, and A. Rondepierre. Global probability of collision: problem modelling via occupation measure. Technical Note 19xxx, LAAS-CNRS, October 2017.

[13] K. Atkinson and W. Han. *Spherical harmonics and approximations on the unit sphere: An introduction.* Springer, Berlin, Heidelberg, Germany, 202.

[14] Y.K. Belyaev. On the number of exits across the boundary of a region by a vector stochastic process. *Theory of Probability and Its Applications*, 13(2):320–324, 1968.

[15] V. I. Bogachev. *Measure theory*, volume I and II. Springer Science & Business Media, 2007.

[16] S. Boyd, L. El Ghaoui, E. Feron, and V. Balakrishnan. *Linear Matrix Inequalities in System and Control Theory.* SIAM Studies in Applied Mathematics. SIAM, Philadelphia, PA, USA, 1994.

[17] S. Boyd and L. Vandenberghe. *Convex Optimization.* Cambridge University Press, New York, NY, USA, 2004.

[18] M.E. Campbell. Collision monitoring within satellite clusters. *IEEE Transactions on Control Systems Technology*, 13(1):42–55, January 2005. `http://dx.doi.org/10.1109/tcst.2004.838550`.

[19] J.R. Carpenter. Conservative analytical collision probability for design of orbital formations. In *2nd International Symposium on Formation Flying*, 2004.

[20] F.K. Chan. Collision Probability Analysis for Earth-orbiting Satellites. *Advances in the Astronautical Sciences*, 96, 1997.

[21] F.K. Chan. *Spacecraft Collision Probability.* American Institute of Aeronautics and Astronautics, 2008.

[22] F.K. Chan. Formulation of collision probability with time-dependent probability density functions. In *AAS/AIAA Space Flight Mechanics Meeting*, number AAS 15-233, Williamsburg, VA, USA, January 2015.

[23] F.K. Chan. Hovering collision probability. In *AAS/AIAA Space Flight Mechanics Meeting*, number AAS 15-234, Williamsburg, VA, USA, January 2015.

[24] K. Chan. Spacecraft collision probability for long-term encounters. Number AAS 03-549, Big Sky, Montana, USA, 2003.

[25] K. Chan. Short-term vs long-term spacecraft encounters. Number AAS 04-5460, Providence, Rhode Island, USA, August 2004.

[26] W.H. Clohessy and R.S. Wiltshire. Terminal guidance system for satellite rendezvous. *Journal of the Astronautical Sciences*, 27(9):653–658, 1960.

[27] V. Coppola. Evaluating the short encouter assumption of the probability of collision formula. In *Proceedings of the AAS-AIAA Astrodynamics Specialist Conference*, number AAS 12-248, Minneapolis, Minnesota, USA, 2012.

[28] V.T. Coppola. Including Velocity Uncertainty in the Probability of Collision between Space Objects. *Advances in the Astronautical Sciences*, 143, 2012.

[29] V.T. Coppola and J. Woodburn. Determination of close approaches based on ellipsoidal threat volumes. *Spaceflight mechanics*, pages 1013–1023, 1999.

[30] F. Dabbene, D. Henrion, and C.M. Lagoa. Simple approximations of semialgebraic sets and their applications to control. *Automatica*, 78:110–118, 2017.

[31] K. DeMars and M. Gualdoni. Information-Theoretic Approaches to Space Object Collision. Paper presented at the 7th European Conference on Space Debris, apr 2017.

[32] K.J. DeMars, Y. Chang, and M.K. Jah. Collision probability with gaussian mixture orbit uncertainty. *Journal of Guidance, Control, and Dynamics*, 37(3):979–985, 2014.

[33] J.C. Dolado-Perez, P. Legendre, R. Garmier, B. Revelin, and X. Pena. Satellite Collision Probability Computation for Long Term Encounters. *Advanced Astronomical Society / American Institute of Aeronautics and Astronautics Astrodynamics Specialist Conference*, 142, 2011.

[34] J. L. Foster and H. S. Estes. A parametric analysis of orbital debris collision probability and maneuver rate for space debris. *NASA/JSC-25898*, August 1992.

[35] J. L. Foster and S. E. Herbert. A Parametric Analysis of orbital Debris Collision Probability and Maneuver Rate for Space Vehicles. Technical report, NASA Johnson Space Center, August 1992.

[36] R.C. Frigm and D. Rohrbaugh. Relative velocity as a metric for probability of collision calculations. In *Proceedings of the 59th International Astronautical Congress*, number IAC-08-A6.2.5, Glasgow, Scotland, UK, October 2008.

[37] R. Garmier, J.C. Dolado-Perez, X. Pena, B. Revelin, and P. Legendre. Collision Risk Assessment for Multiple Encounters, 2009. `http://www.academia.edu/12629726/Collision_Risk_Assessment_for_Multiple_Encounters`.

[38] W.M. Haddad and V. Chellaboina. *Nonlinear Dynamical Systems and Control*. Princeton University Press, 2008.

[39] D.T. Hall. Implementations recommendatioons and usage boundaries for the two-dimensional probability of collision calculation. Number AAS 19-632, Portland, Oregon, USA, August 2019.

[40] D.T. Hall, M.D. Hejduk, and L.C. Johnson. Time Dependence of Collision Probabilities During Satellite Conjunctions. Number AAS 17-271, San Antonio, TX, USA, February 2017.

[41] D. Henrion, J.B. Lasserre, and C. Savorgnan. Approximate volume and integration for basic semialgebraic sets. *SIAM review*, 51(4):722–743, 2009.

[42] R. Illsley. *Crossings of boundaries by vector Gaussian processes with applications to problems in reliability*. PhD thesis, City University, London, UK, 1992.

[43] R. Illsley. The moments of the number of exits from a simply connected region. *Advances in Applied Probability*, 30(1):167–180, 1998.

[44] A.H. Jazwinski. *Stochastic processes and filtering*. Academic Press, New York, NY, USA, 1970.

[45] Z.N. Khutorovsky, V.F. Boikov, and S.Y. Kamensky. Direct method for the analysis of collision probability of artificial space objects in leo: Techniques, results and applications. In *Proceedings of the first European Conference on Space Debris*, Darmstadt, Germany, April 1993.

[46] G. Krier. Satellite Collision Probability for Long-term Encounters and Arbitrary Primary Satellite Shape. Paper presented at the 7th European Conference on Space Debris, apr 2017.

[47] P. Lairez, M. Mezzarobba, and M. Safey El Din. Computing the volume of compact semi-algebraic sets. In *Proceedings of the 2019 on International Symposium on Symbolic and Algebraic Computation*, pages 259–266, 2019.

[48] J.B Lasserre. Global optimization with polynomials and the problem of moments. *SIAM Journal on optimization*, 11(3):796–817, 2001.

[49] J.B. Lasserre. *An Introduction to Polynomial and Semi-Algebraic Optimization*. Cambridge University Press, 2015.

[50] J.B. Lasserre. Volume of sublevel sets of homogeneous polynomials. *SIAM Journal on Applied Algebra and Geometry*, 3(2):372–389, 2019.

[51] J.B. Lasserre and Y. Emin. Semidefinite relaxations for lebesgue and gaussian measures of unions of basic semialgebraic sets. *Mathematics of Operations Research*, 44(4):1477–1493, 2019.

[52] V.I. Lebedev. Values of the nodes and weights of ninth to seventeenth order gauss-markov quafrature formulae invariant under the octahedron group with inversion. *USSR Computational Mathematics and Mathematical Physics*, 15:44–51, 1975.

[53] V.I. Lebedev. Quadratures on a sphere. *USSR Computational Mathematics and Mathematical Physics*, 16(2):10–24, January 1976.

[54] V.I. Lebedev. Spherical quadrature formulas exact to orders 25-29. *Siberian Mathematical Journal*, 18:99–107, 1977.

[55] V.I. Lebedev and D.N. Laikov. A quadrature formula for the sphere of the 131st algebraic order of accuracy. *Doklady Mathematics*, 59:477–481, 1999.

[56] J. Lofberg. YALMIP : a toolbox for modeling and optimization in MATLAB, 2004. `http://yalmip.github.io/`.

[57] J. Mathews. *Numerical Methods for computer science, engineering and mathematics*. Prentice Hall, Englewood Cliffs, NJ, USA, 1992.

[58] D.P. McKinley. Development of a nonlinear probability of collision tool for the Earth observing system. In *AIAA/AAS Astrodynamics Specialist Conference and Exhibit*, number AAS-2006-6295, August 2006.

[59] O. Montenbruck and E. Gill. *Satellite orbits: Models, Methods, Applications*. Springer, Berlin, Germany, 2001.

[60] MOSEK ApS. MOSEK Version 8.0.0.64, April 2017. `https://www.mosek.com/products/mosek`.

[61] R.P. Patera. General Method for Calculating Satellite Collision Probability. *Journal of Guidance, Control, and Dynamics*, 24(4):716–722, July 2001.

[62] R.P. Patera. Satellite collision probability for nonlinear relative motion. *Journal of Guidance Control and Dynamics*, 26(5):728–733, 2003.

[63] M. Phillips and S. Hur-Diaz. On-board estimation of collision probability for cluster flight. In *Proceedings of the AAS/AIAA Space Flight Mechanics Meeting*, 2013.

[64] M. Putinar. Positive polynomials on compact semi-algebraic sets. *Indiana University Mathematics Journal*, 42(3):969–984, 1993.

[65] S.O. Rice. Mathematical analysis of random noise. *Bell Systems Technical Journal*, 23:282–332, 1944.

[66] S.O. Rice. Mathematical analysis of random noise. *Bell Systems Technical Journal*, 24:44–156, 1945.

[67] R.I. Saye. High-order quadrature methods for implicitly defined surfaces and volumes in hyperrectangles. *SIAM Journal on Scientific Computing*, 37(2):A993–A1019, 2015.

[68] V. Schaeffer, S. Laurens, P. Seimandi, and F. Delmas. Collision probability through time integration. In *SpaceOps Conference*, Marseille, France, June 2018.

[69] S. L. Schilling. *Measures, Integrals and Martingales*. Cambridge University Press, 2011.

[70] P. Seimandi. Méthodes pour le calcul de la probabilité de collision. Technical Report SORO-NT-7202-0302-CNES, CNES, June 2016.

[71] R. Serra. *Opérations de proximité en orbite : évaluation du risque de collision et calcul de manoeuvres optimales pour l'évitement et le rendez-vous*. PhD thesis, Université de Toulouse, INSA de Toulouse, 135 Avenue de Rangueil, 31400 Toulouse, France, 12 2015.

[72] R. Serra, D. Arzelier, M.M. Joldes, J.B. Lasserre, A. Rondepierre, and B. Salvy. Fast and accurate computation of orbital collision probability for short-term encounters. *Journal of Guidance Control and Dynamics*, 2016.

[73] R. Serra, D. Arzelier, M.M. Joldes, J.B.-Bernard Lasserre, A. Rondepierre, and B. Salvy. A new method to compute the probability of collision for short-term space encounters. In *AIAA/AAS Astrodynamics Specialist Conference*, page 4366, 2014.

[74] R. Serra, D. Arzelier, M.M. Joldes, and A. Rondepierre. Probabilistic collision avoidance for long-term space encounters via risk selection. In *Advances in Aerospace Guidance, Navigation and Control*, pages 679–698. Springer, 2015.

[75] W.S. Shepperd. Universal Keplerian State Transition Matrix. *Celestial Mechanics*, 35:129–144, 1985.

[76] C.E. Van Daalen and T. Jones. Fast conflict detection using probability flow. *Automatica*, 45:1903–1909, 2009.

[77] C. Wen, Y. Gao, and H. Shi. Three-dimensional relative reachable domain with initial state uncertainty in gaussian distribution. *Proceedings of the Institution of Mechanical Engineers, Part G: Journal of Aerospace Engineering*, 233(5):1555–1570, 2019.

[78] J. Yeh. *Real Analysis - Theory of Measure and Integration*. World Scientific, Singapore, Singapore, 2nd edition, 2000.

[79] O. Zarrouati. *Trajectoires spatiales*. Cepadues, Toulouse France, 1987.